

# **The Highest Oxidation States of the 5d Transition Metals: a Quantum-Chemical Study**

DISSERTATION

zur Erlangung des naturwissenschaftlichen Doktorgrades  
der Bayerischen Julius-Maximilians-Universität Würzburg

vorgelegt von  
Sebastian Hasenstab-Riedel  
aus Groß-Gerau

**Würzburg 2006**

Eingereicht am: .....

Bei der Fakultät für Chemie und Pharmazie

1. Gutachter: .....

2. Gutachter: .....

der Dissertation

1. Prüfer: .....

2. Prüfer: .....

3. Prüfer: .....

Des öffentlichen Promotionskolloquiums: .....

Tag des öffentlichen Promotionskolloquiums: .....

Doktorurkunde ausgehändigt am: .....

*“One of the major goals of inorganic chemistry is to prepare compounds of elements in unusual oxidation states.”*

C. K. Jørgensen,  
*Naturwissenschaften*, 1976, 63, 292



*Für Andrea*



# Abstract

The theoretical work presented in this thesis is concerned with the highest possible oxidation states of the 5d transition metal row. Based on a validation study of several DFT functionals against accurate coupled-cluster CCSD(T) methods we will present calculations on a series of new high oxidation state  $\text{Hg}^{\text{IV}}$  species. Quantum-chemical calculations have also been applied to various fluoro complexes of gold in oxidation states +V through +VII to evaluate the previously claimed existence of  $\text{AuF}_7$ . The calculations indicate clearly that the oxidation state (+V), e.g., in  $[\text{AuF}_5]_2$ , remains the highest well-established gold oxidation state. Further calculations on iridium in oxidation state (+VII) show that  $\text{IrF}_7$  and  $\text{IrOF}_5$  are viable synthetic targets, whereas higher oxidation states of iridium appear to be unlikely. Structures and stabilities of several osmium fluorides and oxyfluorides were also studied in this thesis. It is shown that homoleptic fluorides all the way up to  $\text{OsF}_8$  may exist.

Combining the results of the most accurate quantum-chemical predictions of this thesis and of the most reliable experimental studies, we observe a revised trend of the highest oxidation states of the 5d transition metal row. From lanthanum (+III) to osmium (+VIII), there is a linear increase of the highest oxidation states with increasing atomic number. Thereafter, we observe a linear descent from osmium (+VIII) to mercury (+IV). We will also present a short outlook to the transition metals of the 3d and 4d row and their highest reachable oxidation states.

# Zusammenfassung

In der vorliegenden theoretischen Arbeit wurden mittels quantenchemischer Methoden die höchsten Oxidationsstufen der späten Übergangselemente untersucht. Um eine adäquate Beschreibung dieser Systeme zu gewährleisten, wurde zuerst eine Validierungsstudie verschiedener Dichtefunktionale, die mit hochgenauen coupled-cluster CCSD(T) Berechnungen verglichen wurden, durchgeführt. Das zugrundeliegende Referenzsystem war Quecksilber in der Oxidationsstufe +IV ( $\text{HgF}_4$ ,  $\text{HgCl}_4$ ,  $\text{HgH}_4$ ). Es wurden Strukturoptimierungen von Minima und Übergangszuständen, Atomisierungsenergien sowie die entsprechenden Zerfallsreaktionen für die Systeme betrachtet. Basierend auf diesen Ergebnissen konnten weitere  $\text{Hg}^{\text{IV}}$  Systeme mit sogenannten „Weakly Coordinating Anions“ wie z.B.  $[\text{OTeF}_5]^-$ ,  $[\text{AsF}_6]^-$ ,  $[\text{Sb}_2\text{F}_{11}]^-$  usw. unter Verwendung von Dichtefunktionalmethoden untersucht werden. Die beiden Verbindungen  $\text{Hg}[\text{OTeF}_5]_4$  und  $\text{Hg}[\text{AsF}_6]_4$  scheinen dabei die Oxidationsstufe +IV am besten zu stabilisieren.

Quantenchemische Methoden wurden ebenfalls zur Berechnung von Fluorkomplexen des Goldes in den Oxidationsstufen von +V bis +VII verwendet. Dabei wurde insbesondere überprüft, ob das angeblich experimentell gefundene  $\text{AuF}_7$  tatsächlich existiert. Es konnte gezeigt werden, dass eine Existenz von  $\text{AuF}_7$  unter den in der Literatur angegebenen Bedingungen sehr wahrscheinlich ausgeschlossen werden kann. Diese Instabilität wird ebenfalls für das quantenchemisch untersuchte  $\text{AuF}_6$  beobachtet. Somit bleibt die Oxidationsstufe +V in  $[\text{AuF}_5]_2$  die höchste erreichbare Oxidationsstufe für Gold.

Basierend auf coupled-cluster CCSD(T) Berechnungen konnten die Verbindungen des Iridiums in der Oxidationsstufe +VII ( $\text{IrF}_7$ ,  $\text{IrOF}_5$ ) als thermochemisch stabil vorhergesagt werden, wohingegen die höheren Iridiumverbindungen des  $\text{Ir}^{\text{VIII}}$  und  $\text{Ir}^{\text{IX}}$  sehr unwahrscheinlich sind. Außerdem wurden Strukturen und Stabilitäten verschiedener Osmiumfluoride und Oxyfluoride in dieser Arbeit diskutiert. Es konnte gezeigt werden, dass ausgehend von  $\text{OsF}_6$  auch die höheren Verbindungen  $\text{OsF}_7$  und  $\text{OsF}_8$  experimentell zugänglich sein sollten.

Kombiniert man die in dieser Arbeit vorhergesagten Verbindungen in ihren höchsten Oxidationsstufen mit den verlässlichsten experimentellen Untersuchungen, so beobachtet man einen revidierten Trend der höchsten Oxidationsstufen der 5d-Übergangsmetallreihe: Direkt proportional zur Ordnungszahl steigen die höchsten Oxidationszahlen zunächst linear an, von Os (+VIII) bis hin zu Hg (+IV) kann ein linearer Abfall beobachtet werden.

Abschließend werden in dieser Arbeit die höchsten Oxidationsstufen der 3d und 4d Übergangsmetalle in einer kurzen Übersicht vorgestellt.



# Acknowledgments

I would like to express my particular gratitude to my supervisor Martin Kaupp for his inspiring and honest guidance. He always found the time to listen and help. Especially I have to thank for the freedom to do all the research on high oxidation state species. Whenever a new idea comes to my mind Martin supported me with his enormous knowledge which brought me deeper into the topic. I have also to thank for allowing me to participate in many research schools and conferences over the years.

My deepest thanks to the previous member of our workgroup Michal Straka for his help, explanations, and especially for many fruitful, interesting and inspiring discussions. He was one of the first who guided me through the jungle of quantum-chemical methods and programs.

I owe a lot of gratitude to the present members of our research group: Sylwia Kacprzak, Christian Remenyi, Alexander Patrakov, James Asher, Roman Reviakin, Alexei Arbuznikov, Sandra Schinzel, Hilke Bahmann, Irina Malkin and to our guest Jean-Christophe Tremblay. I thank for all the nice discussions, for technical assistance, for the proof-reading of manuscripts and for the friendly atmosphere.

I especially want to thank Pekka Pyykkö for inviting me for research habitation to his work group in Helsinki and for his great hospitality during my stay. Thanks for the many fruitful and inspiring discussions all the time. My time in Helsinki was excellent due to the nice group members of the Laboratory of Instructions in Swedish: Dage Sundholm, Michael Patzschke, Mikael Johansson, Olli Lehtonen, Jonas Jusèlius, Ying-Chan Lin and Susanne Lundberg.

I also want to thank Carsten Strohmman who was always there with his nice suggestions and motivating remarks and to his former students Daniel Schildbach, Dominik Auer, Katja Strohfeldt, Jan Hörnig and to our guest from the second floor, Krzysztof Radacki.

Last but not least I want to thank my family and friends. I thank my mother Marlies Riedel and my brother Steffen Riedel for their great support during all the years. My family in law Werner, Gabi, Sylvia, Katharina, Peter and the smallest one, Christoph Hasenstab, for just being there. I want also to thank all my friends for the good time, nice campfires and all nice adventures during my time with the scouts.

Finally, I want to express my deepest gratitude to Andrea for her patient and understanding nature. You were always there and you never gave up in keeping my back free. Thanks for just being you.

*Sebastian Hasenstab-Riedel*

*Würzburg, 17.7.2006*

# List of Abbreviations

<b>AE</b>	Atomization energies	<b>KS</b>	Kohn-Sham
<b>AO</b>	Atomic orbital	<b>LDA</b>	Local density approximation
<b>a.u.</b>	Atomic units	<b>LSDA</b>	Local spin density approximation
<b>BO</b>	Born-Oppenheimer approximation	<b>MO</b>	Molecular orbitals
<b>BSSE</b>	Basis-set superposition errors	<b>MP<sub>n</sub></b>	Møller-Plesset perturbation theory of <i>n</i> th order
<b>CASSCF</b>	Complete active space self-consistent field	<b>MCSCF</b>	Multi-configuration self-consistent field
<b>CC</b>	Coupled-cluster	<b>MRCI</b>	Multi-reference configuration interaction
<b>CCSD</b>	Coupled-cluster with singles and doubles	<b>NPA</b>	Natural population analysis
<b>CCSD(T)</b>	Coupled-cluster with singles and doubles including perturbative triples	<b>ND</b>	Non-dynamical correlation
<b>CGTF</b>	Contracted gaussian type functions	<b>PP</b>	Pseudopotentials
<b>CI</b>	Configuration interaction	<b>PT</b>	Perturbation theory
<b>CISD</b>	Configuration interaction with singles and doubles	<b>QCI</b>	Quadratic configuration interaction
<b>CP</b>	Counterpoise correction	<b>RLC</b>	Relativistic large core PP
<b>CSF</b>	Configuration state function	<b>RSC</b>	Relativistic small core PP
<b>DC</b>	Dynamical correlation	<b>SCF</b>	Self-consistent field
<b>dmpe</b>	(bis(dimethylphosphanyl) ethane)	<b>SE</b>	Schrödinger equation
<b>DF</b>	Dirac-Fock calculation	<b>SO</b>	Spin-orbit coupling
<b>DFT</b>	Density functional theory	<b>STO</b>	Slater-type orbitals
<b>DKH</b>	Douglas-Kroll-Hess	<b>SV</b>	Split-valence
<b>DZ</b>	Double zeta	<b>TS</b>	Transition state
<b>GGA</b>	Generalised gradient approximation	<b>VWN</b>	Vosko-Wilk-Nusair local-correlation-energy approximation
<b>GTO</b>	Gaussian type orbitals	<b>WCA</b>	Weakly coordinating anions
<b>HF</b>	Hartree-Fock	<b>ZORA</b>	Zero-order regular approximation
		<b>ZPE</b>	Zero-point energy

# Contents

<b>Abstract</b>	I
<b>Acknowledgments</b>	III
<b>List of abbreviations</b>	IV
<b>1. Introduction</b>	<b>1</b>
<b>2. Methodology</b>	<b>5</b>
<b>2.1. Molecular Energy</b> .....	6
<b>2.2. <i>Ab initio</i> Methods</b>	
2.2.1. Hartree-Fock Approximation (HF) .....	7
2.2.2. Configuration Interaction Methods .....	9
2.2.3. Perturbation Theory (PT) .....	10
2.2.4. Coupled-Cluster Theory (CC).....	12
2.2.4.1. Dynamical and Non-Dynamical Correlation.....	14
2.2.4.2. $T_1$ -Diagnostic.....	15
<b>2.3. Density Functional Theory (DFT)</b>	
2.3.1. Hohenberg-Kohn Theorems .....	17
2.3.2. Kohn-Sham Approach (KS) .....	17
2.3.3. Local Density Approximation (LDA) .....	19
2.3.4. Generalised Gradient Approximation (GGA) .....	20
2.3.5. Hybrid Functionals .....	20
<b>2.4. Basis Sets</b> .....	21
<b>2.5. Relativity</b>	
2.5.1. Relativistic Effects .....	22
2.5.2. Relativistic Methods.....	27
2.5.2.1. 2-Component Methods.....	28
2.5.2.2. Pseudopotentials.....	29

## Corrections

2.5.3. Basis-Set Superposition Error (BSSE).....	30
2.5.4. Zero-Point energy (ZPE).....	31

## 3. Oxidation States and Ligands 33

## 4. The Highest Oxidation States of the Late 5d Transition Metals 37

### 4.1. Validation of Density Functional Methods for Computing Structures and Energies of Hg<sup>IV</sup> Complexes

4.1.1. Introduction.....	37
4.1.2. Computational Details.....	38
4.1.3. Minimum Structures.....	40
4.1.4. Reaction Energies for X <sub>2</sub> -elimination.....	41
4.1.5. Atomization Energies.....	44
4.1.6. Transition States.....	46
4.1.7. Conclusions.....	48

### 4.2. Can Weakly Coordinating Anions Stabilise Mercury in its Oxidation State +IV?

4.2.1. Introduction.....	50
4.2.2. Computational Details.....	51
4.2.3. Structure Optimisation.....	53
4.2.4. Thermochemical Stability of Hg <sup>IV</sup> versus Hg <sup>II</sup> Complexes.....	64
4.2.5. Bonding Analyses.....	70
4.2.6. Discussion and Suggestions for Experimental Investigation.....	72
4.2.7. Conclusions.....	76

### 4.3. Has AuF<sub>7</sub> Been Made?

4.3.1. Introduction.....	77
4.3.2. Computational Details.....	78
4.3.3. Structure Optimisation of Au <sup>V</sup> , Au <sup>VI</sup> , and Au <sup>VII</sup> Fluorides.....	79
4.3.4. Vibrational Frequencies.....	83
4.3.5. Reaction Energies for Concerted and Homolytic Elimination.....	84
4.3.6. Transition States for Elimination Reactions.....	85

4.3.7. Electron Affinities of Hexafluorides .....	87
4.3.8. Bonding Comparison of AuF <sub>5</sub> and AuF <sub>7</sub> .....	87
4.3.9. Conclusions .....	89
<b>4.4. Higher Oxidation States of Iridium: the Case of Ir<sup>VII</sup></b>	
4.4.1. Introduction .....	90
4.4.2. Computational Details.....	91
4.4.3. Structures and Thermochemistry .....	92
4.4.4. Noble-Gas Complexes.....	94
4.4.5. The Iridium Oxyfluoride IrOF <sub>5</sub> .....	95
4.4.6. Cationic Iridium Fluoride Species.....	96
4.4.7. Conclusions .....	96
<b>4.5. Where is the Limit of Highly Fluorinated High Oxidation State Osmium Species?</b>	
4.5.1. Introduction .....	97
4.5.2. Computational Details.....	98
4.5.3. Results and Discussion.....	99
4.5.4. Conclusions .....	106
<b>5. Conclusions and Outlook</b>	<b>107</b>
<b>6. References</b>	<b>116</b>
<b>List of Publications.....</b>	<b>VIII</b>
<b>Curriculum Vitae .....</b>	<b>X</b>



# 1 Chapter

## Introduction

Even 137 years after its discovery, the periodic table of the elements is still yielding up new secrets to inquisitive researchers. The number of new species characterised since D. Mendeleev<sup>[1]</sup> and J. L. Meyer<sup>[2]</sup> published the table is in the millions and still growing, and observation and analysis of periodicities and trends is ongoing.

One major topic in the field of fundamental chemistry is the prediction and experimental verification of novel inorganic species with unusual oxidation states. The discovery of these new states and their properties enhances and expands chemical understanding of the behaviour of the elements and their compounds. Such serendipities can also reveal hitherto-unrecognised trends in the periodic table. But higher oxidation states are by no means only of academic interest – complexes in high oxidation states may serve as fluorinating agents,<sup>[3, 4]</sup> oxidants<sup>[5, 6]</sup> and catalysts.<sup>[7-9]</sup>

For a long time, it was only possible to characterise and explain observations and trends in the periodic table by way of experiment. But with the development of more and more sophisticated methodologies, computational chemistry has reached a high-level of predictive power. For example, the possible existence of the  $[\text{N}_5]^+$  ion, along with its structure, were computationally predicted in 1991 by P. Pykkö and N. Runeberg.<sup>[10]</sup> In 1999, K. O. Christe synthesised it as the salt  $[\text{N}_5][\text{AsF}_6]$ .<sup>[11]</sup>

Today, density functional theory (DFT) provides a most successful tool to calculate at low costs of theory structures, transition states and vibrational spectra of large systems. Even the description of large transition metal complexes is possible, as shown by many validation studies.<sup>[12-14]</sup> But DFT fails for systems where non-dynamical correlation plays a dominant role, for example for systems with stretched bonds. The up to now existing density functionals partly incorporate these effects, but in an uncontrolled way.<sup>[13, 15, 16]</sup> This problem can be solved by using coupled-cluster theory which describes to some extent non-dynamical correlation. It is thus, e.g., possible to use DFT-optimised structures and calculate in a second step single-point coupled-cluster energies. This combination of the new density functionals

with the most modern implementations of coupled-cluster (CC) methods provides an excellent approach for calculating accurate energetics of complexes. Where the coupled-cluster single-point calculations become too computationally expensive, one may resort to DFT for energetics. However, as we will show throughout this thesis, informed selection of suitable DFT methods benefits from calibration by comparison to coupled-cluster results for smaller systems.

In this work we have used this combination of methods, density functional theory and high-level coupled-cluster calculations, to evaluate the structures, frequencies and stabilities of many late 5d transition metal complexes.

In Chapter 4.1 we present a validation study of DFT methods for computing structures and energies of mercury in the +IV oxidation state. The existence of Hg in a higher oxidation state than +II would turn the group 12 element into a genuine transition metal. Normally, the group 12 elements (Zn, Cd, Hg) use only s-orbitals in bonding, and are therefore counted among the main group elements. We will show that several Hg<sup>IV</sup> species have a realistic chance of experimental realisation – see Chapter 4.2. For the left neighbour, gold, we will show in Chapter 4.3 that the claimed experimental discovery of the oxidation state +VII in AuF<sub>7</sub> was very probably erroneous. The study will also indicate that Au<sup>VI</sup> as AuF<sub>6</sub> has an extremely large electron affinity and low stability. Thus, Au<sup>V</sup> remains the highest well-established gold oxidation state. In the case of iridium, our high-level quantum-chemical calculations predict a series of species in the new oxidation state +VII, but we consider the higher oxidation states Ir<sup>VIII</sup>F<sub>8</sub> Ir<sup>IX</sup>F<sub>9</sub> unlikely to exist – see Chapter 4.4. The highest oxidation state of osmium, +VIII, is experimentally well-known in OsO<sub>4</sub>. But we will show in this study that OsF<sub>8</sub>, which is not known experimentally, also has a realistic chance for experimental verification – see Chapter 4.5.

Our quantum-chemical calculations augment the existing experimental knowledge, providing a revised picture of the highest oxidation states of the 5d transition metals, displaying a clear trend: from lanthanum +III to osmium +VIII, there is a linear increase of the oxidation states with increasing atomic number. Thereafter, we observe a linear descent from osmium +VIII to mercury +IV – see Chapters 4.4, 4.5 and 5.

Our results disagree with several publications of Russian research groups which predicted the highest oxidation states for the late 5d transition metals as [Ir<sup>IX</sup>O<sub>4</sub>]<sup>+17</sup>, [Ir<sup>VII</sup>O<sub>4</sub>]<sup>-18</sup>, [Pt<sup>X</sup>O<sub>4</sub>]<sup>+2</sup><sup>[19]</sup>, Pt<sup>VIII</sup>O<sub>4</sub><sup>[18]</sup>, [Au<sup>IX</sup>O<sub>4</sub>]<sup>+19</sup>, Au<sup>VII</sup>F<sub>7</sub><sup>[20]</sup>, and Hg<sup>VIII</sup>O<sub>4</sub><sup>[19]</sup>. Including these improbable oxidation states into the trend, they observe a linear increase up to oxidation state +X for platinum and a linear decrease down to oxidation state +VIII for mercury.<sup>[18, 21]</sup> It was



recently shown by Seppelt *et al.*<sup>[22]</sup> how difficult it is to establish experimentally the existence of high oxidation states. He inspected several published osmium species in oxidation state +VII: OsO<sub>3</sub>F, OsO<sub>2</sub>F<sub>3</sub>, OsOF<sub>5</sub>, [OsO<sub>6</sub>]<sup>5-</sup> and OsF<sub>7</sub> and showed that only OsOF<sub>5</sub> and [OsO<sub>6</sub>]<sup>5-</sup> were correctly assigned, whereas the other species were wrongly characterised, or the experimental observations, were not reproducible.<sup>[22]</sup>

This indicates how controversial the topic of the assignment of the highest reachable oxidation states for the late 5d transition metals is. In this thesis we will discuss the most reliable experimental observations and our own high quality quantum-chemical predictions to show which high-oxidation state species of the late 5d transition metal row are likely to be accessible to experimental discovery.



## 2 Chapter

# Methodology

In the field of quantum chemistry there exist quite a few approaches implemented in several software packages for the solution of quantum-chemical problems. One of the major approaches for very accurate calculations are the so-called *ab initio* methods. These *ab initio* methods do not employ any empirical parameters except for the fundamental constants, as they are directly derived from the theoretical fundamentals of quantum mechanics (*ab initio* = from first principles) and, therefore, are applicable to a wide range of species. The advantage of these methods is the high accuracy in the description of a system under study because such methods may be improved systematically in the *ab initio* framework, using higher-order expansions or corrections. However, the computational cost of these terms grows rapidly with their order, thus allowing the application of the most highly accurate methods only for systems with small to moderate size.

Another successful tool in computational chemistry is the so-called density functional theory (DFT). This method has become one of the major workhorses for a wide range of species, especially when the system size of the complexes is enlarged. This is mainly due to the lower computational costs of DFT while yet good accuracy as compared to the *ab initio* methods. Thus DFT is commonly the first choice to assess for example minima structures, transition states and vibrational spectras of such complexes. The disadvantage of this method is that it is not possible to improve the method systematically. This leads to a constant need to validate DFT methods either against reliable experiments or against high-level *ab initio* methods. There is always a need to find a reasonable compromise between accuracy and cost of a calculation, that is, to find the most effective method for a system under study.

This chapter will give a brief overview of the methods used throughout this thesis. For a deeper understanding the reader is referred to textbooks, the references of which are provided at the end of this thesis.<sup>[23-26]</sup>

## 2.1 Molecular Energy

The energy of a quantum system is described by the Schrödinger equation (SE):

$$\hat{H}\Psi = E\Psi \quad (2.1)$$

where  $\Psi$  is the wave function,  $\hat{H}$  the Hamilton operator, and  $E$  is the energy of the system. The expression for the full energy of a system is then,

$$E = \int (\Psi \cdot \hat{H} \cdot \Psi dV) \quad (2.2)$$

where the integration is done over the whole space. The non-relativistic Hamiltonian in the absence of external electromagnetic fields may be written as:

$$\hat{H} = \underbrace{-\sum_i \frac{1}{2} \nabla_i^2}_{E_{\text{kin}} \text{ electrons}} - \underbrace{\sum_A \frac{1}{2M_A} \nabla_A^2}_{E_{\text{kin}} \text{ nuclei}} - \underbrace{\sum_i \sum_A \frac{Z_A}{r_{iA}}}_{\text{Coulomb attraction between nucleus and electrons}} + \underbrace{\sum_{i < j} \frac{1}{r_{ij}}}_{\text{repulsion between electrons}} + \underbrace{\sum_{A < B} \frac{Z_A Z_B}{R_{AB}}}_{\text{repulsion between nuclei}}, \quad (2.3)$$

where  $M_A$  describes the ratio of the mass of the nucleus  $A$  to the mass of an electron, and  $Z_A$  is the atomic charge of nucleus  $A$ . The nuclei and the electrons are described by position vectors  $R_A$  and  $r_i$ , respectively. The distances of nuclei and electrons are given by  $R_{AD}$ ,  $r_{iA}$  and  $r_{ij}$ .<sup>[23]</sup> The Laplace operators  $\nabla_i^2$  and  $\nabla_A^2$  operate on the coordinates of an electron  $i$  and a nucleus  $A$ , respectively.

The SE is greatly simplified by the separation of the nuclear and electronic motions by means of the so-called Born-Oppenheimer approximation. It is based on the fact that the nuclei are much heavier than the electrons and as a result the electrons move much faster compared to the nuclear motions. So the electrons can “adjust” quickly to the slow motions of the nuclei. This is the reason why to a first approximation the nuclei could be regarded as fixed in space, and to consider the motion of the electrons only. It means that the wave function of a system might now be written as a product of two independent parts – the nuclear  $\Psi_N(R)$  and the electronic  $\Psi_e(R, r)$  wave functions

$$\Psi(R, r) = \Psi_N(R) \cdot \Psi_e(R, r) \quad (2.4)$$

and after the separation of the variables in eq. (2.1) the corresponding electronic Hamiltonian (2.5) will lack the term describing the kinetic energy of the nuclei, while the nuclear repulsion

will remain as a constant  $c = \sum_{A<B} \frac{Z_A Z_B}{R_{AB}}$ .

$$\hat{H}_{el} = \underbrace{-\sum_i \frac{1}{2} \nabla_i^2}_{E_{\text{kin}} \text{ electrons}} - \underbrace{\sum_i \sum_A \frac{Z_A}{r_{iA}}}_{\text{coulomb attraction between nucleus and electrons}} + \underbrace{\sum_{i<j} \frac{1}{r_{ij}}}_{\text{repulsion between electrons}} \quad (2.5)$$

## 2.2 Ab initio Methods

### 2.2.1 Hartree-Fock Approximation

The Hartree-Fock (HF) procedure is the oldest and simplest *ab initio* method available. It represents also the starting point for more accurate *ab initio* methods (which are called post-Hartree-Fock methods) as well as the basis of the vast range of semiempirical approaches.

The procedure, first proposed by Hartree is the method of solving the SE equation (2.1) with the Hamiltonian of the form (2.5) and the total  $n$ -electron wave function  $\Psi_{el}(1,2,\dots,n)$  written as a product of one-electron wave functions  $\Psi(1), \Psi(2), \dots, \Psi(n)$ , or in other words,  $\Psi_{el}$  is describing a system with  $n$  independently moving electrons. However, the Pauli principle is not fulfilled by such a wave function, as it is symmetric with regard to the interchange of the electrons. For the wave function to become antisymmetric, Fock has proposed to use a Slater determinant instead of the simple product of the one-electron wave functions:

$$\Psi(1,2,3,\dots,N) = \sqrt{(N!)} \begin{vmatrix} \Psi_1(1) & \Psi_1(2) & \cdots & \Psi_1(N) \\ \Psi_2(1) & \Psi_2(2) & \cdots & \Psi_2(N) \\ \vdots & \vdots & & \vdots \\ \Psi_n(1) & \Psi_n(2) & \cdots & \Psi_n(N) \end{vmatrix} \quad (2.6)$$

where  $\Psi_i(j)$  is called a spin-orbital and depends on space and spin coordinates of an electron  $j$ . The Hartree-Fock system of equations is obtained then by substituting the determinantal wave function (2.6) into the total energy expression (2.2) with the additional constraint of

functions  $\Psi_i$  being orthonormalised. One takes then the functional variation with respect to the one-electron wave function  $\Psi_i$  in order to find the energy minimum

$$\hat{H}_i(1)\Psi_i(1) + \sum_{j=1}^n \left( 2\Psi_i(1) \int \frac{\Psi_j^2(2)}{r_{12}} d\tau_2 - \Psi_j(1) \int \frac{\Psi_j(2)\Psi_i(2)}{r_{12}} d\tau_2 \right) = \varepsilon_i \Psi_i(1) \quad (2.7)$$

The  $\hat{H}_i$  term of eq. (2.7) is the one-electron part of the Fock operator containing the kinetic energy term and the attraction to the nuclei. The first term in parentheses is an averaged electrostatic interaction of an electron  $i$  with all other electrons, and the second one is the so-called exchange term that could be regarded as a decrease in the energy of the electrostatic interaction of the electrons with parallel spins. The first term is already present in Hartree's method, whereas the second one results entirely from determinantal wave function antisymmetry needed to fulfill the Pauli principle that the electrons with parallel spins try to avoid each other.

As far as the two-electron part of the Fock operator depends on the sought-for one-electron wave functions  $\Psi_i$  it is not possible to solve the set of equations (2.7) explicitly. An iterative procedure is used instead, where the  $\Psi_i$  obtained in an iteration step are used to construct the two-electron part of the Fock operator in the next one. The procedure continues until the total energy difference calculated with the wave functions obtained in the next iteration and the previous one becomes negligible. As the iterations are carried out until the orbitals are consistent within a given threshold with the potential derived from them the procedure is often called the self-consistent field procedure (SCF). The reason one cannot get an energy below the exact energy of the system during the SCF procedure is the so-called variational principle: the energy obtained with a trial wave function is always higher (or equal) than the exact ground-state energy of a system. A method that complies with this principle is called variational.

As far as the Hartree-Fock approximation treats each electron in a system as moving in an averaged field of all other electrons, not accounting for the correlation of the electron movement at a point in time, the energy obtained with this method does not represent the true energy of a system. The electron correlation lowers the probability of two electrons on different orbitals to be located close to each other, thus reducing the electron repulsion and the total energy. The difference between the single-determinant Hartree-Fock energy and the

exact energy of a system is called the electron correlation energy – see eq. (2.8) and Chapter 2.2.4.1.

$$E_{corr} = E_{exact} - E_{HF} \quad (2.8)$$

## 2.2.2 Configuration Interaction Methods

The configuration interaction method (CI) is the conceptually simplest way to account for the electron correlation of a system – see Chapters 2.2.1 and 2.2.4.1. The total wave function of a system is written as a linear combination of Slater determinants describing different electron configurations. The determinants are built from the orbitals obtained in the Hartree-Fock ground-state calculation, and the excited-state configurations are constructed on the basis of different electron arrangement over all orbitals – by transferring electrons from the occupied orbitals to the vacant ones:

$$\Psi_{CI} = c_0 \Psi^{HF} + \sum_{ia} c_i^a \Psi_i^a + \sum_{i>j} \sum_{a>b} c_{ij}^{a,b} \Psi_{ij}^{a,b} + \dots \quad (2.9)$$

where the  $\Psi^{HF}$  is the ground-state determinant and the  $\Psi_i^a$ ,  $\Psi_{ij}^{ab}$ ,  $\Psi_{ijk}^{abc}$  etc. are the so-called single-, double-, triple- etc. excited determinants, differing from the ground-state one in either one, two, three or more occupied orbitals  $i, j, k...$  being substituted in the determinantal expansion by the vacant orbitals  $a, b, c...$

The coefficients of all the determinants enter the linear expansion with could be found by the variational method. Provided the complete basis set and all possible excited determinants were used (full CI) one would obtain the exact total energy of a system. In reality, however one works with a finite basis set. As the number of excited determinants grows drastically with the excitation level included, the CI expansion (2.9) is truncated at some level. The most popular truncated CI method used is CISD, which corresponds to the inclusion of single and double excitations in the CI expansion only. However, the shortcomings of the truncated CI are the so-called size-consistency and size-extensivity problems which are closely interrelated: the energy of a many-particle system should be proportional to the number of particles  $N$  in the limit  $N \rightarrow \infty$ , which is not true in case of truncated CI.<sup>[23]</sup> The truncated CI deteriorates as the size of the system increases. A simple example for the lack of the size-consistency in, say, CISD is that the energy of a dimer composed of two identical non-

interacting systems will not be twice the energy of the monomers. This is explained by the fact that the CISD approximation excludes the possibility of both monomers being doubly excited simultaneously, as that would correspond to the quadruple excitation in the dimer. Keeping the above said theoretical aspects in mind one must confess that in practice the truncated CI is yet effectively size-consistent, provided one goes for the higher excitations as the size of a system grows: i.e. CI including quadruple<sup>[27]</sup> excitations performs well for the molecules with the number of electrons still under 50.<sup>[23]</sup>

The canonical Hartree-Fock orbitals used in the construction of the determinants of the CI expansion lead to its rather slow convergence and thus are not the best choice of orbitals in fact. One of the possibilities is to vary the orbitals along with the optimization of the CI coefficients used in the expansion (2.9). This method is called multiconfiguration SCF (MCSCF). As long as the cost of such complex optimisations is even greater than that of the CI, the configuration space is often being carefully selected in real calculations. Modern methods based on the MCSCF select configurations in a systematic manner, partitioning the orbital space into active, inactive and secondary subspaces. For instance, in the complete active space (CASSCF) method the inactive orbitals are doubly occupied, secondary – unoccupied, and the active orbitals are subject to no restrictions on their occupation in all configurations.

### 2.2.3 Perturbation Theory

Perturbation theory is in many cases an effective method to take the correlation energy into account at a relatively low cost. The idea of this method is to treat a part of the Hamilton operator as the perturbation to the ground-state Hamiltonian  $\hat{H}_0$ :

$$\hat{H} = \hat{H}_0 + \lambda\hat{H}_1. \quad (2.10)$$

Such a partitioning is only allowed if the perturbation  $\lambda\hat{H}_1$  is small compared to the ground-state Hamiltonian  $\hat{H}_0$ . The SE (2.1) will now look like,

$$\hat{H}\Psi_i = (\hat{H}_0 + \lambda\hat{H}_1)\Psi_i = E\Psi_i. \quad (2.11)$$



If all the eigenvalues  $E_i$  of the operator  $\hat{H}$  are different, or in other words, there are no degenerate solutions among  $\Psi_i$ , one may expand  $E_i$  and  $\Psi_i$  in (2.11) into a Taylor series in powers of  $\lambda$  to get

$$\left(\hat{H}_0 + \lambda\hat{H}_1\right)\left(\lambda^0\Psi^{(0)} + \lambda^1\Psi^{(1)} + \lambda^2\Psi^{(2)} + \lambda^3\Psi^{(3)} + \dots\right) = \left(\lambda^0E^{(0)} + \lambda^1E^{(1)} + \lambda^2E^{(2)} + \lambda^3E^{(3)} + \dots\right)\left(\lambda^0\Psi^{(0)} + \lambda^1\Psi^{(1)} + \lambda^2\Psi^{(2)} + \lambda^3\Psi^{(3)} + \dots\right). \quad (2.12)$$

For this equation to hold for different values of  $\lambda$  terms with the same power of  $\lambda$  should be equal on both sides. To find the  $n$ -th order energy correction one has to solve an equation for the corresponding power of  $\lambda$ . In solving equations, one goes from the lower powers of  $\lambda$  to higher ones, expanding the unknown functions  $\Psi_i^n$  into the series of  $\Psi_i^{n-1}$  and using the orthonormality conditions in integration of the corresponding energy expressions. For calculation of the correlation energy corrections to the Hartree-Fock energy the so-called Møller-Plesset perturbation theory is used, where the Hamiltonian is

$$\hat{H} = \hat{H}_0 + \nu. \quad (2.13)$$

$\hat{H}_0$  is now the HF Hamiltonian,

$$\hat{H}_0 = \sum_i \left[ h(i) + \nu^{HF}(i) \right] \quad (2.14)$$

and the perturbation is given by

$$\nu = \sum_{i < j} r_{ij}^{-1} - \sum_i \nu^{HF}(i) \quad (2.15)$$

where  $h(i)$  and  $\nu^{HF}(i)$  are the one- and two-electron parts of the HF Hamiltonian correspondingly – see for example, eq. (2.7). The HF energy is the sum of the zeroth and first-order energies. Thus the first correction to the HF energy occurs in the second order of perturbation theory.

$$E_0^{(2)} = \frac{1}{4} \sum_{ijab} \frac{|\langle ij || ab \rangle|^2}{\varepsilon_i + \varepsilon_j - \varepsilon_a - \varepsilon_b} \quad (2.16)$$

The occupied and unoccupied orbitals are  $i, j$  and  $a, b$  respectively, where  $\varepsilon_n$  are the corresponding HF orbital energies. The electron correlation is accounted for 80-90%. This method can be used for systems where electron correlation is moderately important – see below. The MP2 method is size-consistent and size-extensive (see Chapter 2.2.2) but fails for degenerate and multireference systems. Higher order energy corrections could be recovered by including the higher order terms through MP3 or MP4. However one should note that higher order MP theory is may be unstable and should only be used carefully.

## 2.2.4 Coupled-Cluster Theory

Coupled-cluster (CC) theory solves the size-consistency and size-extensivity problem of the CI formalism (see Chapter 2.2.2) by formulating the wave function using exponential excitation operators.

$$\Psi_{CC} = \exp(T) \Psi_0 \quad (2.17)$$

The coupled-cluster wave function (2.17) can be formulated outgoing from the reference HF wave function  $\Psi_0$ . The cluster operator  $T$  can be written as a sum of single, double, triple up to  $N$ -tuple excitation operators

$$\begin{aligned} T &= T_1 + T_2 + T_3 + \dots + T_N \\ &= T_S + T_D + T_T + \dots + T_N \end{aligned} \quad (2.18)$$

where the cluster operator is defined as

$$T_n = \sum_{\substack{i,j,k,\dots \\ a,b,c,\dots}} t_{i,j,k,\dots}^{a,b,c,\dots} \hat{a}_{i,j,k,\dots}^{a,b,c,\dots} \quad (2.19)$$

The first factor in equation (2.19) describes the cluster amplitudes (expansion coefficients) and the second factor is the so-called excitation operator (electrons from the  $i,j,k,\dots$  occupied

orbitals are excited to  $a,b,c,\dots$  vacant ones, accordingly). The exponential part of equation (2.17) can be now written as an infinite Taylor expansion

$$\exp(T) = 1 + T + \frac{1}{2}T^2 + \frac{1}{6}T^3 + \dots + \frac{1}{N!}T^N = \sum_{n=0}^N \frac{1}{n!}T^n. \quad (2.20)$$

Using eq. (2.18) and (2.20) the exponential operator  $T$  can be written as

$$\begin{aligned} \exp(T) &= \exp(T_1 + T_2 + T_3 + T_4 + \dots + T_N) \\ &= 1 + T_1 \\ &\quad + \left( T_2 + \frac{1}{2}T_1^2 \right) \\ &\quad + \left( T_3 + T_2T_1 + \frac{1}{6}T_1^3 \right) \\ &\quad + \left( T_4 + T_3T_1 + \frac{1}{2}T_2^2 + \frac{1}{2}T_2T_1^2 + \frac{1}{24}T_1^4 \right) \\ &\quad + \dots + T_N \end{aligned} \quad (2.21)$$

The first term of the expanded form (2.21) gives simply the reference HF wave function whereas the second describes all singly excited-states. Doubly excited-states are generated by the first term in parentheses, in which  $(T_2)$  is considered as a “*linked*” and  $(T_1^2)$  as an “*unlinked*” operator. This means that the total contribution from double excitations is the sum of these two operators. This description of the excitations by “*linked*” and “*unlinked*” operators is the main difference between coupled-cluster and CISD methods, because in the latter the “*unlinked*”  $(T_2^2)$  quadruple excitation operator is missing and therefore the CISD method is not size-extensive – see Chapter 2.2.2.

The advantage of this method is that it is possible to truncate the coupled-cluster expression (2.21) after every excitation operator. Normally this truncation takes place after the double contributions  $(T_2)$  due to the fact that these contributions are the most important for the inclusion of electron correlation, as in the CI method – see Chapter 2.2.2. Electron correlation can be treated up to 95% for equilibrium structures. This truncation corresponds to the so-called coupled-cluster with singles and doubles substitutions (CCSD) and can be written as

$$\begin{aligned}
\exp(T_1 + T_2) = & 1 + T_1 \\
& + \left( T_2 + \frac{1}{2} T_1^2 \right) \\
& + \left( T_1 T_2 + \frac{1}{6} T_1^3 \right) \\
& + \left( \frac{1}{2} T_2^2 + \frac{1}{2} T_2 T_1^2 + \frac{1}{24} T_1^4 \right)
\end{aligned} \tag{2.22}$$

Truncating the coupled-cluster expression after the triple contributions (CCSDT) is only a good choice for small systems due to the highly demanding computational effort. An alternative to CCSDT is to calculate the triple contributions perturbationally. The triples are calculated using the MP4 formula (see Chapter 2.2.3) but the perturbation coefficients are exchanged with the CCSD amplitudes for the wave function corrections. In addition, an MP5 term is also included to describe the coupling between singles and triples. This method is called coupled-cluster with singles, doubles and inclusion of perturbative triple excitations, abbreviated as CCSD(T). The treatment of correlation effects is better than in CCSD theory, and is therefore the most accurate (and expensive) methodology used in this thesis.

This coupled-cluster methodology gives highly accurate results for energies and properties.<sup>[28, 29]</sup> But the disadvantage of this method is the large computational effort – the scaling with the system size is CCSD ( $N^6$ ), CCSD(T) ( $N^7$ ), and CCSDT ( $N^8$ ) compared to the ( $N^4$ ) of HF method – which makes this method only useable for relatively small or highly symmetrical molecules. But to obtain good accuracy with CCSD or CCSD(T) calculations, the basis set should be large enough to recover the correlation effects quantitatively.<sup>[29]</sup>

#### 2.2.4.1 Dynamical and Non-Dynamical Correlation

As we have mentioned in the previous chapters, electron correlation is a vital part of the accurate treatment of quantum-chemical problems. To discuss electron correlation in more detail it can be useful to separate it, as suggested by Sinanoğlu<sup>[30]</sup>, into two different parts: the so-called non-dynamical and dynamical correlation. The former of these describes the influence of other configurations that are low-lying in energy and that mix strongly with the HF configuration.<sup>[31]</sup> This effect is often small in closed-shell systems near their equilibrium

structure, but it increases as molecules are distorted, for example, in stretched bonds (long-range effects). This is clearly shown by the comparison of the electron correlation energies for  $\text{H}_2$  at equilibrium ( $E_{\text{corr}} \approx 106 \text{ kJ mol}^{-1}$ ) and as infinitely separated H atoms, ( $E_{\text{corr}} \approx 656 \text{ kJ mol}^{-1}$ ). This large difference reflects the difficult character of the dominant configuration state functions (CSF)<sup>1</sup>: for the description of the  $\text{H}_2$  equilibrium only one CSF ( $\sigma_g^2$ ) is necessary, but for the infinitely separated H atoms two CSFs are important ( $\sigma_g^2, \sigma_u^2$ ).<sup>[31]</sup> Non-dynamical correlation is also important for open-shell systems like excited-states and transition metal complexes, and in particular for changes in the transition metal oxidation states. High oxidation states have strained bonds due to the combination of compact d-orbitals with a larger number of ligands in the coordination sphere. Repulsive interactions between the ligands (and with the outermost metal core shells)<sup>[32, 33]</sup> prevent the relaxation of the metal-ligand bonds. Together with the shrunken d-orbitals, this results in a distorted bonding situation in which non-dynamical correlation cannot be neglected. The other part, called dynamical correlation, can be “defined” as a short-range effect and arises by reduction of the repulsion energy at short interelectronic distances.

These discussions give an impression of how complicated the description of electron correlation is.<sup>[31]</sup> Not all methods perform well in the presence of strong non-dynamical correlations. A reliable approach in the presence of moderate non-dynamical correlation is to expand the coupled-cluster theory to triple excitations, CCSD(T) – see above. But this method works only for moderately distorted molecules where the  $T_1$ -diagnostic – see next chapter – is below certain thresholds. In other cases, multireference methods should be used.

Given that most systems treated in this thesis are not “multireference cases” we have opted to use the CCSD(T) method as a reliable benchmark approach – see Chapter 4.

#### 2.2.4.2 $T_1$ -Diagnostic

A fundamental question in performing quantum-chemical calculations is always that of choosing a suitable method for the problem at hand. To judge the appropriate level, several diagnostics of  $N$ -particle space problems have been developed.<sup>[34-38]</sup> These diagnostics analyse the sufficiency of the given level based on the calculation itself. Usually they examine the CI coefficients, the CC amplitudes, or the norms of the wave function in PT theory.

---

<sup>1</sup> A configuration state function (CSF) is a symmetry-adapted linear combination of Slater determinants.

As we have seen in Chapter 2.2.4 coupled-cluster theory at CCSD level recovers up to 95% of electron correlation and is therefore one of the most accurate methods available in quantum chemistry. This is, however, only the case for systems displaying little non-dynamical correlation – see above – i.e. in which near-degeneracy effects or other major problems with the HF reference wave function are not showing up.

One example in which non-dynamical correlation cannot be omitted is the small transition-metal compound CuH. The ground-state of this species is dominated by the  $d^{10}s$  configuration (SCF MOs). However, this configuration alone does not describe the system well, as the  $d^9s^2$  configuration does also contribute strongly to the wave function. But the  $d^{10}s$  form of the SCF orbitals is biased against the  $d^9s^2$  state and therefore the contribution to the wave function is much less than it should be. This “orbital bias” effect is much more important for CISD than for CCSD calculations. To describe bond-breaking processes properly, for example in  $N_2$  or  $C_2H_4$ , non-dynamical correlation must be treated, using multiple excitations.<sup>[26, 39]</sup>

To estimate the importance of non-dynamical correlation, Lee and Taylor have developed the so-called  $T_1$ -diagnostic.<sup>[40, 41]</sup>

$$T_1 = \frac{|t_1|}{\sqrt{N}} \quad (2.23)$$

The factor  $t_1$  is the norm of the single-excitation cluster amplitudes where  $N$  is the number of correlated electrons. Empirical comparisons of a variety of closed-shell systems suggest that for  $T_1$ -values above 0.02 non-dynamical correlation effects begin to seriously degrade the reliability of the single-reference treatment. The value of  $T_1$  decreases slightly by improving the basis set, but this normally affects only the fourth decimal place. If the  $T_1$ -diagnostic is larger than 0.02, it becomes necessary to include higher-order excitations. The simplest reliable correction for treating non-dynamical correlation is to expand the coupled-cluster theory to triple excitations for example CCSD(T). If the  $T_1$ -diagnostic is 0.04 or larger, then multireference methods should be used. For open-shell systems, the  $T_1$ -diagnostic can show much larger values than 0.02. A modified diagnostic called  $D_1$  or  $D_2$  was been suggested for open-shell systems.<sup>[34-38]</sup>

## 2.3 Density Functional Theory

### 2.3.1 Hohenberg-Kohn Theorems

As we have seen in the previous chapters, the wave function is the fundamental quantity of all *ab initio* methods. In 1964 Hohenberg and Kohn<sup>[42]</sup> have showed that it is in principle possible to use only the ground-state electron density instead of the complicated wave function formalism to describe the ground-state energy of a molecule, eq. (2.24). They pointed out that the functional that delivers the ground-state energy of a system describes the lowest energy only when the input density is the real ground-state density. This is the fundamental principle of density functional theory (DFT) and can be formulated as a kind of variational principle – see equation (2.25).

$$E[\rho] = T[\rho] + E_{ne}[\rho] + E_{ee}[\rho] \quad (2.24)$$

$$E_0 \leq E[\tilde{\rho}] \quad (2.25)$$

where  $E_0$  is the real ground-state energy and  $E[\rho]$  is the energy calculated from a trial electron density  $\tilde{\rho}$ .  $T[\rho]$  describes the kinetic energy,  $E_{ne}[\rho]$  is the nucleus-electron attraction, and  $E_{ee}[\rho]$  is the electron-electron repulsion. This approach is based on a functional of the density that delivers the exact energy of the system. There are two serious problems in this approach: a) we need to know the exact density of the system and b) we have to know the exact form of the functional.

### 2.3.2 Kohn-Sham Approach

One year after the Hohenberg-Kohn theorem was published, Kohn and Sham developed a scheme for a practical use of density functional theory. They introduced an approximation to describe the unknown kinetic energy functional  $T[\tilde{\rho}]$  of eq. (2.24). To treat this kinetic energy better a fictitious system of non-interacting electrons described by a single-determinantal wave function (Kohn-Sham determinant) was introduced. The latter is characterised by the ground-state density  $\rho_s$  which is identical to that of the fully interacting system,  $\rho_0$ . The orbitals entering the Kohn-Sham determinant (called Kohn-Sham Orbitals)

are thus employed for (exact) calculation of the non-interacting kinetic energy,  $T_s[\rho]$ , which is supposed to comprise the major part of  $T[\tilde{\rho}]$ .

The predominant part of the electron-electron interaction energy  $E_{ee}[\rho]$  of eq. (2.24) consists of the classical Coulomb repulsion  $J[\rho]$  between the electrons. We can now define:

$$E[\rho] = T_s[\rho] + E_{ne}[\rho] + J[\rho] + E_{xc}[\rho] \quad (2.26)$$

where the unknown part  $E_{xc}[\rho]$  is

$$E_{xc}[\rho] \equiv (T[\rho] - T_s[\rho]) + (E_{ee}[\rho] - J[\rho]) = T_c[\rho] + E_{ne}[\rho]. \quad (2.27)$$

This exchange-correlation energy term  $E_{xc}[\rho]$  is the most complicated part because it consists everything what is non-classical and unknown. It contains the self-interaction correction to the Coulomb part, exchange and correlation contributions to the potential energy of the system, and the difference between the kinetic energy of the interacting system and that of the non-interacting system.

Similar to the HF approximation, we can now apply the Hohenberg-Kohn variational principle (2.25) to the energy functional (2.26), that results in the one-electron Kohn-Sham determinant, resulting in equations:

$$\left( -\frac{1}{2} \nabla_1^2 + V_s(\vec{r}_1) \right) \varphi_i(\vec{r}_1) = \varepsilon_i \varphi_i(\vec{r}_1). \quad (2.28)$$

The  $\varepsilon_i$  is the eigenvalue of the Kohn-Sham orbitals  $\varphi_i$  and the  $V_s(\vec{r}_1)$  is an effective local potential:

$$V_s(\vec{r}_1) = \int \frac{\rho(\vec{r}_2)}{r_{12}} d\vec{r}_2 + V_{xc}(\vec{r}_1) - \sum_A^M \frac{Z_A}{r_{1A}} \quad (2.29)$$

where  $V_{xc}$  is the so-called exchange-correlation potential which is defined as the functional derivative of the exchange-correlation energy with respect to the density:



$$V_{xc} \equiv \frac{\delta E_{xc}}{\delta \rho}. \quad (2.30)$$

The one-electron Kohn-Sham equations (2.28) can now be solved in an iterative procedure like in the HF approximation. The problematic term of equation (2.29) is the potential  $V_{xc}$ . If we would know the exact form of this term it would be possible to calculate the exact ground-state energy of the system. As this is not the case,  $E_{xc}$  and  $V_{xc}$  have to be approximated. This is one of the central tasks of density functional theory.

### 2.3.3 Local Density Approximation

As we have seen in the chapter above, one of the main objectives of DFT is to find better and better approximations to the exchange-correlation functional  $E_{xc}$ . The simplest approach is the so-called Local Density Approximation (LDA).<sup>[14]</sup> The advantage of the LDA approach is the assumption that we can formulate the exchange-correlation energy  $E_{xc}$ :

$$E_{xc}^{LDA}[\rho] = \int \rho(\vec{r}) \varepsilon_{xc}(\rho(\vec{r})) d\vec{r}. \quad (2.31)$$

where  $\varepsilon_{xc}(\rho(\vec{r}))$  describes the exchange-correlation energy density per particle of a uniform electron gas with electron density  $\rho(\vec{r})$ . The  $\varepsilon_{xc}(\rho(\vec{r}))$  term can be split in the exchange  $\varepsilon_x$  and correlation  $\varepsilon_c$  parts.<sup>[14]</sup> The exchange part  $\varepsilon_x$  is called the Slater-exchange<sup>[43]</sup> energy density. For the correlation part  $\varepsilon_c$  no similar expression is known, but several authors have presented analytical fits for the correlation part  $\varepsilon_c$  based on accurate numerical quantum Monte-Carlo simulations. One of the frequently used correlation functionals  $\varepsilon_c$  is the so-called Vosko-Wilk-Nusair (VWN) local-correlation-energy approximation.<sup>[44]</sup>

For open-shell systems, we have to use the Local-Spin-Density-Approximation (LSDA) with different  $V_{xc}$  for spin up and spin down electrons.<sup>[14]</sup> LDA/LSDA underestimates the exchange energy by ca. 10%.<sup>[24]</sup> This error is often larger than the whole correlation energy. LDA/LSDA overestimates significantly the bond forces and is inaccurate for thermochemical applications.

### 2.3.4 Generalised Gradient Approximation

To improve the DFT accuracy, the Generalised Gradient Approximation (GGA) was developed. It describes much better energetics compared to the LDA method. In addition to the density  $\rho(r)$  at each point, GGA applications use also the information of the density gradients,  $\nabla\rho(r)$ , to take into account the description of the density inhomogeneities.

$$E_{XC}^{GGA} = [\rho_\alpha, \rho_\beta] = \int f(\rho_\alpha, \rho_\beta, \nabla\rho_\alpha, \nabla\rho_\beta) d\vec{r} \quad (2.32)$$

Examples for gradient-corrected exchange functionals are Becke86<sup>[45]</sup>, Becke88<sup>[46]</sup>, PW91<sup>[47]</sup>, and the PBE96<sup>[48]</sup>. The most frequently used gradient-corrected correlation functionals are the P86<sup>[49]</sup> and LYP<sup>[50]</sup> functionals which have empirical parameters included, and the parameter free PW91<sup>[51]</sup> and PBE<sup>[48]</sup>. In principle one can combine every exchange functional with every correlation functional as for example Becke88 and LYP (BLYP<sup>[46, 50]</sup>), Becke88 and P86 (BP86<sup>[46, 49]</sup>), and Becke88 and PW91 (BPW91<sup>[46, 51]</sup>).

### 2.3.5 Hybrid Functionals

Hybrid functionals use a certain admixture of the exchange energy of the HF method, the “exact exchange”. One of the first hybrid functionals was the Becke’s *half and half* (BHandH)<sup>[52]</sup> functional with 50% of the exact exchange. The currently most popular hybrid functional is the Becke’s 3-parameter exchange functional combined with the correlation functional LYP, called (B3LYP)<sup>[50, 53]</sup> functional.

$$E_{XC}^{B3LYP} = a \cdot E_X^{exact} + (1-a) E_X^{LDA} + b \cdot \Delta E_X^{Becke88} + (1-c) E_C^{VWN} + c \cdot E_C^{LYP} \quad (2.33)$$

The parameters of eq. (2.33) a, b, and c were optimised on ionization energies, atomisation energies, and proton affinities of G1 set of molecules (in B3 scheme, a = 0.2, b = 0.72, and c = 0.81). Among other hybrid functionals one can mention also B3PW91<sup>[53]</sup>, and PBE1PBE<sup>[48, 54]</sup>.

## 2.4 Basis Sets

The wave function of a system under study is built of molecular orbitals which are constructed in their turn from functions that could be regarded as one-electron wave functions of separate atoms – atomic orbitals. A set of atomic orbitals of the same atom is called a basis set. A natural choice of the form of atomic orbitals is to take functions which closely resemble the orbitals obtained from the exact solution of the SE for hydrogen atom – the so-called “Slater Type Orbitals” (STOs) [55]:

$$\chi_{\zeta nlm}^{STO}(r, \theta, \varphi) = NY_{lm}(\theta, \varphi) r^{n-1} e^{-\zeta r}. \quad (2.34)$$

The  $n$  is the principle quantum number,  $N$  is the normalization constant,  $\zeta$  the orbital exponents and the  $Y_{lm}(\theta, \varphi)$  spherical harmonic function of the angular quantum number  $l$  and the magnetic quantum number  $m$ . Such functions show correct asymptotic behaviour, but the two-electron integrals over them that arise in the quantum-chemical treatment are quite cumbersome to be computed analytically.<sup>[24]</sup> That is why another type of functions is commonly used for construction of basis sets in real calculations instead – the “Gaussian Type Orbitals” (GTOs) [56]:

$$\chi_{\zeta nlm}^{GTO}(r, \theta, \varphi) = NY_{lm}(\theta, \varphi) r^{2n-2-1} e^{-\zeta r^2}. \quad (2.35)$$

The two-electron integrals could be evaluated analytically with ease when the GTOs are used in a basis, however as they have incorrect behaviour near the nuclear region, multiple GTOs with different exponents need to be combined to overcome this problem.

$$\chi^{CGTF} = \sum_i d_i \chi_i^{GTF} \quad (2.36)$$

Such linear combinations are called “Contracted Gaussian Type Functions” (CGTF) and are employed in most modern quantum-chemical programs (basis set libraries).

A minimal basis set is described by one basis function for each occupied orbital like the STO-3G<sup>[57]</sup> basis set. When the number of basis functions is doubled than the basis set is called “Double- $\zeta$ ” (DZ).

An extension of these basis sets is for example the aug-cc-pVDZ where the “aug” denotes that this basis set is augmented by diffuse functions – see below. The “cc” description explains that the basis set provides a systematic improvement that converges toward the complete basis set limit. The “p” notation indicates that polarization functions are used. The VDZ stands for valence double zeta so that every valence orbital is described by two contractions. In this study we have mainly used the aug-cc-pVTZ basis set.

Another type of standard basis is known as “Split-Valence” (SV) where the core region is described by a minimal basis and the valence region is described by a DZ basis set – see above. The advantage of this basis set is the better description of the valence space compared to the use of minimal basis set. It is also cheaper to use the “Split-Valence” basis set than the more expensive  $x-\zeta$  basis set.

For a flexible description of the valence space it is possible to augment the basis set by higher angular quantum number  $l$  basis functions. These functions are called polarization functions. They improve the description of the anisotropic density distribution around the atom in question by mixing one function with a higher angular quantum number to some other function, like the d-function polarizing the p-function and so on. A good example is 6-31G\*, also called 6-31G(d) basis set, where a d-function is added for each atom.<sup>[58]</sup>

The description of anions or lone pairs, where the diffuse electron density is important, can be improved by using diffuse orbitals. These orbitals have a small orbital exponent.

## 2.5 Relativity

### 2.5.1 Relativistic Effects

When considering for the first time in 1929 the relativistic description of an electron, Dirac supposed that this effect would not be relevant for chemistry due to the weakly bound valence electrons, which have only a small kinetic energy.<sup>[59, 60]</sup> Fifty years later two fundamental papers were published by Pyykkö and Desclaux<sup>[61]</sup> and by Pitzer<sup>[62]</sup>. They showed that relativistic effects cannot be neglected for heavy-element chemistry.

Relativistic effects in atoms and their compounds can be separated into two parts. The kinematic effects, also called scalar relativistic effects, and the effects of Spin-orbit coupling (SO). The scalar relativistic effects are caused by the proximity of the core electrons and the nucleus. In the classical description the core electrons have a high velocity due to the nuclear

Coulomb potential. This high velocity will increase the rest mass ( $m_{rest}$ ) of the inner electrons to some kinematic mass ( $m_{kin}$ ) due to equation (2.37).

$$m_{kin} = \frac{m_{rest}}{\sqrt{1-(v/c)^2}} \quad (2.37)$$

The  $v$  is the velocity of the electrons,  $c$  is the speed of light and  $Z$  is the nuclear charge in atomic units. Consequently the effective Bohr radius decreases with the increase of the electron velocity, as

$$a_B = \frac{\hbar^2}{mc^2} = a_B^0 \sqrt{1-(v/c)^2}. \quad (2.38)$$

The relativistic effect of 1s-electron of a  $Z=1$  nucleus with a Bohr radius of 53 pm and a velocity of 1/137.036 atomic units (a.u.) gives rise to a 1.00003 increase of the kinematic mass. This indicates that the kinetic energy of an electron around an hydrogen nucleus is not large enough to increase significantly the kinetic mass. This observation is not anymore true for the heavier elements like  $_{78}\text{Pt}$ ,  $_{79}\text{Au}$ ,  $_{80}\text{Hg}$  or beyond where the 1s-electrons exhibit much larger kinetic energies due to the large nuclear Coulomb potential. For  $\text{Hg}^{79+}$  ( $Z = 80$ ) we obtain for the 1s-orbit a velocity of  $(80/137.036) \cdot c = 0.58c$ , in other words the 1s-electron of  $\text{Hg}^{79+}$  has 58% of the speed of light. Due to this high velocity the electron has a 23% kinetic mass increase and therefore a 20% shrunken Bohr radius, see equation (2.38).<sup>[61, 63]</sup> This contraction is even larger (43%) for element 112 eka-mercury where the 1s-electron velocity is 82% of the speed of light.<sup>[64]</sup>

How the relativistic kinematics of the inner electrons affect the valence shell? This is mainly due to the “inner tails” of the outer s-orbital and, to a lesser extent, of the outer p-orbitals. These orbitals are “core-penetrating” and have therefore a probability to be in the vicinity of the nucleus. Thus the electrons of the valence shell are also influenced by the nuclear Coulomb potential and this interaction will not only contract and stabilise the inner orbitals (s and p) but it will also affect the outer ones.<sup>[65, 66]</sup> This contraction and stabilisation effect is called the “direct” relativistic effect. Consider, for example, the 7s-orbital of element

105 Db, where the relativistic contraction can be calculated as  $\Delta_R \langle r \rangle_{7s} = (\langle r \rangle_{nr} - \langle r \rangle_{rel}) / \langle r \rangle_{nr} = 25\%$  – see Figure 2.5-1.

Shells with a higher angular momentum like the d and f orbitals have no “core-penetrating” parts and therefore no spatial probability at the nucleus. These d and f orbitals are influenced by the so-called “indirect” relativistic effect which is caused by the contraction of the s and p core shell, leading to a more effective shielding of the nuclear Coulomb potential, which destabilises and expands the d- and f-orbitals.

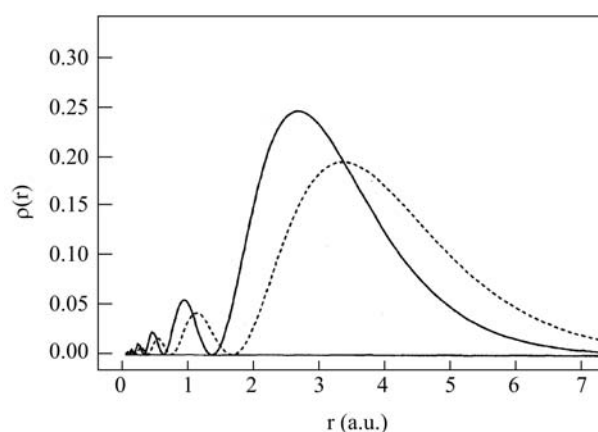


**Figure 2.5-1** Relativistic (solid line) and non-relativistic (dashed line) radial distribution of the 7s-valence density in element 105 Db.<sup>[67]</sup>

This destabilizing effect of the valence d-orbitals affects the next higher s- and p-orbitals by a small additional indirect stabilisation. This partially explains the relativistic stabilisation of the 6s- and 7s-orbitals in Au and eka-mercury 112 because the d-orbitals become fully occupied (this is also the case for the f-orbitals) at the end of the transition metal row and therefore a maximum in the stabilisation of the valence s-orbitals occurs.<sup>[68-70]</sup> This effect of orbital stabilisation and contraction reaches the maximum in the 6<sup>th</sup> period at the “gold maximum” – see Figure 2.5-2 – and in the 7<sup>th</sup> period on eka-mercury 112 (group-12 maximum).<sup>[66, 71]</sup> The shift of the gold maximum in the 6<sup>th</sup> period to the group-12 maximum in the 7<sup>th</sup> period is related to the ground-state electron configuration of elements 111 and 112. Both elements have the same  $d^9s^2$  orbital occupancy whereas the ground-state electron configuration in the 6<sup>th</sup> period changes from Au ( $d^{10}s^1$ ) to Hg ( $d^{10}s^2$ ).

Scalar relativistic effects have a direct influence on the chemical properties like excitation energies, ionization potentials, and electron affinities. For example, higher oxidation states for

the late transition metals, as we will discuss in this thesis, are mainly available due to the partly lower relativistic ionization potentials. This is connected to the destabilised d-orbitals in which electrons feel less attracted to the nucleus. But in the case of  $\text{HgF}_4$  the role of relativistic effects in stabilizing  $\text{Hg}^{\text{IV}}\text{F}_4$  against reductive elimination was found to arise mainly from a relativistic destabilisation of  $\text{Hg}^{\text{II}}\text{F}_2$ , due to the relativistic contraction of the mercury 6s-orbital. This high oxidation state is directly connected to the scalar relativistic effects and is therefore not seen for the lighter elements of group 12, cadmium and zinc.<sup>[12, 72-75]</sup> Eka-mercury, element 112, shows an even larger stabilisation of oxidation state +IV due to relativistic effects.<sup>[76]</sup>

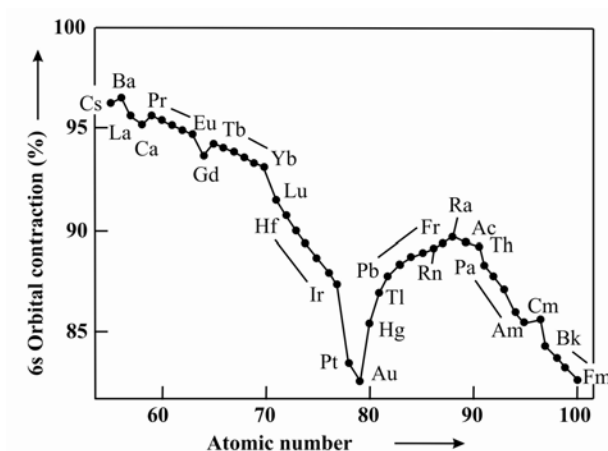


**Figure 2.5-2** Relativistic contraction (%) of the 6s orbitals from cesium to fermium.

As we have mentioned in the beginning of this chapter there is a second relativistic effect which has to be considered, the so-called Spin-orbit coupling (SO). This effect is important for higher angular momenta,  $l > 0$ , like p-, d-, and f-orbitals. In the quantum mechanical description a rotating electron around the nucleus generates a magnetic moment. This rotating electron also has a spin and is therefore generating a second magnetic moment. These two magnetic moments can interact with each other, causing the splitting of the orbitals into different levels, as shown in Figure 2.5-3. (This is only a semiclassical description, but is adequate for qualitative understanding of the effect.)

The problem occurs now in the right description of the heavier elements because neither the orbital angular momentum  $l$  nor the spin angular momentum  $s$  is a good quantum number anymore. Therefore the vector sum  $\vec{j} = \vec{l} + \vec{s}$  is used. The p-electrons with  $l = 1$  can be separated in two possible values of  $j = 1/2$  and  $j = 3/2$ , noted as  $p_{1/2}$  and  $p_{3/2}$ . SO splitting

is a relativistic effect and becomes similar or even larger than the typical bonding energies for heavy or superheavy species. As shown in Figure 2.5-3 the SO coupling becomes larger with the increase of atomic number for the group 12 elements up to eka-mercury 112. In eka-mercury the  $6d_{5/2}$  orbital is even higher in energy than the  $7s$  orbital.

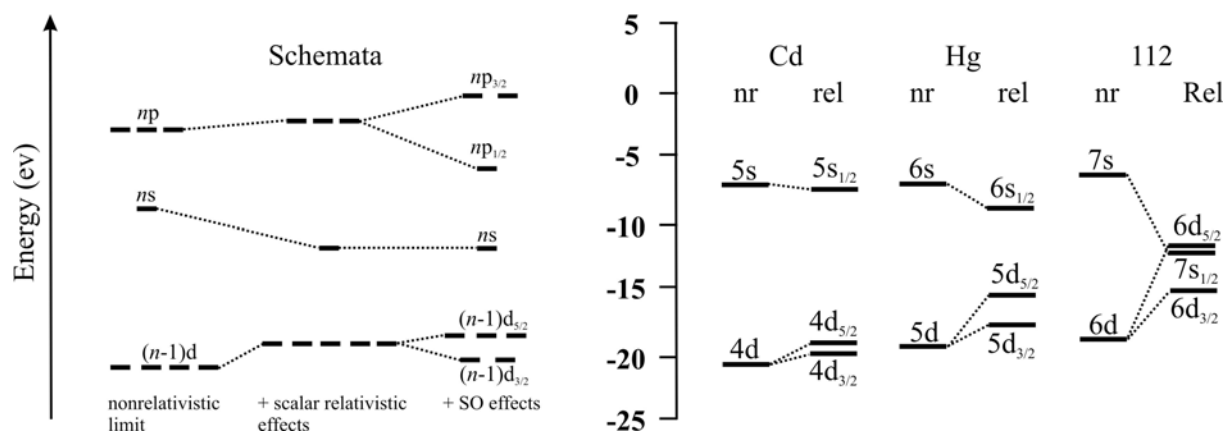


**Figure 2.5-3** Schemata of the relativistic effects and relativistic (DF)<sup>[77]</sup> and nonrelativistic (HF)<sup>[71]</sup> energy levels of the valence  $ns$  and  $(n-1)d$ -electrons of the group 12 elements.<sup>[64]</sup>

All these relativistic effects (scalar and SO) are important for the understanding of chemical and physical properties of the elements. The yellow colour of gold<sup>[61, 78]</sup> and the liquid state of mercury<sup>[79]</sup> at room temperature are due to relativistic effects. It is also known from relativistic quantum mechanical calculations that the triple bond radius of Rg is even smaller than for copper.<sup>[80]</sup> Relativistic effects are also the reason why tungsten is used in light bulbs. This is related to the relativistic increase of the melting points for heavier 5d elements such as W, Re, Os, and Ir. Furthermore, no lead accumulator would work in a non-relativistic world.<sup>[81]</sup>



### 2.5.2 Relativistic Methods

Several relativistic quantum-chemical methods were developed to describe the effects of relativity on heavy and superheavy elements and their compounds. The fundamental structure of the Schrödinger equation (SE) – see Chapter 2.1 – does not describe correctly the relativistic because the SE is not Lorentz invariant.<sup>1</sup> Dirac proposed to use for a free electron the following equation instead of the time-dependent SE.

$$\left[ c\alpha \cdot p + \beta mc^2 \right] \Psi = i \frac{\partial \Psi}{\partial t} \quad (2.39)$$

The corresponding Dirac-Coloumb (DC) or the Dirac-Coulomb-Breit (DCB) Hamiltonians can be formulated as

$$\hat{H}_{DC} = -\sum_i \left[ c\alpha_i \cdot p_i + \beta_i c^2 + \sum_A V_A(r_{iA}) \right] + \sum_{i<j} \frac{1}{r_{ij}} + \sum_{A<B} \frac{Z_A Z_B}{R_{AB}} \quad (2.40)$$

$$\hat{H}_{DCB} = H_{DC} - \sum_{i<j} \frac{1}{2r_{ij}} \left[ \alpha_i \cdot \alpha_j + \frac{(\alpha_i \cdot r_{ij})(\alpha_j \cdot r_{ij})}{r_{ij}^2} \right]. \quad (2.41)$$

Here  $\alpha$  and  $\beta$  are  $4 \times 4$  matrices,  $c$  the speed of light, and the  $p_i$  is the momentum operator of electron  $i$ . The external potential  $V_A$  is caused by the nucleus  $A$  with charge  $Z_A$ . The Dirac expressions has four-dimensional spinors and the relativistic wave function can be conventionally written as

$$\Psi = \begin{pmatrix} \Psi_{L\alpha} \\ \Psi_{L\beta} \\ \Psi_{S\alpha} \\ \Psi_{S\beta} \end{pmatrix}. \quad (2.42)$$

---

<sup>1</sup> The differential operators of the spatial coordinates are second derivatives whereas the time coordinate shows up as a first derivative. A correct physical description would have to treat both the spatial and the time coordinate equivalently.

Working with a full 4-component wave function is demanding due to the fact that the relativistic theory considers simultaneously for every particle the degrees of freedom of its charge-conjugated particle. Therefore approximate relativistic methods have been developed to reduce the complexity of the problem.

### 2.5.2.1 2-Component Methods

As we have mentioned above the 4-component treatment of relativistic effects is computationally very expensive. It is possible to separate out the charge-conjugated degrees of freedom from the start because the valence shells of neutral and slightly ionised molecules are not excited at low energies.<sup>1</sup> This decoupling leads to a reduced Hamiltonian which operates on a 2-component wave function. This transformed Hamiltonian annihilates the coupling between the “electron-like” and the “positron-like” degrees of freedom. In other words there is no coupling anymore between the positive energy states (electrons) and the negative energy states (positrons) which renders the solution of the relativistic expressions easier.

The Foldy-Wouthuysen<sup>[82]</sup> transformation was one of the first attempts to reduce the Dirac or the Dirac-Coulomb-Breit Hamiltonian to the electronic degrees of freedom. An improvement on the Foldy-Wouthuysen transformation is provided by the Douglas-Kroll-Hess (DKH) Hamiltonian, which offers cleaner decoupling of the charge-conjugated parts and gives results in better agreement with those of the Dirac equation.<sup>[83-85]</sup> Another efficient approximation was developed by the Amsterdam group<sup>[86-88]</sup>, the so-called zero- and first-order regular approximation (ZORA) and (FORA). This method describes the relativistic effects in the vicinity of the nucleus very well. A more detailed description and discussion of relativistic methods is given in ref. <sup>[85, 89, 90]</sup>.

Furthermore it is possible to separate the spin-dependent terms from the 2-component treatment and generate a spin-averaged 1-component wave function, which corresponds to a scalar relativistic formalism.<sup>[91]</sup> A further separation such as the elimination of the degrees of freedom associated with the core electrons will give rise to a nonlocal effective potential, which will be discussed below.

In this thesis we have used the DKH method to compute the SO effects of IrF<sub>7</sub>, IrF<sub>6</sub> and IrF<sub>5</sub> – see Chapter 4.4.

---

<sup>1</sup> The pair-creation shows up at 1 MeV and is therefore not important for neutral or slightly ionised molecules because their electronic energies are mostly around 100 eV.

### 2.5.2.2 Pseudopotentials

A different approach to treat relativistic effects is the so-called pseudopotential (PP). This approach is based on the idea of Hellmann<sup>[92]</sup> and Gombas<sup>[93]</sup> that the inner core electrons of an atom (from the third row or even higher) do not contribute to the chemical behaviour like, e.g., chemical reactions. Only the valence electrons are responsible for the chemical properties. Due to this observation it is possible to describe the sum of the core electrons by a PP.<sup>[94, 95]</sup> The theoretical description to separate the core and valence electrons by modification of the Hamiltonian is based on the work of Phillips and Kleinmann<sup>[96]</sup> and can be written as

$$\hat{H}_{PP} = \sum_{i=1}^{mv} \left[ -\frac{1}{2} p_i^2 + \sum_A V_A^{PP}(r_{iA}) \right] + \sum_{i < j} \frac{1}{r_{ij}} + \sum_{A < B} \frac{Q_A Q_B}{R_{AB}}. \quad (2.43)$$

The pseudopotential  $V_A^{PP}$  describes the influence of the core electrons of atom  $A$  on the valence electrons. The separation of the electrons in the core and valence electrons to create a good approximation for the element is of course not an easy task and several different strategies for generating PP have been developed. The consideration of the outer  $nd$ - and  $(n+1)s$ -orbitals in the valence region of a transition metal will describe the so-called “large-core” pseudopotentials (rlc). When the outer region of a transition metal is extended to the  $ns$ - and  $np$ -orbitals then the pseudopotential is known as “small-core” PP (rsc). The description for main group elements is different. In the rlc pseudopotentials only the outer valence  $s$ - and  $p$ -orbitals are included whereas the rsc is also extended to the semicore  $d$  and even often to the semicore  $p$ - and  $s$ -orbitals. For example the relativistic rlc pseudopotential of iodine includes 46 core electrons whereas the relativistic rsc includes only 28 core electrons in the pseudopotential.

It is shown that for a good description of transition metals it is necessary to use the relativistic “small-core” pseudopotentials instead of the “large-core” ones.<sup>[94]</sup> Two of the most important advantages of the pseudopotential approach are the smaller number of electrons which have to be considered in the calculations and the inclusion of relativistic effects.

## 2.6 Corrections

### 2.6.1 Basis-Set Superposition Error

The basis-set superposition error (BSSE) is related to the use of incomplete nucleus-centred basis sets. Fixing the basis functions to the position of the nuclei allows the use of a compact basis set. The problem which occurs in use of this kind of basis sets is the difference in comparing energies at different geometries. This discrepancy is due to the fact that the electron density around one nucleus is not only described by its own basis functions but also by basis functions centred at other nuclei around and this is the reason for the geometry dependency. This is of course particularly pronounced in molecules where weak influences like hydrogen bonds or van der Waals interactions are calculated. It was been shown for accurate calculations of the potential curve of helium dimers ( $\text{He}_2$ ) that the BSSE gives a much deeper well compared to experiment.<sup>[97]</sup> Therefore the BSSE should be considered in calculations where accuracy is important. In the limit of a complete basis set the BSSE is zero. This means that an improvement of the basis set will decrease the BSSE.<sup>[24]</sup>

Usually the so-called counterpoise correction (CP)<sup>[98]</sup> is used to approximate the BSSE. Here we have to calculate the difference between the fragment energies with the regular fragment basis set and with the full set of basis functions of the whole complex. The complexation energy can be computed as the difference between the energies of the optimised  $A$  and  $B$  fragments and the energy of the optimised geometry of the complex  $AB$  where the complex geometry is denoted as  $*$ .

$$\Delta E_{\text{complexation}} = E(AB)_{ab}^* - E(A)_a - E(B)_b \quad (2.44)$$

To estimate how large the BSSE is we have to calculate several energies.  $E(A)_a^*$ , the energy of fragment  $A$  with basis set  $a$ , and  $E(B)_b^*$ , the energy of fragment  $B$  with basis set  $b$  have to be calculated using the geometry of the complex. In addition we need also two calculations with the fragment  $A$   $E(A)_{ab}^*$ , and  $B$   $E(B)_{ab}^*$  using the complex of the geometry  $*$  and the full basis set  $ab$ . Thus we can define the CP correction as

$$\Delta E_{CP} = E(A)_{ab}^* + E(B)_{ab}^* - E(A)_a^* - E(B)_b^* \quad (2.45)$$

The counterpoise-corrected complexation energy is then given by

$$\Delta E_{\text{correction}} = \Delta E_{\text{complex}} - \Delta E_{\text{CP}}. \quad (2.46)$$

It is important to realise that  $\Delta E_{\text{CP}}$  gives only an estimate of BSSE, as it does not provide an upper or lower limit. CP corrections are somewhat larger and more sensitive for methods which include electron correlation, explicitly post-HF methods.

### 2.6.2 Zero-Point Energy

One important correction for thermochemical calculations is the so-called zero-point energy (ZPE) correction. This energy describes the discrepancy between the calculated energy and the real physical molecular energy. This is due to quantum mechanics where the Heisenberg uncertainty principle states that the momentum and the position of a system cannot be accurately observed for both properties at the same time, i.e.  $\Delta E \Delta t \geq \hbar$ . This physical result means that the energy of a system cannot be zero, i.e.  $E > 0$ .

To estimate the value of the ZPE for the description of the thermochemistry, the ZPE correction is calculated from a sum of harmonic oscillator frequencies for all  $i$  vibrational modes. In the  $\text{H}_2$  example there is only one vibrational mode  $\omega = 4416.0376 \text{ cm}^{-1}$  which we can convert into  $\frac{1}{2}hc = 2.27827 \cdot 10^{-6} \text{ cm Hartree}$ , and we obtain a ZPE of 0.01006 Hartree (26.4  $\text{kJ mol}^{-1}$ ). This ZPE is added to the calculated energy and will consequently lower the dissociation energy of the molecule. This is even more the case for systems with lower mass because there is an inverse relation between mass and harmonic frequency.



### 3 Chapter

## Oxidation States and Ligands

As we will discuss in this thesis there are several high oxidation state species for which it has to be explained how to define them. The definition of oxidation states is one of the fundamental principles in chemistry and also important for other scientific subjects like physics, biology and medicine. The definition is based on a formalism where the oxidation state of a central atom in a coordination sphere is defined as the charge of the central atom, when every ligand of the coordination sphere is removed in its most stable form. Therefore we assign the bonding electron pairs between the metal centre and the ligands exclusively to the most electronegative bonding partners.<sup>[99-101]</sup> This is often no easy task because the bonding situation is predominantly not purely ionic, and the difference between the electronegativities of ligands and central atom is often not large enough for a clear separation. The situation will be even more complicated when delocalised bonds, for example in non-innocent<sup>[101]</sup> ligands, are involved. This was recently shown in the literature for the complex  $[\text{Pd}(\text{dmpe})\{1,2\text{-C}_6\text{H}_4(\text{SiH}_2)_2\}]$  where the Pd centre was thought to be coordinated by six silyl ligands. The authors assigned this species to be a palladium complex where the Pd has the highly unusual oxidation state +VI.<sup>[102]</sup> But several other groups have presented arguments why the formulation of oxidation state +VI is not favoured, and Pd<sup>II</sup> is preferred.<sup>[103-105]</sup> Further ambiguities can arise with the definition of the formal oxidation state when the ligand system has low-lying unoccupied molecular orbitals of the appropriate symmetry to be involved in back-bonding. It is also complicated to specify the formal oxidation state when metal-metal bonds involving different or similar metals with very different ligand sets are included in the bonding situation.<sup>[106]</sup>

In order to assign accurate oxidation states of the predicted species in this study we have used a variety of redox-inert<sup>[101]</sup> ligand systems. These ligands are known to be the most electronegative ligands: fluoride, oxo,  $[\text{AsF}_6]^-$ ,  $[\text{SbF}_6]^-$ ,  $[\text{OSeF}_5]^-$ , and  $[\text{OTeF}_5]^-$ .<sup>[107, 108]</sup> Especially fluoride is an ideal ligand to stabilise high oxidation states, as the F-F bond in  $\text{F}_2$  is one of the weakest known covalent bonds. This is mainly due to the large electron/electron

repulsion effects between the F atoms arising from lone-pair interactions.<sup>[109, 110]</sup> This weakness favours the stabilisation of transition metal fluorides in high oxidation states. The disadvantage in using fluorides as ligands for high oxidation states is some times the large number of coordinated fluorine ligands, for example in Os<sup>VIII</sup>F<sub>8</sub>. The coordination number can be reduced by using oxo ligands. The amount of ligands can be halved, e.g. as in Os<sup>VIII</sup>O<sub>4</sub>. On the other side, the related thermochemistry will be less favourable for the transition metal complexes due to the large binding energy of the oxygen (-494 kJ mol<sup>-1</sup>). This explains the lower stability of oxyfluorides and oxides compared to the pure fluoride species (F<sub>2</sub> bonding energy -158 kJ mol<sup>-1</sup>). As can be seen by comparison of stabilities between XeF<sub>4</sub> and XeO<sub>4</sub> complexes where the former is a stable species and the latter is highly explosive.<sup>[111]</sup> A compromise between coordination number and O<sub>2</sub> elimination is the use of mixed ligand systems like the monooxofluoride-complexes OsOF<sub>5</sub> or IrOF<sub>5</sub>.<sup>[112]</sup> The corresponding OF species is much less stable (-205 kJ mol<sup>-1</sup>) than O<sub>2</sub> and therefore the complex is more stable. Of course homolytic bond dissociation can also take place and favours the decomposition of the complex as it is seen, e.g., by the reaction  $\text{IOF}_5 \xrightarrow{\Delta} \text{IF}_5 + \frac{1}{2}\text{O}_2$ . This indicates clearly the formation tendency of molecular oxygen. Interestingly, the stronger bond of this complex is the I-O and not the I-F bond.<sup>[111]</sup> One can avoid bimolecular decomposition channels by using the gas-phase or matrix-isolation techniques.

In the case of Hg<sup>IV</sup> also other ligand systems have been chosen to avoid stabilisation of Hg<sup>II</sup> vs. Hg<sup>IV</sup> due to better aggregation.<sup>[73]</sup> These ligands are called “weakly coordinating anions” (WCAs) and the idea of using WCAs is equivalent to creating an environment of the metal in the condensed phase that is as close as possible to the gas-phase situation.<sup>[113]</sup> In particular, we want to avoid high coordination numbers of the Hg<sup>II</sup> elimination products. Our choice of WCAs was based on a) their known abilities to stabilise high oxidation states, b) their experimental availability, and c) a reasonably moderate size to allow calculation of the complexes at an appropriate theoretical level.

[AlF<sub>4</sub>]<sup>-</sup> was chosen as a very small WCA. It is expected to provide less stabilisation than larger ligands and therefore served mainly for comparison purposes for other ligand systems. During the optimisations (Chapter 4.2) we saw in some cases the formation of the dinuclear Al<sub>2</sub>F<sub>7</sub>-ligand and therefore included a few complexes of this anion as well. [AsF<sub>6</sub>]<sup>-</sup> and [SbF<sub>6</sub>]<sup>-</sup> are WCAs that are well known to stabilise unusual cations and high oxidation states, including noble-gas species.<sup>[113, 114]</sup> These anions are furthermore known to condense exothermically to the dinuclear anions [Sb<sub>2</sub>F<sub>11</sub>]<sup>-</sup> and [As<sub>2</sub>F<sub>11</sub>]<sup>-</sup>,<sup>[115, 116]</sup> which are supposed to be even more weakly coordinating, as their negative charge is still more delocalised (the



trinuclear  $[\text{Sb}_3\text{F}_{16}]^-$  and tetra-nuclear  $[\text{Sb}_4\text{F}_{21}]^-$  ions are also known<sup>[115, 116]</sup>, and we included them for comparison. It was furthermore interesting to compare  $[\text{Sb}_2\text{F}_{11}]^-$  with  $[\text{As}_2\text{F}_{11}]^-$ , as the latter tends to be less stable relative to the corresponding mononuclear ligand  $[\text{EF}_6]^-$  – see Chapter 4.2.

The very effective WCAs  $[\text{E}(\text{OTeF}_5)_6]^-$  (E = As, Sb, Bi, Nb)<sup>[108, 113, 114]</sup> were too large for our purposes, given our available computational resources. However, the experimentally known pentafluorooxotellurate “teflate” anion  $[\text{OTeF}_5]^-$ , and its selenium homologue  $[\text{OSeF}_5]^-$ , appeared promising ligands. They are often discussed as “bulky fluoride analoga” and are well known to stabilise high oxidation states<sup>[108]</sup> and unusual cations.<sup>[108, 114]</sup> The group electronegativity of these kind of ligands is thought to be comparable to that of fluorine, and these ligands are unlikely to favour high coordination numbers in the  $\text{Hg}^{\text{II}}$  product complexes.<sup>[108]</sup> The  $[\text{OEF}_5]^-$  ligands are also unlikely to favour elimination reactions by condensing to larger units, and they are stable to fluoride abstraction – see Chapter 4.2.<sup>[114]</sup>



## 4 Chapter

# The Highest Oxidation States of the Late 5d Transition Metals

### 4.1 Validation of Density Functional Methods for Computing Structures and Energies of Hg<sup>IV</sup> Complexes<sup>[12]</sup>

#### 4.1.1 Introduction

The possible existence of species with mercury in an oxidation state higher than +II has been puzzling experimentalists and theoreticians for almost three decades. An experimental verification of such high-valent mercury complexes is a fascinating target, as it would turn a group 12 element into a true transition metal. An initial report of an electrochemically generated, spectroscopically characterised short-lived [Hg<sup>(III)</sup>(cyclam)][BF<sub>4</sub>]<sub>3</sub> species by Deming *et al.* in 1976<sup>[117]</sup> has never been confirmed. But it stimulated Jørgensen<sup>[118, 119]</sup> to predict the possible existence of HgF<sub>4</sub>. Analogous to the 5d<sup>8</sup> Au<sup>III</sup> oxidation state, a 5d<sup>8</sup> Hg<sup>IV</sup> species should be more stable than a Hg<sup>III</sup> d<sup>9</sup> state.

In 1993, Kaupp *et al.* reported the first application of quantum-chemical methods to the problem.<sup>[72, 73]</sup> Using high-level quasirelativistic pseudopotential QCISD(T) calculations with, at the time, respectable basis sets, the square-planar *D*<sub>4h</sub> symmetrical HgF<sub>4</sub> was predicted to be thermodynamically stable in the gas-phase with respect to the elimination reaction HgF<sub>4</sub> → HgF<sub>2</sub> + F<sub>2</sub>. Comparison with nonrelativistic pseudopotential results showed that the stability of the higher oxidation state is of relativistic origin.<sup>[73]</sup> Most notably, the results showed that a better description of electron correlation should increase the reaction energy. This was confirmed five years later by Liu *et al.*<sup>[120]</sup> using larger basis sets and CCSD(T) methods. HgCl<sub>4</sub> was in contrast suggested to be thermodynamically unstable<sup>[120]</sup> with respect to Cl<sub>2</sub> elimination. Seth *et al.* predicted that the eka-mercury analogue of HgF<sub>4</sub>, (112)F<sub>4</sub>, should be

even more stable than HgF<sub>4</sub> with respect to F<sub>2</sub> elimination.<sup>[76]</sup> Recently, Pyykkö *et al.*<sup>[74]</sup> showed computationally that HgH<sub>4</sub> and HgH<sub>6</sub> are significantly endothermic, but have moderate activation barriers to H<sub>2</sub> elimination.

Up to date, none of the discussed high-valent mercury compounds systems has been confirmed experimentally. The technical difficulties for their synthesis have apparently been too large. As aggregation energies disfavour HgF<sub>4</sub> against HgF<sub>2</sub> in the condensed phase, molecular beam or matrix-isolation techniques would seem appropriate. However, the use of aggressive fluorine compounds and of mercury does not make the former route attractive for experimentalists, and the latter route also has not produced evidence for high-valent mercury.<sup>[121]</sup> The quest for Hg<sup>IV</sup> complexes remains thus a major challenge, and we have recently started to consider new synthetic targets and routes, including electrochemical access using chelate or macrocyclic ligands and/or oxidising matrix environments.<sup>[75, 122, 123]</sup> A problem arising with quantum-chemical predictions is that the accurate coupled-cluster methods employed previously in this field are computationally too expensive to be applied to larger complexes. The only alternative is currently to use density functional theory (DFT) methods. However, as the accuracy of the various DFT approaches may not be improved systematically towards the exact result, and the most appropriate functional is not immediately obvious, it is necessary to validate DFT methods on smaller models, for which accurate coupled cluster methods may still be used. In this chapter we provide such a systematic validation study of various density functionals and basis sets on structures and stability of small HgX<sub>4</sub> complexes (X = F, Cl, H; n = 2, 4) against accurate benchmark CCSD(T) calculations.

### 4.1.2 Computational Details

The benchmark calculations employed the coupled-cluster method with single and double, as well as perturbative triple excitations [CCSD(T) level]. For comparison, CCSD and MP2 calculations are also reported. All of these *ab initio* calculations used a quasirelativistic small-core 20-valence-electron (20-VE) pseudopotential<sup>[124]</sup> with a (11s10p9d4f3g)/[9s6p5d3f2g] valence basis set<sup>[124]</sup> for Hg, as well as aug-cc-pVQZ<sup>[125, 126]</sup> basis sets for F, Cl, and H. This ECP/basis-set combination will be denoted basis A. Bond lengths were optimised by fitting a fifth-order polynomial to about 7 single-point energy calculations, which were done with the MOLPRO 2000.1<sup>[127]</sup> program.

DFT calculations used the Gaussian98<sup>[128]</sup> program and gradient methods. The following exchange-correlation functionals were scrutinised: the local density approximation in form of the SVWN5<sup>[44]</sup> functional, the gradient-corrected BP86<sup>[46, 129]</sup> functional, and the hybrid functionals B1LYP<sup>[130, 131]</sup>, B3LYP<sup>[128]</sup> (based on the work of Becke)<sup>[53]</sup>, MPW1PW91<sup>[130]</sup>, and BHandHLYP<sup>[52]</sup>. Basis-set requirements in the DFT calculations are expected to be somewhat less dramatic than in the post-HF treatments. Moreover, future applications to larger systems require a reasonable compromise between accuracy and computational effort. Three different basis-set combinations were compared, denoted B, C, and D – see Table 4.1-1.

In the following chapter the computational levels are reported by the notation method/basis. Unrestricted Kohn-Sham calculations on nonspherical atoms were performed to obtain atomization energies.

Basis-set superposition errors (BSSE) were considered using the counterpoise correction (CP)<sup>[98]</sup> at optimised minimum structures. Zero-point energy (ZPE) corrections were computed at the B3LYP/C level. Spin-orbit corrections were not considered in this chapter. They have previously been found to be small for the elimination reaction  $\text{HgF}_4 \rightarrow \text{HgF}_2 + \text{F}_2$ ,<sup>[73]</sup> and the theory against theory comparison is not affected by them.

**Table 4.1-1** Basis sets and pseudopotentials used

Basis set combination	Element	ECP	Basis set
A	Hg	20-VE ECP <sup>[124]</sup>	(11s10p9d4f3g)/[9s6p5d3f2g] <sup>[124]</sup>
	F		aug-cc-pVQZ <sup>[126]</sup>
	Cl		aug-cc-pVQZ <sup>[125]</sup>
	H		aug-cc-pVQZ <sup>[126]</sup>
B	Hg	20-VE ECP <sup>[124]</sup>	(8s8p7d2f)/[6s6p4d2f] with f-exponents $\alpha=1.5$ and $\alpha=0.5$ . <sup>[124]</sup>
	F		(9s5p1sp1d)/[4s2p1sp1d]-Dunning-DZ+P <sup>[132]</sup>
	Cl		(12s8p1sp1d)/[6s4p1sp1d]-Dunning-DZ+P <sup>[132-134]</sup>
	H		DZ+P (5s1p)/[3s1p] <sup>[132]</sup>
C	Hg	20-VE ECP <sup>[124]</sup>	(8s8p6d2f)/[6s6p3d1f] <sup>[124]</sup> with contraction of the two f functions to one f function with $\alpha=1.5$ $c_1 = -0.064334$ and $\alpha=0.5$ $c_2 = 1.032173$ .
	F	7-VE ECP <sup>[135]</sup>	(4s4p1d)/[2s2p1d] <sup>[136]</sup>
	Cl	7-VE ECP <sup>[135]</sup>	(4s4p1d)/[2s2p1d] <sup>[136]</sup>
	H		(4s1p)/[2s1p] <sup>[132]</sup>
D	Hg	20-VE ECP <sup>[137]</sup>	(8s7p6d)/[6s5p3d] segmented <sup>[137]</sup>
	F	7-VE ECP <sup>[135]</sup>	(4s4p1d)/[2s2p1d] <sup>[136]</sup>
	Cl	7-VE ECP <sup>[135]</sup>	(4s4p1d)/[2s2p1d] <sup>[136]</sup>
	H		(4s1p)/[2s1p] <sup>[132]</sup>

### 4.1.3 Minimum Structures

The HgX<sub>4</sub> systems were generally found to have  $D_{4h}$  minima at all computational levels. The calculated Hg-X bond lengths are shown in Table 4.1-2. Using the CCSD(T)/A results as benchmark, CCSD/A underestimates the bond lengths for HgH<sub>4</sub> and HgF<sub>4</sub>. MP2/A overestimates the distances for HgF<sub>4</sub> but underestimates them for HgCl<sub>4</sub> and HgH<sub>4</sub>. The large and non-systematic differences document the previously discussed<sup>[73]</sup> importance of non-dynamical correlation in these systems, particularly for HgF<sub>4</sub> and HgCl<sub>4</sub>. The non-iterative triple excitations in CCSD(T) are known to partially recover the non-dynamical correlation<sup>[138]</sup>. The CCSD  $T_1$ -diagnostics<sup>[40]</sup> at the CCSD(T) minima are 0.017, 0.011, and 0.012 for HgF<sub>4</sub>, HgCl<sub>4</sub>, and HgH<sub>4</sub>, respectively. This suggests a reasonable quality of the coupled-cluster results. The largest  $T_1$  value for HgF<sub>4</sub> is consistent with large variations between MP2, CCSD, and CCSD(T) results. This suggests to view MP2 and CCSD energies with caution.<sup>[73]</sup>

**Table 4.1-2** Calculated M-X distances (pm) for HgX<sub>4</sub> (X = F, Cl, H).<sup>[a]</sup>

Method	Basis set	Hg-F	Hg-Cl	Hg-H
<b>CCSD(T)</b>	<b>A</b>	<b>188.5</b>	<b>223.6</b>	<b>162.3</b>
CCSD	A	186.8	223.5	161.8
MP2	A	188.9	223.4	160.6
SVWN5	B	189.4	230.9	164.9
BP86	B	193.7	236.7	166.0
B1LYP	B	191.7	236.8	165.3
B3LYP	B	192.1	236.9	165.4
MPW1PW91	B	190.1	233.3	164.5
BHandHLYP	B	188.5	233.7	164.0
SVWN5	C	190.0	232.4	165.0
BP86	C	193.7	237.6	166.2
B1LYP	C	192.0	237.5	165.5
B3LYP	C	192.3	237.7	165.6
MPW1PW91	C	190.5	234.2	164.6
BHandHLYP	C	189.0	234.4	164.2
SVWN5	D	192.0	233.0	164.1
BP86	D	195.3	234.4	163.4
B1LYP	D	193.7	237.6	164.3
B3LYP	D	194.0	237.8	164.4
MPW1PW91	D	192.2	234.4	162.9
BHandHLYP	D	190.7	238.0	165.1

<sup>[a]</sup>At  $D_{4h}$  minimum structures.

Compared to the CCSD(T)/A benchmark results, all DFT calculations overestimate the Hg-X bond lengths – see Table 4.1-2. This may in part be due to the neglect of dispersion effects<sup>[139]</sup> in present-day functionals, which would further decrease the distances. Consistent with this, the discrepancies are by far largest for HgCl<sub>4</sub>. Among the various functionals, the BHandHLYP and SVWN5 results are closest to the CCSD(T) values for HgF<sub>4</sub> and HgCl<sub>4</sub>. While this may be attributed to error compensation with the typical overbinding of the local density approximation for the SVWN5 case<sup>[14]</sup>, the large fraction of Hartree-Fock exchange shortens the bond lengths for the BHandHLYP functional.

As might be expected, basis B provides the shortest DFT bond lengths and thus the best agreement with the benchmark CCSD(T)/A results. This is largely due to the inclusion of f-functions for mercury and in part to the still relatively flexible basis sets for X. Basis set C provides results similar to basis set B for HgF<sub>4</sub> and HgH<sub>4</sub> at lower computational cost. The results indicate that the best DFT structure results for HgX<sub>4</sub> are obtained using basis sets B or C, and SVWN5 or BHandHLYP functionals.

#### 4.1.4 Reaction Energies for X<sub>2</sub>-elimination

Calculated energies for the elimination reactions  $\text{HgX}_4 \rightarrow \text{HgX}_2 + \text{X}_2$  (X = F, Cl, H) are provided in Table 4.1-3 and in Figure 4.1-1. CCSD underestimates and MP2 overestimates the elimination energies in all cases. This appreciable level dependence of the results indicates again a significant influence of non-dynamical correlation – see Chapter 2.2.4.1. As has been discussed previously,<sup>[73]</sup> these effects arise mainly for the “true transition-metal” Hg<sup>IV</sup> d<sup>8</sup> species, while non-dynamical correlation effects are much smaller for the Hg<sup>II</sup> d<sup>10</sup> complexes, where metal d-orbitals are unimportant for the bonding – see atomization energies below and in Table 4.1-5. The resulting lack of error compensation between these effects for the two sides of the reaction is responsible for the appreciable level dependence. Comparison with previous results<sup>[73, 120]</sup> confirms the notion of larger elimination reactions for larger basis sets.

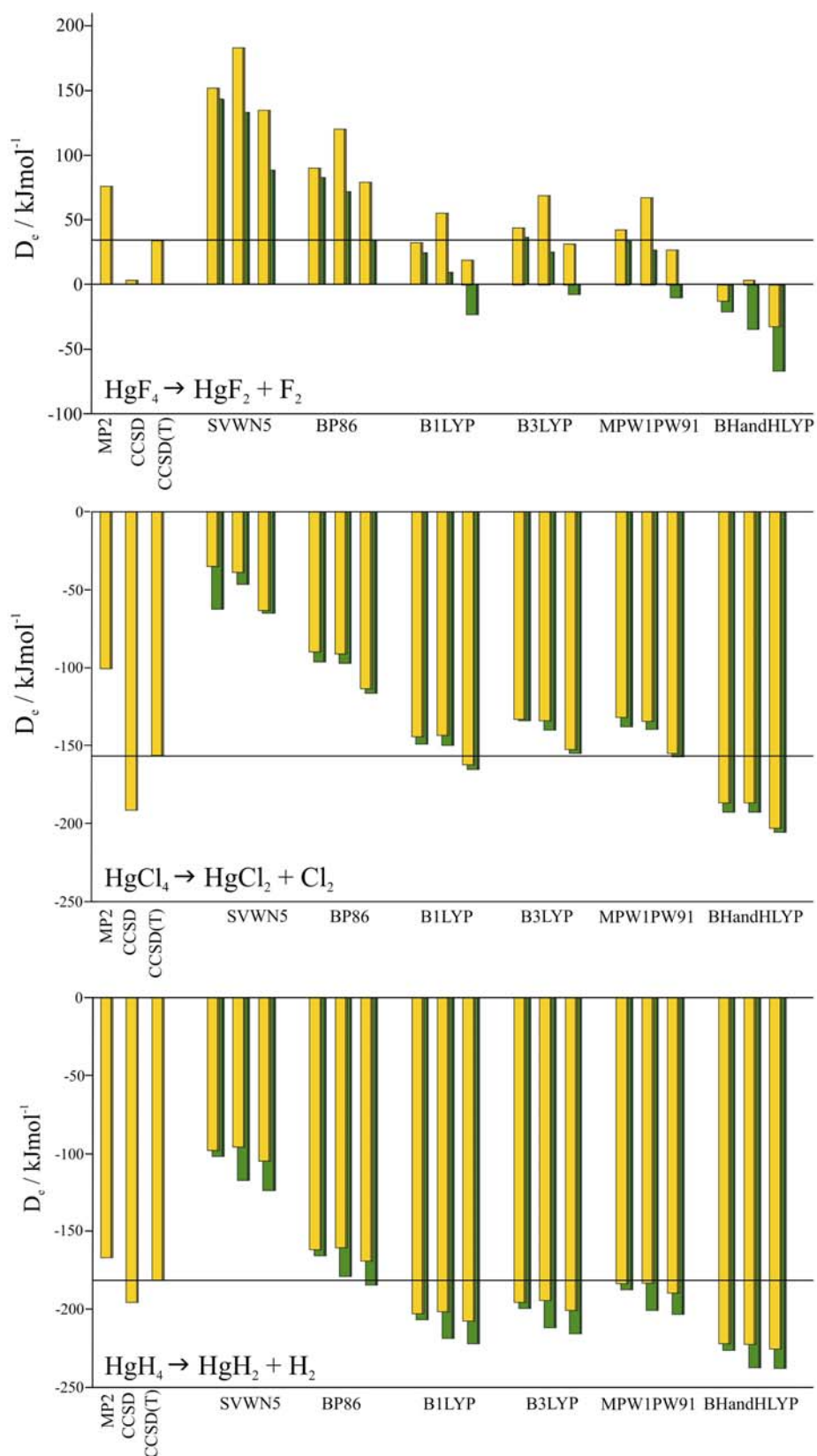


**Figure 4.1-1** Computed energies for elimination reactions  $\text{HgX}_4 \rightarrow \text{HgX}_2 + \text{X}_2$ . ■ Without CP correction. ■ With CP correction. From left to right: *ab initio* basis set combination A and for DFT basis set combinations B, C, and D.



The full CP procedure to correct for BSSE was not possible at CCSD(T)/A level for HgF<sub>4</sub> and HgCl<sub>4</sub>, as the large dimension of the problem combined with the low symmetry of the CP calculation for the halogen atoms exceeded the available computational resources. Given the close agreement between CCSD and CCSD(T) CP corrections for the hydride, we may assume that the CCSD values provide also a good estimate for the CCSD(T) CP correction in the other two cases. In general, the CP corrections tend to lower the reaction energies moderately by ca. 10-15 kJ mol<sup>-1</sup>. We estimate this to be less than the underestimate of correlation effects due to basis-set incompleteness errors, which are expected to cause an underestimate of the reaction energies.<sup>[73]</sup> We presume therefore, that the CCSD(T)/A values in Table 4.1-3 provide still lower bounds to the true reaction energies.

**Table 4.1-3** Calculated reaction energies (kJ mol<sup>-1</sup>) for HgX<sub>4</sub> → HgX<sub>2</sub> + X<sub>2</sub> (X=F,Cl,H) elimination.<sup>[a]</sup>

X	Basis set	MP2	CCSD	CCSD(T)	SVWN5	BP86	B1LYP	B3LYP	MPW1PW91	BHandHLYP
F	A	75.9	3.1 (-8.2)	34.0 <sup>[b]</sup>						
	B				151.7 (143.4)	90.1 (82.5)	32.6 (24.7)	44.0 (36.3)	42.0 (33.6)	-12.4 (-21.0)
	C				182.9 (133.1)	120.0 (72.0)	55.0 (9.5)	68.5 (25.1)	67.2 (26.8)	3.5 (-34.2)
	D				134.7 (88.4)	79.2 (34.4)	18.9 (-23.0)	31.5 (-7.5)	26.6 (-10.3)	-32.1 (-66.2)
Cl	A	-100.4	-191.5 (-200.1)	-156.4 <sup>[b]</sup>						
	B				-35.1 (-62.7)	-89.7 (-96.4)	-144.1 (-148.9)	-133.1 (-134.2)	-132.0 (-137.9)	-186.7 (-192.7)
	C				-39.0 (-46.5)	-91.2 (-97.2)	-143.3 (-149.9)	-134.1 (-140.0)	-134.4 (-139.7)	-186.6 (-192.6)
	D				-63.3 (-64.9)	-113.4 (-116.4)	-162.1 (-165.4)	-152.2 (-154.8)	-155.0 (-157.0)	-202.9 (-205.5)
H	A	-166.8	-195.5 (-208.7)	-181.4 (-195.6)						
	B				-98.1 (-102.0)	-161.9 (-165.7)	-203.0 (-206.6)	-195.5 (-199.4)	-183.5 (-187.5)	-222.3 (-226.3)
	C				-96.1 (-117.5)	-160.7 (-178.8)	-201.8 (-219.0)	-194.4 (-212.0)	-183.3 (-200.7)	-222.5 (-237.7)
	D				-104.9 (-123.6)	-169.2 (-184.5)	-207.7 (-222.3)	-200.9 (-215.6)	-189.7 (-203.4)	-225.8 (-238.0)

<sup>[a]</sup>Results with CP corrections in parentheses. <sup>[b]</sup>No CP correction was possible, due to system size.

Turning now to DFT methods, the best agreement with the benchmark CCSD(T)/A results is achieved using those hybrid functionals (B1LYP, B3LYP, and MPW1PW91) that exhibit about 20% Hartree-Fock (HF) exchange. Functionals with higher HF exchange admixture,

such as BHandHLYP (50% HF exchange) give too low elimination energies, whereas the gradient-corrected BP86, and in particular the local SVWN5 functional overestimate the elimination energies significantly.

The comparison of basis sets B, C, and D (Table 4.1-3 and Figure 4.1-1) indicates a moderate basis-set dependence. After inclusion of CP corrections, the intermediate basis C results are relatively close to those with the larger basis B (i.e., both provide good agreement with the CCSD(T) data when using a hybrid functional like B3LYP). However, the CP corrections obtained for basis C are considerably larger than for basis B with HgF<sub>4</sub> and HgH<sub>4</sub>, making basis B the overall more reliable method of choice, provided the size of system to be studied allows the use of the larger basis. In particular, CP corrections are not easily applicable in all energy calculations (e.g. for intramolecular processes), and thus a basis with an inherently smaller BSSE may be preferable. Finally, the basis D results for HgF<sub>4</sub> and HgCl<sub>4</sub> (including a segmented valence basis for Hg, cf. Table 4.1-1) exhibit large BSSE and still appreciable deviations from the basis B results after CP correction.

Zero-point energy (ZPE) corrections calculated at the B3LYP/C level are listed in Table 4.1-4. The ZPE corrections lower the elimination energy almost negligibly for the fluoride and chloride and moderately so for the hydride.

**Table 4.1-4** Zero-point energy corrections (kJ mol<sup>-1</sup>) to elimination energies.<sup>[a]</sup>

Reaction	ZPE	Other studies
HgF <sub>4</sub> → HgF <sub>2</sub> + F <sub>2</sub>	6.5	7.1 <sup>[b]</sup> , 7.1 <sup>[c]</sup>
HgF <sub>2</sub> → Hg + F <sub>2</sub>	2.0	
HgCl <sub>4</sub> → HgCl <sub>2</sub> + Cl <sub>2</sub>	3.5	3.7 <sup>[d]</sup>
HgCl <sub>2</sub> → Hg + Cl <sub>2</sub>	1.3	
HgH <sub>4</sub> → HgH <sub>2</sub> + H <sub>2</sub>	15.7	
HgH <sub>2</sub> → Hg + H <sub>2</sub>	0.6	

<sup>[a]</sup>At B3LYP/C level. <sup>[b]</sup>HF<sup>[72]</sup>. <sup>[c]</sup>QRPP-CCSD(T)<sup>[120]</sup>. <sup>[d]</sup>DFT-BP<sup>[120]</sup>.

### 4.1.5 Atomisation Energies

Table 4.1-5 provides computed atomization energies (AE) for the X<sub>2</sub>, HgX<sub>2</sub>, and HgX<sub>4</sub> systems (with CP corrections but without ZPE corrections). These data allow us to further analyze the contributions from individual species to the elimination reactions in Table 4.1-3. Triple excitations in the coupled-cluster calculations increase the AE notably for HgF<sub>4</sub>, HgCl<sub>4</sub>, and for F<sub>2</sub>, consistent with nonnegligible non-dynamical correlation effects – see above. In the same three cases, the MP2 calculations overestimate the AE appreciably. In the

other cases, the MP2 results are either somewhat above or slightly below the CCSD(T) data. In the case of F<sub>2</sub>, Cl<sub>2</sub>, and H<sub>2</sub>, experimental data are available for comparison – see footnote [a] to Table 4.1-5. The CCSD(T)/A results deviate only by a few kJ mol<sup>-1</sup> from experiment, indicating an approximate convergence of the halogen (hydrogen) basis sets and of the correlation level in this case. Any remaining errors in the CCSD(T)/A results for the elimination reactions (Table 4.1-3) will thus be due mostly to the description of the metal complexes themselves, probably in particular that of the Hg<sup>IV</sup> species.

**Table 4.1-5** Calculated atomization energies (kJ mol<sup>-1</sup>) for HgX<sub>4</sub>, HgX<sub>2</sub>, and X<sub>2</sub> (X = F, Cl, H).<sup>[a]</sup>

Species	Basis	MP2 <sup>[c]</sup>	CCSD	CCSD(T)	Basis	SVWN5	BP86	B1LYP	B3LYP	MPW1PW91	BHandHLYP
HgF <sub>4</sub>	A	789.9	606.1	693.0 <sup>[c]</sup>	B	1240.0	921.8	704.3	761.4	740.7	551.9
					C	1188.6	829.0	616.9	677.5	669.0	482.4
HgF <sub>2</sub>	A	545.4	487.7	515.1	B	776.1	623.7	551.3	574.1	571.6	512.5
					C	738.5	565.1	492.2	514.3	525.3	465.3
F <sub>2</sub> <sup>[b]</sup>	A	179.8	126.6	156.4	B	311.2	207.1	120.1	142.5	126.9	52.3
					C	317.0	192.0	115.3	154.7	116.9	51.4
HgCl <sub>4</sub>	A	597.5	440.4	501.6 <sup>[c]</sup>	B	844.8	627.6	486.1	521.2	563.6	427.9
					C	874.5	616.3	472.5	505.8	551.4	418.7
HgCl <sub>2</sub>	A	451.3	412.6	431.6	B	590.5	487.4	445.4	454.1	492.1	453.8
					C	601.5	477.0	435.1	446.5	482.8	446.7
Cl <sub>2</sub> <sup>[b]</sup>	A	255.7	218.4	236.2	B	316.9	227.3	189.7	201.3	209.5	166.8
					C	319.4	236.5	187.4	199.3	208.3	164.6
HgH <sub>4</sub>	A	587.4	606.7	619.8	B	826.4	699.6	625.0	644.1	634.2	614.3
					C	824.8	697.6	622.5	641.7	631.3	611.4
HgH <sub>2</sub>	A	329.3	358.6	358.7	B	455.6	399.8	377.0	383.7	382.6	387.3
					C	455.0	398.9	376.1	382.9	382.0	386.4
H <sub>2</sub> <sup>[b]</sup>	A	438.1	456.8	456.8	B	472.7	465.5	454.7	459.9	439.1	453.3
					C	487.2	477.4	465.3	470.8	450.1	462.7

<sup>[a]</sup>CP corrected values, unless noted otherwise. No ZPE corrections included. <sup>[b]</sup>The experimental values for X<sub>2</sub> (F, Cl, H) are 159.7<sup>[140]</sup>, 239.7±0.4<sup>[141]</sup>, and 432.0±0.4<sup>[141]</sup> kJ mol<sup>-1</sup>, respectively. After subtraction of ZPE corrections at B3LYP/C level, the values to compare to are: 165.8, 242.9, and 458.8 kJ mol<sup>-1</sup>, respectively. <sup>[c]</sup>Including CP corrections at CCSD level.

While any of the density functionals tested should perform reasonably well for the AE of H<sub>2</sub> (the MPW1PW91/B results appear a bit low), the more complicated electronic structure of the dihalogens is reflected in larger variations between the functionals. Again, hybrid functionals with ca. 20% Hartree-Fock exchange (B1LYP, B3LYP, MPW1PW91) tend to perform best (with an underestimate of ca. 10-30 kJ mol<sup>-1</sup>), whereas the BHandHLYP functional underestimates the AE of both F<sub>2</sub> and Cl<sub>2</sub> appreciably, and the gradient-corrected BP86 overestimates the AE for F<sub>2</sub> (the local SVWN5 functional overestimates both AEs appreciably).

Similar behaviour of the functionals is seen for the tetrahalide complexes: again B1LYP, B3LYP, and MPW1PW91 appear to perform best, BHandHLYP underbinds compared to the CCSD(T)/A benchmark results, whereas BP86 and particularly the local SVWN5 overbind appreciably. In these cases, deviations for the tetrahalides are much larger than for the dihalides. This translates into appreciable errors in the energies of the elimination reactions (cf. Table 4.1-3). While the B3LYP/B AE are too high by ca. 70 and 60 kJ mol<sup>-1</sup> for HgF<sub>4</sub> and HgF<sub>2</sub>, respectively, these errors compensate largely for the elimination reaction. Similar comparisons apply to the B1LYP and MPW91PW91 functionals. In consequence, these types of hybrid functionals (with basis B) reproduce most reliably the CCSD(T)/A thermochemistry.

#### 4.1.6 Transition States for Elimination Reaction

We have also attempted to calculate the transition states and activation barriers for the concerted elimination of X<sub>2</sub> (Table 4.1-6). Full structure optimization at the CCSD(T)/A level exceeded the available computational resources. In the case of the post-HF methods, we were thus restricted to single-point energy calculations at various DFT-optimised structures. Full optimisations were, however, attempted for all density functionals. The transition states located are structurally similar to that computed for the HgH<sub>4</sub> case by Pyykkö *et al.*<sup>[74]</sup>, a planar arrangement with C<sub>2v</sub> symmetry – see Figure 4.1.2.

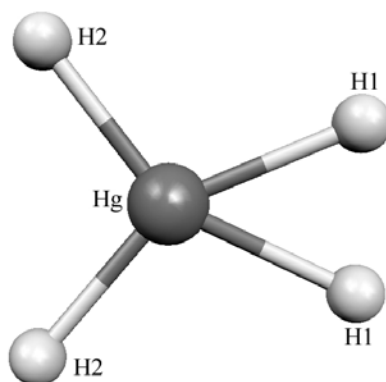


**Figure 4.1-2** Optimised transition state (C<sub>2v</sub>) on B3LYP/B level.

For HgF<sub>4</sub>, the computed activation barriers appear to be very large and vary over a wide range (Table 4.1-6). Already the variation of the structure with different functionals changes the CCSD(T)/A barrier over a range of more than 100 kJ mol<sup>-1</sup>. The DFT barriers are only

about half of the CCSD(T) results but still appear unrealistically large relative to the average Hg-F binding energies deducible from the atomization energies in Table 4.1-5. Matters are less dramatic for HgCl<sub>4</sub> and HgH<sub>4</sub>, where the computed barriers range from ca. 60 to 80 kJ mol<sup>-1</sup>, and from ca. 40 to 50 kJ mol<sup>-1</sup>, respectively. In the latter two cases, the DFT results are not very far from the best CCSD(T) values.

**Table 4.1-6** Calculated activation barriers (in kJ mol<sup>-1</sup>) for HgX<sub>4</sub> → HgX<sub>2</sub> + X<sub>2</sub> (X = F, Cl, H) elimination reactions.<sup>[a]</sup>

	Basis//Structure	MP2	CCSD	CCSD(T)	SVWN5	BP86	B1LYP	B3LYP	MPW1PW91	BHandHLYP
HgF <sub>4</sub>	A //SVWN5	626.2	584.4	542.9						
	A //B3LYP	624.1	696.1	633.2						
	A //BHandHLYP	558.3	592.7	514.6						
	B //B						258.8	252.1	275.4	307.8
	C //C						247.5	240.9	262.0	323.1
	D //D						242.8	235.2	254.8	288.5
HgCl <sub>4</sub>	A //SVWN5	160.3	86.8	66.7						
	A //B3LYP	159.4	102.5	69.8						
	A //BHandHLYP	128.5	90.7	66.7						
	B //B				60.5	40.1	51.7	49.9	61.4	64.8
	C //C				51.6	37.1	49.4	47.4	56.8	61.3
	D //D				53.9	40.7	55.8	53.3	63.0	69.9
HgH <sub>4</sub>	A //SVWN5	50.8	48.2	48.0						
	A //B3LYP	57.4	51.8	51.1						
	A //BHandHLYP	51.8	48.4	47.7						
	B //B				41.2	41.6	39.5	40.2	38.6	36.9
	C //C				40.9	41.2	39.0	39.7	38.0	36.2
	D //D				49.3	49.7	48.2	48.8	47.5	46.1
	other studies	34 <sup>[b]</sup>						39 <sup>[b]</sup>		

<sup>[a]</sup>Single-points at DFT-optimised structures for MP2, CCSD, and CCSD(T). Fully optimised structures for DFT methods. <sup>[b]</sup>Ref. [74].

Closer inspection of the electronic structure at the F<sub>2</sub> elimination transition state for HgF<sub>4</sub> suggests very small HOMO-LUMO gaps already for the hybrid functionals (ca. 1-1.7 eV for B3LYP, B1LYP, and MPW1PW91 and ca. 3-3.5 eV for BHandHLYP). With gradient-corrected and local functionals, no electronically stable Kohn-Sham wavefunction could be obtained. This suggests appreciable multi-reference character for the transition state, and both approximate DFT and single-reference coupled-cluster theory appear problematic. Matters are not much better for the HgCl<sub>4</sub> case (although here the BP86 and SVWN5 calculations afford small gaps of ca. 0.1-0.2 eV), and it is presently unclear why the computed barriers are less level dependent. In contrast, the HgH<sub>4</sub> case exhibits appreciable HOMO-LUMO gaps at any of the levels employed (ca. 4.5 eV with BP86 and SVWN5, ca. 6 eV with the “regular” hybrid

functionals, and ca. 8 eV with BHandHLYP). It appears that the simpler electronic structure of the HgH<sub>4</sub> transition state, and possibly the relatively large Hg-H covalency, make this system an easier case for single-reference methods ( $T_1$ -diagnostics at CCSD level in this case are only ca. 0.015, compared to values around 0.04-0.06 for HgF<sub>4</sub> and HgCl<sub>4</sub>). In particular, we think that repulsive effects between the nonbonding electron pairs of the halogen ligands and the 5p semi-core shell on mercury may be responsible<sup>[32]</sup> for the generally larger non-dynamical correlation effects in the tetrahalides compared to the tetrahydride. The present results for the HgH<sub>4</sub> system agree well with the previous study by Pyykkö *et al.*<sup>[74]</sup> – see Table 4.1-7.

**Table 4.1-7** Structure of the transition state for H<sub>2</sub> elimination from HgH<sub>4</sub> calculated at different levels.<sup>[a]</sup>

	Geometry	SVWN5	BP86	B1LYP	B3LYP	MPW1PW91	BHandHLYP
this work, basis B	r g-H1	169.9	170.9	169.3	169.6	168.3	167.2
	r Hg-H2	167.4	168.7	168.4	168.4	167.5	167.4
	r H1-H1	132.4	135.3	139.4	138.6	138.2	142.2
	∠ H2-Hg-H2	104.1	102.8	101.7	101.9	101.7	101.2
	∠ H2-Hg-H1	105.0	105.3	104.8	105.0	104.9	104.3
ref. <sup>[74]</sup>	r Hg-H1				169.2		
	r Hg-H2				166.8		
	r H1-H1				132.9		
	∠ H2-Hg-H2				103.6		
	∠ H2-Hg-H1				105.1		

<sup>[a]</sup>Bond lengths in pm, bond angles in deg. See Figure 4.1-2 for atom labels.

## 4.1.7 Conclusions

This validation study of various density functionals and basis sets against accurate benchmark CCSD(T) results for structures and energetics of small Hg<sup>IV</sup> complexes provides a basis for our ongoing studies on larger target systems of potential interest for experimental studies – see Chapter 4.2. While relatively reliable structures of minima (except for HgCl<sub>4</sub>) may already be obtained with the local SVWN5 or the hybrid BHandHLYP functionals (due to error compensation), the energetics are better described by hybrid functionals like B1LYP, B3LYP, and MPW1PW91, that incorporate ca. 20% Hartree-Fock exchange. The choice of basis sets will depend on the size of system to be studied. Optimisations may employ the moderate-sized, economical basis C, whereas accurate DFT energy calculations may require the larger basis B that exhibits considerably lower BSSE.

A search for transition states and activation barriers for X<sub>2</sub>-elimination from HgX<sub>4</sub> (X = F, Cl, H) indicated considerably larger multi-reference character for X = F, Cl than for the previously studied HgH<sub>4</sub> system, possibly due to the presence of nonbonding electron pairs at the halogens<sup>[32]</sup>. At least for X = F, no reliable activation barriers could thus be computed with the available methods. Unfortunately, multi-configurational approaches would currently also be prohibitively expensive in this case, due to the large active orbital space that would be required. However, based on the comparison with the other two cases, we expect an appreciable activation barrier for concerted F<sub>2</sub> elimination, in view of the multi-reference character of the transition state probably the largest of the three systems studied. In any case, the calculations confirm clearly the previously noted exothermic character of HgF<sub>4</sub> as a gas-phase species, in contrast to HgH<sub>4</sub> and HgCl<sub>4</sub>.

## 4.2 Can Weakly Coordinating Anions Stabilise Mercury in its Oxidation State +IV? <sup>[75]</sup>

### 4.2.1 Introduction

Can we turn group 12 of the Periodic Table into a true transition metal group, with the valence d-orbitals involved in bonding? As we have seen in Chapter 4.1 this should be possible for the heaviest group member mercury ( $\text{HgF}_4$ ). The predicted square-planar  $D_{4h}$   $\text{HgF}_4$  is thermochemically stable in the gas-phase with respect to the principle decomposition pathway  $\text{HgF}_4 \rightarrow \text{HgF}_2 + \text{F}_2$ . In spite of this computed favourable gas-phase thermochemistry,  $\text{HgF}_4$  has not yet been confirmed experimentally. Molecular-beam experiments with fluorine and mercury are not attractive to experimentalists, and matrix-isolation spectroscopy has not yet produced evidence for  $\text{HgF}_4$  either.<sup>[121, 142]</sup> In the condensed bulk phase, elimination of  $\text{F}_2$  is strongly favoured by the much higher aggregation energy of solid  $\text{HgF}_2$  in its ionic, high-coordinate fluorite structure compared to aggregation of a more covalent square-planar  $\text{HgF}_4$ .<sup>[73]</sup> While we consider the matrix-isolation route towards  $\text{HgF}_4$  to be still insufficiently investigated, it is appropriate at this point in time to explore alternative  $\text{Hg}^{\text{IV}}$  targets that might offer easier experimental access.

As the major obstacle to a condensed-phase  $\text{Hg}^{\text{IV}}$  chemistry is the energy gain of the corresponding  $\text{Hg}^{\text{II}}$  compounds by aggregation, it seems natural to consider ligands that will not allow high-coordinate  $\text{Hg}^{\text{II}}$  aggregation. One option involves weakly coordinating anions, several of which are well known to stabilise high oxidation states as well as unusual and otherwise unstable cations.<sup>[113, 114]</sup> In weakly coordinating anions (WCA), the negative charge is typically delocalised over several centres, and the nucleophilicity of individual connecting ligand atoms is thus low. The idea is that aggregation of  $\text{Hg}^{\text{II}}$  complexes existing in superacid environments that produce WCAs should be considerably less pronounced than that of  $\text{HgF}_2$  itself – see Chapter 3.

This chapter reports structure optimisations and thermochemical stabilities of  $\text{Hg}^{\text{IV}}$  complexes with a variety of WCAs by quantum-chemical methods. The aim is to identify appropriate targets for experimental access. We investigate in particular  $\text{HgX}_4$  as well as



*cis* and *trans*  $\text{HgF}_2\text{X}_2$  complexes, where  $\text{X}^-$  is one of the following WCAs:  $[\text{AlF}_4]^-$ ,  $[\text{AsF}_6]^-$ ,  $[\text{SbF}_6]^-$ , the dinuclear anions  $[\text{Al}_2\text{F}_7]^-$ ,  $[\text{As}_2\text{F}_{11}]^-$ ,  $[\text{Sb}_2\text{F}_{11}]^-$ , and the pentafluorooxotellurate and -selenate anions  $[\text{OEF}_5]^-$  (E = Te, Se). For comparison, a number of noble-gas compounds will also be investigated.

### 4.2.2 Computational Details

Previous quantum-chemical calculations on the stability of  $\text{Hg}^{\text{IV}}$  have involved mainly high-level coupled-cluster *ab initio* calculations.<sup>[12, 72, 73]</sup> These computationally demanding post-Hartree-Fock methods are currently not applicable to systems of the size envisioned here. We will thus resort to density functional theory (DFT). To provide a sound methodological basis for our exploration, we have recently calibrated different DFT methods in detail against accurate coupled-cluster data for the smaller complexes  $\text{HgX}_4$  (X = F, Cl, H) – see Chapter 4.1.<sup>[12]</sup> In the absence of experimental data, this theory-against-theory comparison has enabled us to identify exchange-correlation functionals and basis sets that are expected to faithfully reproduce the structures and stabilities of  $\text{Hg}^{\text{IV}}$  complexes. While the structural parameters of  $\text{Hg}^{\text{IV}}$  complexes were best reproduced by the local SVWN and hybrid BHandHLYP functionals, the thermochemistry was best described by hybrid functionals like B3LYP, B1LYP or MPW1PW91 that incorporate about 20% Hartree-Fock exchange.<sup>[12]</sup> In this chapter we use the popular B3LYP functional<sup>[50, 53, 143]</sup> (implementation as in the Gaussian program,<sup>[128]</sup> as requested by the keyword `b3-lyp_Gaussian` in the Turbomole program suite<sup>[144]</sup> used in this study). The comparison in Table 4.2-1 shows that B3LYP with the basis used also in the present work (see below) provides only slightly more endothermic elimination energies than the much more involved CCSD(T) calculations. Similar results were noted for decomposition reactions of high-oxidation-state compounds in the neighbouring group 11.<sup>[145]</sup> Note that basis-set convergence for the coupled-cluster results is slower than for DFT, and still larger basis sets than those employed in ref. <sup>[12]</sup> will probably bring the CCSD(T) energetics even closer to the B3LYP data.

We use a pseudopotential/basis-set combination based on the one labelled basis-B in ref. <sup>[12]</sup>. This basis set was found to provide excellent structures and energetics. In particular, it exhibited very small basis-set superposition errors in DFT calculations – cf. Table 4.2-1.

**Table 4.2-1** Comparison of DFT and coupled-cluster elimination, fragmentation and atomization energies (in kJ mol<sup>-1</sup>) for small HgX<sub>4</sub> and HgX<sub>2</sub> (X = F, Cl, H) complexes.<sup>[a]</sup>

System	B3LYP <sup>[b]</sup>	CCSD(T)
HgF <sub>4</sub> → HgF <sub>2</sub> + F <sub>2</sub>	+44.0 (+36.3)	+34.0 (+22.7) <sup>[c]</sup>
HgCl <sub>4</sub> → HgCl <sub>2</sub> + Cl <sub>2</sub>	-133.1 (-134.2)	-156.4 (-165.5) <sup>[c]</sup>
HgH <sub>4</sub> → HgH <sub>2</sub> + H <sub>2</sub>	-195.5 (-199.4)	-181.4 (-195.6) <sup>[b]</sup>
HgF <sub>4</sub> → Hg + 4F	+779.7 (+761.4)	+719.8 (+693.0) <sup>[c]</sup>
HgCl <sub>4</sub> → Hg + 4Cl	+530.4 (+521.2)	+522.8 (+501.6) <sup>[c]</sup>
HgH <sub>4</sub> → Hg + 4H	+651.6 (+644.1)	+648.4 (+619.8) <sup>[b]</sup>
HgF <sub>2</sub> → Hg + 2F	+583.6 (+574.1)	+528.1 (+515.1) <sup>[b]</sup>
HgCl <sub>2</sub> → Hg + 2Cl	+461.1 (+454.1)	+442.0 (+431.6) <sup>[b]</sup>
HgH <sub>2</sub> → Hg + 2H	+387.2 (+383.7)	+373.0 (+358.7) <sup>[b]</sup>
HgF <sub>4</sub> → HgF <sub>2</sub> + 2F	+196.0 (+187.2)	+191.6 (+179.1) <sup>[c]</sup>
HgCl <sub>4</sub> → HgCl <sub>2</sub> + 2Cl	+69.4 (+63.9)	+80.8 (+78.8) <sup>[c]</sup>
HgH <sub>4</sub> → HgH <sub>2</sub> + 2H	+295.6 (+264.9)	+275.4 (+261.2) <sup>[b]</sup>

<sup>[a]</sup>Cf. ref. <sup>[12]</sup>. B3LYP/basis-B and CCSD(T)/basis-A results. <sup>[b]</sup>Results with CP corrections in parentheses. <sup>[c]</sup>Results with CCSD/basis-A CP corrections in parentheses.

A quasi-relativistic small-core 20-valence-electron pseudopotential<sup>[124]</sup> is used for Hg, with a (8s8p7d2f)/[6s6p4d2f] valence basis set including two uncontracted f-functions with exponents  $\alpha = 1.5, 0.5$ . Quasirelativistic large-core PPs were used for Al, As, Sb, Se, and Te.<sup>[135]</sup> The (4s4p)/[2s2p] valence basis sets<sup>[135]</sup> for Al, As, and Sb were augmented by one polarization d-function (see ref. <sup>[146]</sup> for Al and ref. <sup>[147]</sup> for the other atoms) to arrive at basis sets of DZP valence quality. For Se, and Te, (4s5p)/[2s3p] valence basis sets<sup>[135]</sup> were augmented by one diffuse s-function (obtained by dividing the smallest s-exponent in the 4s set by a factor of three) and one d-function,<sup>[147]</sup> resulting in a DZ+P-quality (5s5p1d)/[3s3p1d] valence basis. In comparative calculations on noble-gas compounds, quasirelativistic 8-valence-electron PPs and (6s6p3d1f)/[4s4p3d1f] valence basis sets were used for Xe and Kr.<sup>[148]</sup> Fluorine and oxygen were treated at all-electron level, using Dunning's DZP basis augmented by a diffuse sp-set<sup>[133]</sup> (DZ+P), resulting in a (10s6p1d)/[5s3p1d] basis. While the valence basis sets on Al, As, Sb, Se, and Te are of very slightly lower quality than those for the other atoms, the basis-set incompleteness errors for these "inner" atoms are expected to cancel for the reaction energies studied here. Our previous experience<sup>[12]</sup> (cf. Table 4.2-1) suggests that the basis sets used exhibit small basis-set superposition errors at DFT level. Energies will thus be reported without counterpoise corrections (CP).

All calculations were done with the Turbomole 5.6<sup>[144]</sup> program. Structures were fully optimised without symmetry restrictions. Except for a few of the largest systems (complexes of  $E_2F_{11}$  ligands and dimers of  $Hg[OTeF_5]_2$  and  $Hg[OTeF_5]_4$ ), where this turned out to be computationally too demanding, minima on the potential energy surface were characterised by harmonic vibrational frequency analyses, using numerical second derivatives based on energies and analytical gradients. We provide relative energies without zero-point vibrational corrections, as these do not alter the thermochemistry significantly.<sup>[12]</sup> Spin-orbit effects were also previously found to be almost negligible for the elimination reactions.<sup>[73]</sup> Natural population analyses (NPA)<sup>[149]</sup> used a standalone version of the NBO4.M program,<sup>[150]</sup> interfaced to Turbomole in our group.<sup>[151]</sup>

### 4.2.3 Structure Optimisation

$[X]^- = [AlF_4]^-$ ,  $[Al_2F_7]^-$ . The computed structures of *cis* and *trans*  $HgF_2[AlF_4]_2$  exhibit the expected square planar primary coordination of low-spin  $5d^8$   $Hg^{IV}$ , with slightly shorter Hg-F[F] than Hg-F[ $AlF_4$ ] distances (Figure 4.2-1b,c). In contrast, the coordination is distorted for  $Hg[AlF_4]_4$ , with deviations from planarity and unequal primary Hg-F distances (Figure 4.2-1a). The primary coordination is in all three cases augmented by one weaker axial fluorine contact from each  $AlF_4$  ligand (for  $Hg[AlF_4]_4$  the primary distances are somewhat longer and the secondary distances shorter than for the other two species). The optimised structures exhibit  $C_1$  symmetry for  $Hg[AlF_4]_4$ ,  $C_2$  symmetry for *cis*- $HgF_2[AlF_4]_2$ , and  $D_{2h}$  symmetry for *trans*- $HgF_2[AlF_4]_2$ .

During one structure optimization of the *cis*-isomer, an  $AlF_3$ -unit was transferred from one of the coordinated  $AlF_4$ -ligands to the other, forming a coordinated  $Al_2F_7$ -ligand. The resulting  $C_1$ -symmetrical  $HgF_3[Al_2F_7]$  has one weak axial contact from a fluorine of the  $Al_2F_7$ -ligand in form of a 6-membered chelate ring (Figure 4.2-1d). This complex is ca.  $62.3 \text{ kJ mol}^{-1}$  more stable than *cis*- $HgF_2[AlF_4]_2$ , which in turn is  $5.4 \text{ kJ mol}^{-1}$  more stable than its *trans* isomer. The condensed binuclear ligand appears thus to provide an energy sink in these systems. This led us to consider also  $HgF_2[Al_2F_7]_2$ . In the optimised, nonsymmetric structure (Figure 4.2-1e), each  $[Al_2F_7]^-$  ligand coordinates two equatorial positions in a compressed octahedron, and the terminal fluorine ligands occupy the axial positions.

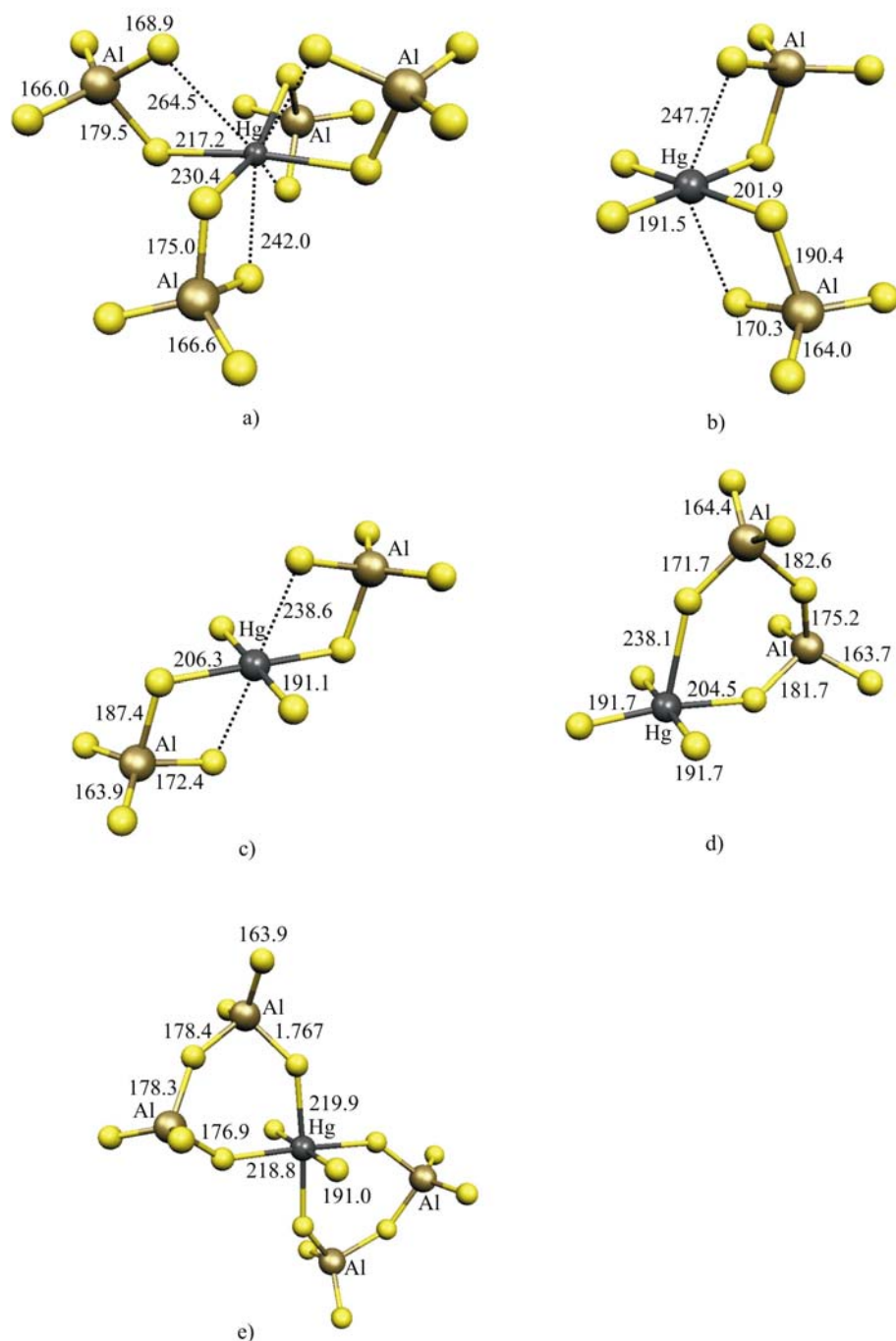


**Figure 4.2-1** Optimised structures for  $\text{Hg}^{\text{IV}}$  complexes with  $\text{AlF}_4^-$ - or  $\text{Al}_2\text{F}_7^-$ -ligands. a)  $\text{Hg}[\text{AlF}_4]_4$ . b) *cis*- $\text{HgF}_2[\text{AlF}_4]_2$ . c) *trans*- $\text{HgF}_2[\text{AlF}_4]_2$ . d)  $\text{HgF}_3[\text{Al}_2\text{F}_7]$ . E)  $\text{HgF}_2[\text{Al}_2\text{F}_7]_2$ .

Possible elimination products for these systems include the  $\text{Hg}^{\text{II}}$  complex  $\text{Hg}[\text{AlF}_4]_2$ , which exhibits  $D_{2d}$  symmetry and tetrahedral mercury coordination via bidentate binding of both ligands (Figure 4.2-2a). The most stable structure found for  $\text{Hg}[\text{Al}_2\text{F}_7]_2$  ( $C_2$  symmetry) exhibits a bidentate chelate binding mode of the dinuclear ligand and also tetrahedral coordination of Hg (Figure 4.2-2b).

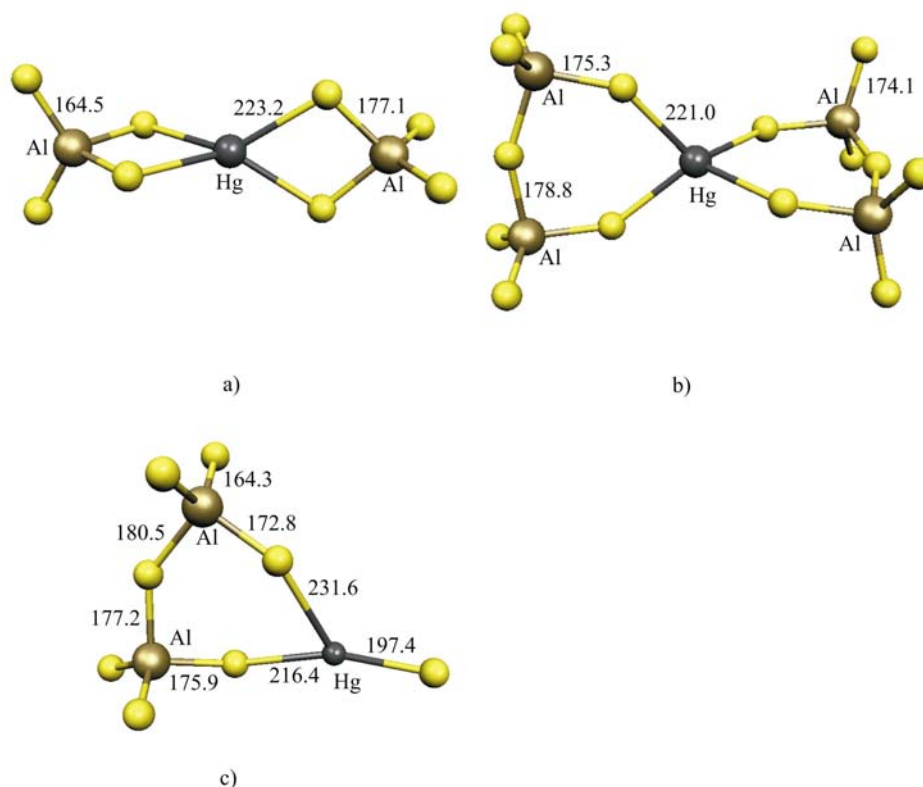


**Figure 4.2-2** Optimised structures for  $\text{Hg}^{\text{II}}$  complexes with  $\text{AlF}_4^-$  or  $\text{Al}_2\text{F}_7^-$  ligands. a)  $\text{Hg}[\text{AlF}_4]_2$ . b)  $\text{Hg}[\text{Al}_2\text{F}_7]_2$ . c)  $\text{HgF}[\text{Al}_2\text{F}_7]$ .

$[\text{X}]^- = [\text{EF}_6]^-$  ( $\text{E} = \text{As}, \text{Sb}$ ). Figure 4.2-3 shows again square-planar primary coordination to mercury in all  $\text{Hg}^{\text{IV}}$  complexes, augmented by two further, weaker axial contacts - four in the case of  $\text{Hg}[\text{SbF}_6]_4$  (Figure 4.2-3b). Primary Hg-F distances to the  $\text{EF}_6$  ligands tend to be in the 195-196 pm range, shorter than the 205-206 pm for  $\text{AlF}_4^-$  ligands above (cf. Figure 4.2-1) but slightly longer than the distances to fluoride. In contrast, the secondary contacts range from 259-277 pm, considerably longer than the 238-239 pm of the aluminum systems. This indicates a lower tendency towards bidentate bonding.

In all bound octahedral  $\text{EF}_6^-$  ligands, the E-F bond to the coordinating fluorine atom is lengthened substantially compared to the other bonds within the ligand, and the equatorial fluorine atoms are bent towards the fluorine atom that coordinates to mercury. This indicates substantial weakening of the metal-coordinated E-F bond in all cases (as a consequence, the E-F bond in *trans* position is shortened). Indeed, optimisation of  $\text{Hg}[\text{AsF}_6]_4$  led to dissociation of two  $\text{AsF}_5$  molecules from two  $\text{AsF}_6^-$  ligands in *cis* position, leading to *cis*- $\text{HgF}_2[\text{AsF}_6]_2$  with two loosely attached  $\text{AsF}_5$  molecules (Figure 4.2-3a, cf. the very similar structure parameters of free *cis*- $\text{HgF}_2[\text{AsF}_6]_2$ , Figure 4.2-3c). This seems to be a relatively general observation for the arsenium-based systems – see below. In contrast, all four  $\text{SbF}_6^-$  ligands stay intact in  $\text{Hg}[\text{SbF}_6]_4$  (Figure 4.2-3b; the

structure has  $C_2$  symmetry), but the F-Sb bond of the coordinated fluorine is lengthened substantially.

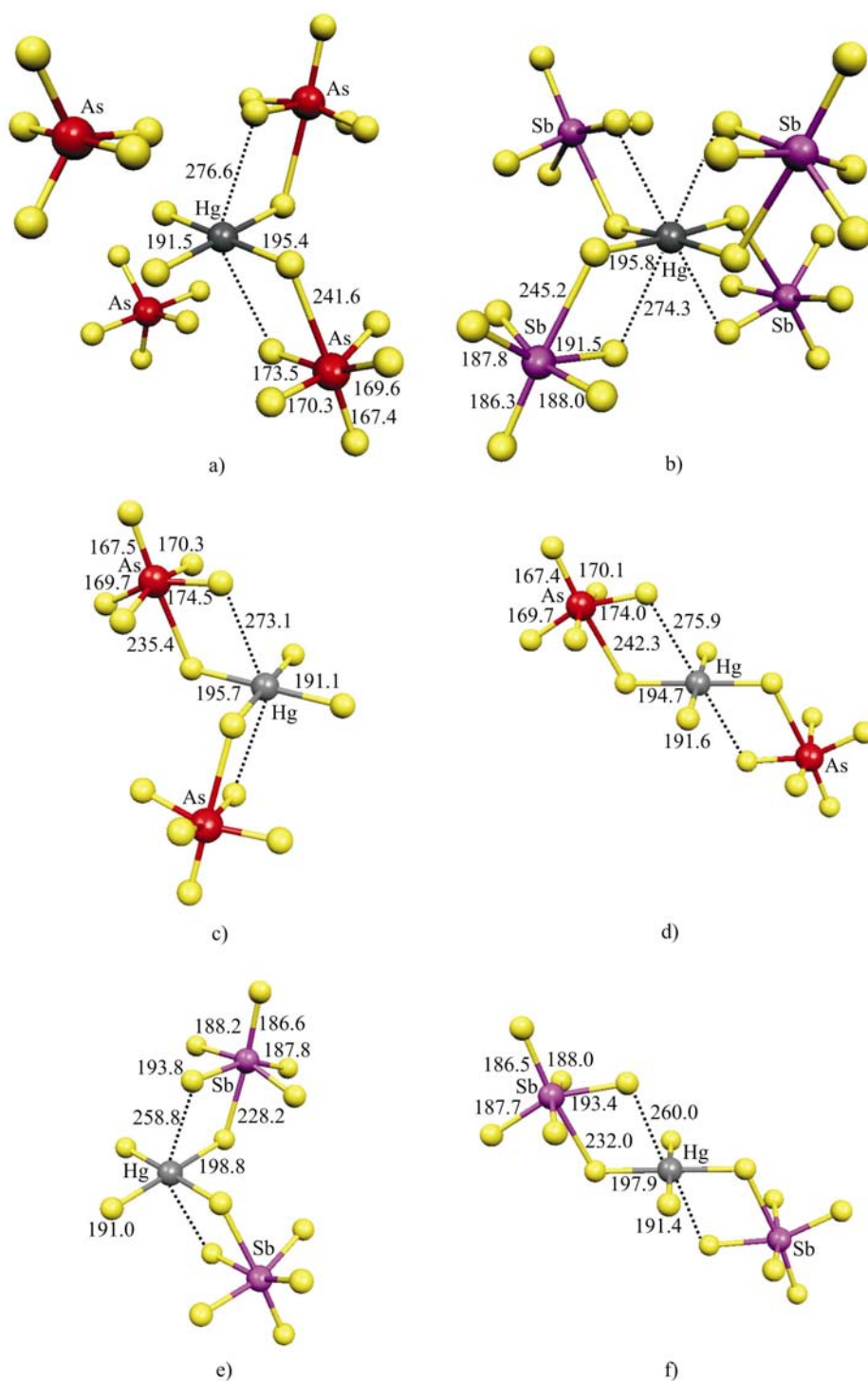


**Figure 4.2-3** Optimised structures for  $\text{Hg}^{\text{IV}}$  complexes with  $\text{AsF}_6^-$  or  $\text{SbF}_6^-$  ligands. a)  $\text{Hg}[\text{AsF}_6]_4$ . b)  $\text{Hg}[\text{SbF}_6]_4$ . c) *cis*- $\text{HgF}_2[\text{AsF}_6]_2$ . d) *trans*- $\text{HgF}_2[\text{AsF}_6]_2$ . e) *cis*- $\text{HgF}_2[\text{SbF}_6]_2$ . f) *trans*- $\text{HgF}_2[\text{SbF}_6]_2$ .

The greater resistance of the  $\text{SbF}_6$  ligands towards loss of  $\text{SbF}_5$  (see below for the associated energetics) may also be discerned in the other cases from the somewhat less pronounced lengthening of the E-F bonds involved in metal coordination (cf. Figure 4.2-3c vs. Figure 4.2-3e for *trans*- $\text{HgF}_2[\text{EF}_6]_2$  and Figure 4.2-3d vs. Figure 4.2-3f for the *cis* complexes). In general, equatorial E-F bonds involved in secondary coordination to mercury are lengthened more moderately, as one might expect. Due to the less pronounced bond expansion of the E-F bond to the coordinated fluorine in the  $\text{HgF}_2[\text{EF}_6]_2$  systems compared to  $\text{Hg}[\text{EF}_6]_4$ , we may consider the  $\text{AsF}_6$ -ligands still whole in these complexes (Figure 4.2-3c,d). The *cis*-isomers of  $\text{HgF}_2[\text{AsF}_6]_2$  and  $\text{HgF}_2[\text{SbF}_6]_2$  are more stable than their *trans* isomers by ca.  $4 \text{ kJ mol}^{-1}$  and ca.  $10 \text{ kJ mol}^{-1}$ , respectively. This may be interpreted as a slightly larger *trans* influence of free fluoride compared to  $[\text{EF}_6]^-$ .

In view of the discussion in the introduction regarding aggregation of the  $\text{Hg}^{\text{II}}$  elimination products, the structures of the  $\text{Hg}[\text{EF}_6]_2$  complexes are of particular interest. As shown in Figure 4.2-4, these exhibit both almost regular octahedral coordination to mercury (the complexes have  $D_{3d}$  symmetry), where three fluorine atoms on one face of each  $\text{EF}_6$ -unit bind to the metal in a tridentate fashion.

While the computed Hg-F distances are significantly longer than the ca. 200 pm of a full single bond, the relatively high coordination number is notable – see below. The E-F bond lengths of the coordinated fluorines are significantly expanded, but much less than the single coordinating E-F bond in the  $\text{Hg}^{\text{IV}}$  complexes – cf. Figure 4.2-3. The  $\text{AsF}_6$ -ligand is much less distorted than in the  $\text{Hg}^{\text{IV}}$  case. Together, these observations signal three moderate Hg-F bonding interactions to each ligand.

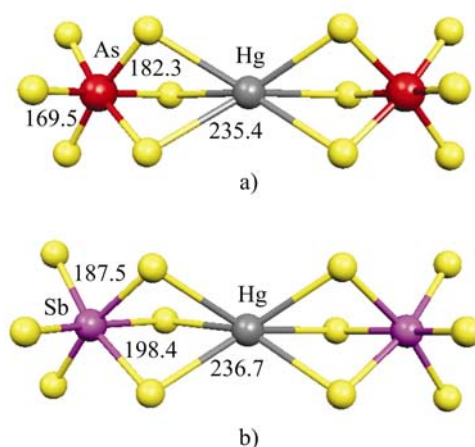


**Figure 4.2-4** Optimised structures for  $\text{Hg}^{\text{II}}$  complexes with  $\text{AsF}_6^-$  or  $\text{SbF}_6^-$  ligands. a)  $\text{Hg}[\text{AsF}_6]_2$ . b)  $\text{Hg}[\text{SbF}_6]_2$ .

$[\mathbf{X}]^- = [\mathbf{E}_2\mathbf{F}_{11}]^-$  ( $\mathbf{E} = \mathbf{As}, \mathbf{Sb}$ ). Optimised structures of  $\text{Hg}^{\text{IV}}$  complexes with the dinuclear  $\text{E}_2\text{F}_{11}$ -ligands are shown in Figure 4.2-5. Optimization of  $\text{Hg}[\text{As}_2\text{F}_{11}]_4$  leads to dissociation of  $\text{AsF}_5$  from all four ligands, forming a system best described as  $\text{Hg}[\text{AsF}_6]_4 \cdot 4\text{AsF}_5$  (Figure 4.2-5a; cf. the structure of  $\text{Hg}[\text{AsF}_6]_4$  in Figure 4.2-3a), or maybe even as  $\text{HgF}_4 \cdot 8\text{AsF}_5$ . We have not been able to locate a stable minimum for  $\text{Hg}[\text{Sb}_2\text{F}_{11}]_4$ : in one optimization, spontaneous reductive elimination of  $\text{F}_2$  occurred, with formation of  $\text{Hg}[\text{Sb}_2\text{F}_{11}]_2 + 2 \text{SbF}_5$ . In another optimisation,  $\text{Sb}_2\text{F}_{10}$  was extruded, with formation of  $\text{HgF}[\text{Sb}_2\text{F}_{11}]_3$  (Figure 4.2-5b). This does not necessarily mean that  $\text{Hg}[\text{Sb}_2\text{F}_{11}]_4$  does not exist, but the size of the system prevented us from more extensive searches for a minimum structure. It seems in any case that there is not much gain in stability in going from the  $\text{SbF}_6^-$  to the  $\text{Sb}_2\text{F}_{11}$ -ligand, or from  $\text{HgF}_2[\text{Sb}_2\text{F}_{11}]_2$  to  $\text{Hg}[\text{Sb}_2\text{F}_{11}]_4$  – see below.

Minima were found for the  $\text{HgF}_2[\text{E}_2\text{F}_{11}]_2$  complexes. The structures differ also appreciably between  $\mathbf{E} = \mathbf{As}$  and  $\mathbf{E} = \mathbf{Sb}$  (Figure 4.2-5c-f). In the case of  $\mathbf{E} = \mathbf{As}$ , again two  $\text{AsF}_5$  units dissociate and are only loosely connected to the remaining  $\text{AsF}_6$ -ligand, turning both *cis* and *trans* complexes essentially into  $\text{HgF}_2[\text{AsF}_6]_2 \cdot 2\text{AsF}_5$  (Figure 4.2-5c,e), similar to the result of structure optimization of  $\text{Hg}[\text{AsF}_6]_4$  (see above), and with the same stoichiometrical composition. In contrast to the latter case, where the  $\text{AsF}_5$  units are closest to metal-bound fluoride (cf. Figure 4.2-3a), here they are bound very weakly to an axial fluorine of the  $\text{AsF}_6$ -ligand (*trans* to mercury). While the two structures are also minima, the binding is slightly less favourable in the latter case, making the *cis* complex in Figure 4.2-5c about  $8 \text{ kJ mol}^{-1}$  less stable than the arrangement in Figure 4.2-3a. The *trans* complex (Figure 4.2-5e) is another  $4 \text{ kJ mol}^{-1}$  less stable. For  $\text{HgF}_2[\text{Sb}_2\text{F}_{11}]_2$ , the *cis* isomer is also about  $8 \text{ kJ mol}^{-1}$  more stable than the *trans*-isomer – see also above. Here the dinuclear ligands remain whole (but with unsymmetrical F-E-F bridges), and the  $\text{Sb}_2\text{F}_{11}$ -ligands bend around to allow secondary contacts to mercury by the “remote”  $\text{SbF}_5$  groups (this appears to be preferable over bidentate bonding from fluorine atoms attached to the same Sb centre, as found for the  $\text{SbF}_6^-$ -complexes; cf. Figure 4.2-3). The somewhat unsymmetrical bridges are similar to those found in the solid state or, e.g., in *ab initio* molecular dynamics studies of liquid  $\text{SbF}_5$  or of  $\text{HF-SbF}_5$  solutions.<sup>[152-154]</sup>



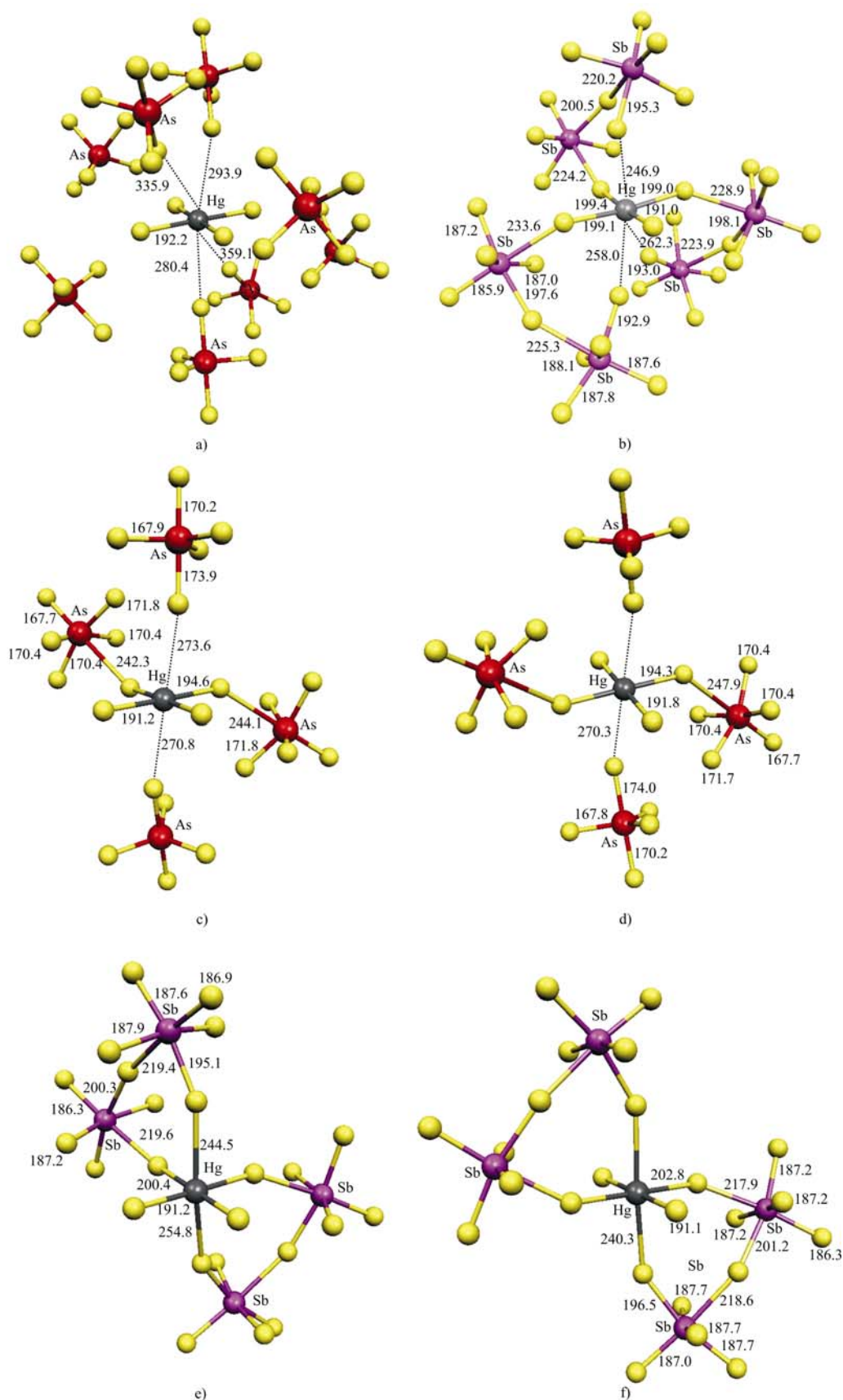


**Figure 4.2-5** Optimised structures for  $\text{Hg}^{\text{IV}}$  complexes with  $\text{As}_2\text{F}_{11}^-$  or  $\text{Sb}_2\text{F}_{11}^-$  ligands. a)  $\text{HgF}_4 \cdot 8\text{AsF}_5$ . b)  $\text{HgF}[\text{Sb}_2\text{F}_{11}]_3$ . c) *cis*- $\text{HgF}_2[\text{AsF}_6]_2 \cdot 2\text{AsF}_5$ . d) *trans*- $\text{HgF}_2[\text{AsF}_6]_2 \cdot 2\text{AsF}_5$ . e) *cis*- $\text{HgF}_2[\text{Sb}_2\text{F}_{11}]_2$ . f) *trans*- $\text{HgF}_2[\text{Sb}_2\text{F}_{11}]_2$ .

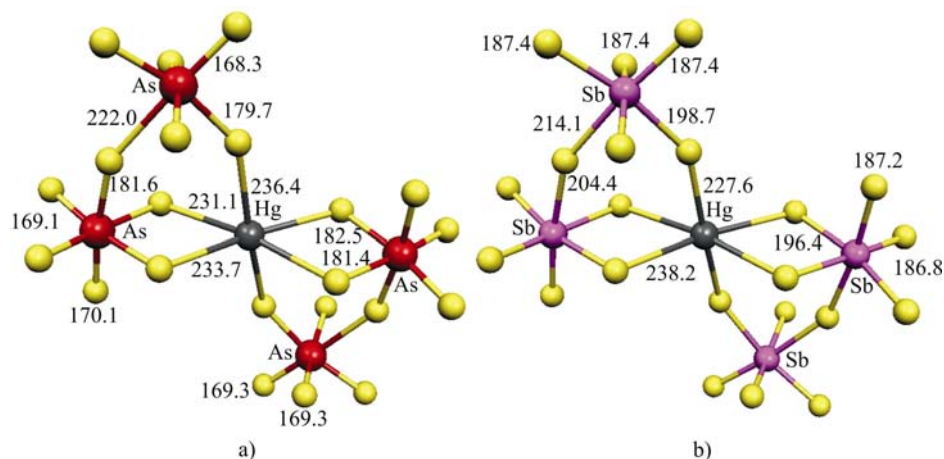


**Figure 4.2-6** Optimised structures for  $\text{Hg}^{\text{II}}$  complexes with  $\text{As}_2\text{F}_{11}$ - or  $\text{Sb}_2\text{F}_{11}$ -ligands. a)  $\text{Hg}[\text{As}_2\text{F}_{11}]_2$ . b)  $\text{Hg}[\text{Sb}_2\text{F}_{11}]_2$ .

The  $\text{Hg}^{\text{II}}$  products of reductive  $\text{F}_2$  elimination,  $\text{Hg}[\text{E}_2\text{F}_{11}]_2$ , have  $C_i$  symmetry (Figure 4.2-6). As for the complexes  $\text{Hg}[\text{EF}_6]_2$  above, the coordination of mercury is distorted octahedral. However, now only two of the three bonding contacts of each ligand derive from one chelate-bonded  $\text{EF}_6$ -unit, whereas the second  $\text{EF}_5$ -unit bends around to provide a third, slightly shorter contact in a 6-ring chelating fashion. Notably, the  $\text{As}_2\text{F}_{11}$ -ligands remain whole in this case, in contrast to the  $\text{Hg}^{\text{IV}}$  species in Figure 4.2-5 (Sb-F-Sb bridges in the  $\text{Sb}_2\text{F}_{11}$ -ligands are also somewhat more symmetrical than in the  $\text{Hg}^{\text{IV}}$  case).

$[\text{X}]^- = [\text{OEF}_5]^-$  (E = Se, Te). The optimisations produce structures of relatively high symmetry ( $D_{2d}$ ) for  $\text{Hg}[\text{OEF}_5]_4$  (Figure 4.2-7a,b). The *trans*  $\text{HgF}_2[\text{OEF}_5]_2$  complexes exhibit  $C_{2h}$  symmetry (Figure 4.2-7c,d) and the *cis* complexes  $C_2$  symmetry (Figure 4.2-7e,f). As expected,<sup>[108]</sup> the  $\text{OEF}_5$ -ligands coordinate primarily via their oxygen atom (with Hg-O distances between 201 and 204 pm) and thus form square-planar  $\text{HgO}_4$ - or  $\text{HgF}_2\text{O}_2$ -type primary coordination. Secondary interactions involve again one equatorial fluorine of each ligand. Distances of these secondary interactions tend to be between 274 and 288 pm, longer than in the previously discussed systems (similar, weak axial secondary  $\text{M}\cdots\text{F}$  contacts have been found by X-ray crystallography in - dimeric - square-planar coordinated  $\text{Au}[\text{OTeF}_5]_3$ <sup>[155]</sup>). Hg-O-E angles are similar in all complexes, close to  $118.0^\circ$ . This is smaller than the typical values of ca.  $125$ - $135^\circ$  found for other coordinated  $\text{OEF}_5$ -anions<sup>[114, 155]</sup> but similar to the values found for  $[\text{Au}(\text{OTeF}_5)_3]_2$ <sup>[155]</sup>, consistent with the presence of secondary  $\text{M}\cdots\text{F}$  contacts.

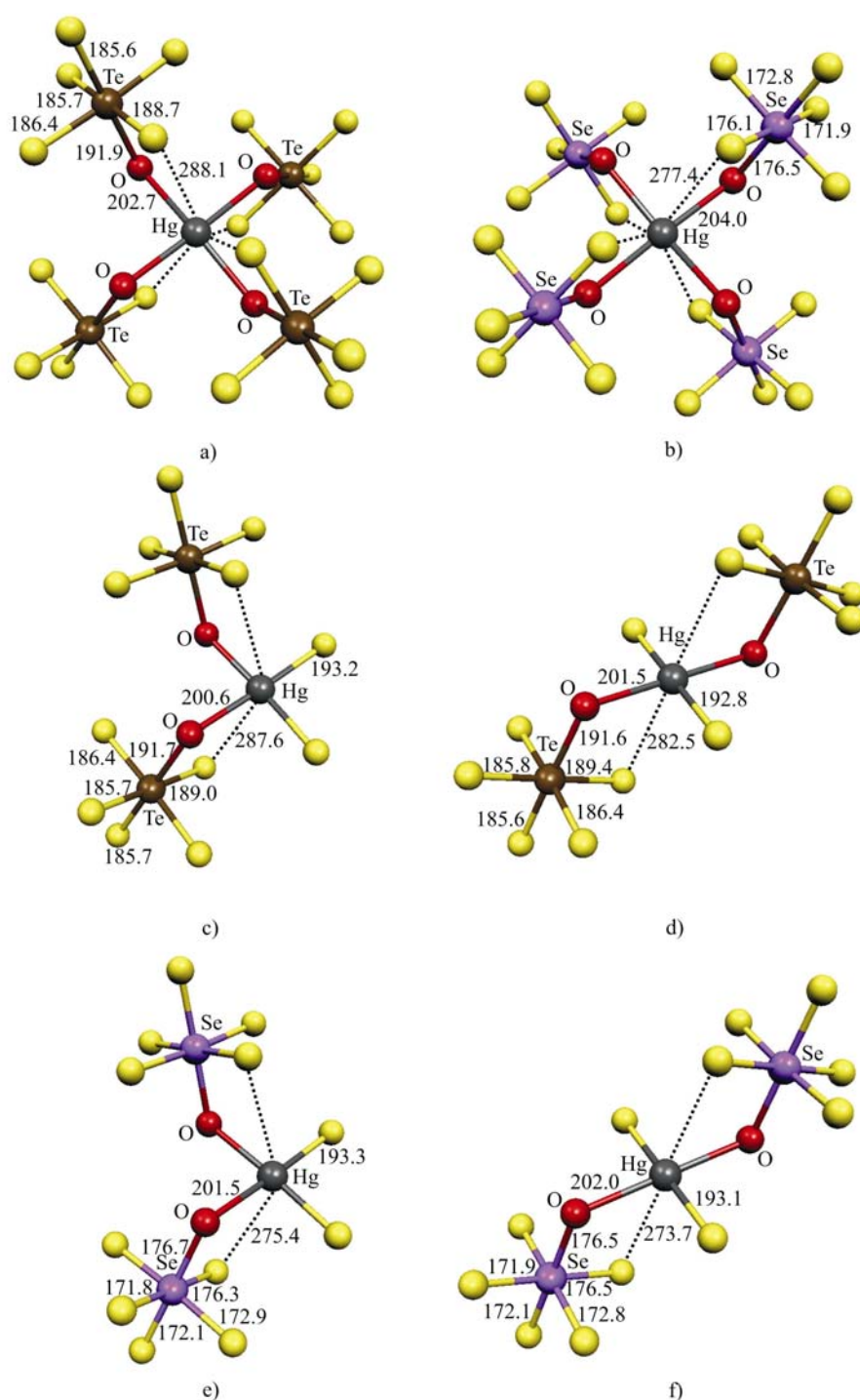


**Figure 4.2-7** Optimised structures for  $\text{Hg}^{\text{IV}}$  complexes with  $\text{OEF}_5$ -ligands. a)  $\text{Hg}[\text{OTeF}_5]_4$ . b)  $\text{Hg}[\text{OSeF}_5]_4$ . c) *cis*- $\text{HgF}_2[\text{OTeF}_5]_2$ . d) *trans*- $\text{HgF}_2[\text{OTeF}_5]_2$ . e) *cis*- $\text{HgF}_2[\text{OSeF}_5]_2$ . f) *trans*- $\text{HgF}_2[\text{OSeF}_5]_2$ .

The computed  $D_{2d}$  structure for  $\text{Hg}[\text{OTeF}_5]_4$  is similar to the experimentally determined X-ray structure of  $\text{Xe}[\text{OTeF}_5]_4$ <sup>[156]</sup>, except for a few details: a) the secondary axial  $\text{Xe}\cdots\text{F}$  contacts are much longer (around 320 pm,  $\text{Xe-O-Te}$  angles are around  $130^\circ$ ) than the optimised  $\text{M}\cdots\text{F}$  contacts; b) the orientation of the  $\text{OTeF}_5$ -ligands in

Xe[OTeF<sub>5</sub>]<sub>4</sub> was found to be up-up-down-down (*C*<sub>2h</sub>), in contrast to the more intuitive up-down-up-down alternating structure favored for the mercury complex – cf. Figure 4.2-7a. The latter point appears to be due to packing effects in the solid for the xenon system.<sup>[156]</sup> Our optimisations of Xe[OTeF<sub>5</sub>]<sub>4</sub> favour the alternating *D*<sub>2d</sub> arrangement over the nonalternating *C*<sub>2h</sub> one by ca. 10 kJ mol<sup>-1</sup>. The somewhat longer primary Hg-F bonds in the *cis*- compared to *trans*-HgF<sub>2</sub>[OEF<sub>5</sub>]<sub>2</sub> complexes reflect a very slightly larger *trans* influence of the OEF<sub>5</sub>-ligand compared to fluoride (whereas the Hg-O distances are somewhat longer in the *trans* complexes). The *cis* isomer of HgF<sub>2</sub>[OTeF<sub>5</sub>]<sub>2</sub> is slightly (about 6 kJ mol<sup>-1</sup>) more stable than the *trans* complex, in contrast to the other systems discussed above. The *trans*-isomer of the OSeF<sub>5</sub>-complex is favoured marginally (by ca 1.1 kJ mol<sup>-1</sup>). These results confirm that electronegativity and *trans* influence of the OEF<sub>5</sub>-anions are similar to those of the fluoride ion<sup>[108]</sup> – but see below for differences. This makes these ligands particularly attractive.

In contrast to the EF<sub>6</sub> ligands, the angles in the OEF<sub>5</sub> ligands are all close to ideal octahedral, as is well known for the coordinated ligand<sup>[108]</sup> (in the free anions, the O-E-F<sub>eq</sub> angles tend to be closer to 95°<sup>[157]</sup>). A slight lengthening of E-F distances for those equatorial fluorine atoms involved in secondary coordination to mercury is again apparent – see above. The other equatorial E-F bond lengths are similar to the axial bond *trans* to oxygen. This reflects a reduction of the *trans* influence of the oxygen atom within the ligand, due to its involvement in bonding to mercury. Structures of the OSeF<sub>5</sub>- and OTeF<sub>5</sub>-complexes are very similar, apart from the naturally shorter E-F and E-O bonds in the selenium systems. Dimensions within the ligands agree well with known structures.<sup>[108, 114]</sup>

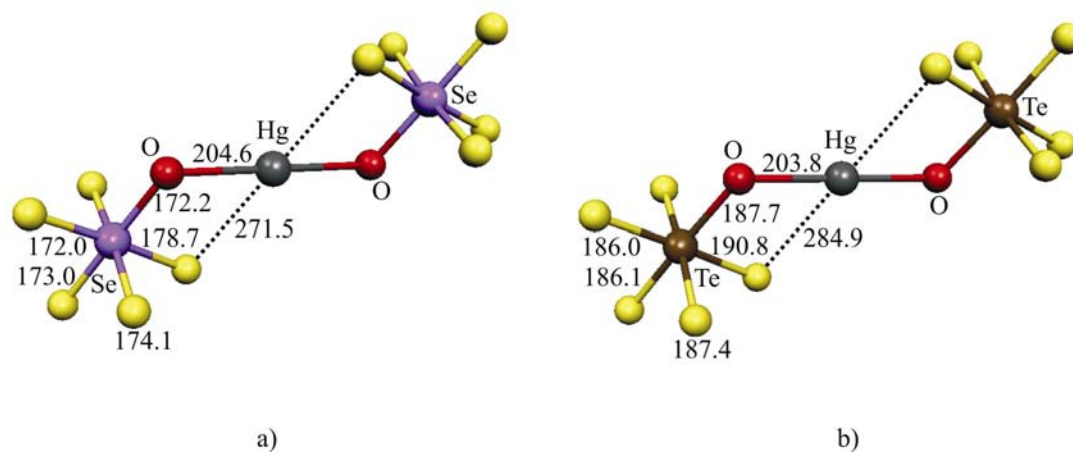


**Figure 4.2-8** Optimised structures for Hg<sup>II</sup> complexes with OEF<sub>5</sub>-ligands. a) Hg[OTeF<sub>5</sub>]<sub>2</sub>. b) Hg[OSeF<sub>5</sub>]<sub>2</sub>.

Computed structures for the  $C_{2h}$  symmetrical  $Hg^{II}$  complexes obtained after  $F_2$  elimination are shown in Figure 4.2-8. Notably, the coordination of mercury is not sixfold as with  $EF_6^-$  or  $E_2F_{11}$ -ligands, but effectively fourfold: Two primary bonds from the oxygen atoms of the two  $OEF_5$ -ligands are supplemented by substantially weaker secondary bonds from equatorial fluorine atoms of the ligands (the two secondary bonds are oriented mutually *trans* and thus render the overall metal coordination planar). Notably, the primary bond is slightly shorter with  $E = Te$ , whereas the secondary contact is appreciably longer. Interestingly, the secondary  $Hg^{II} \cdots F$  interactions feature distances that do not differ much from those seen in the  $Hg^{IV}$  complexes – cf. Figure 4.2-7.

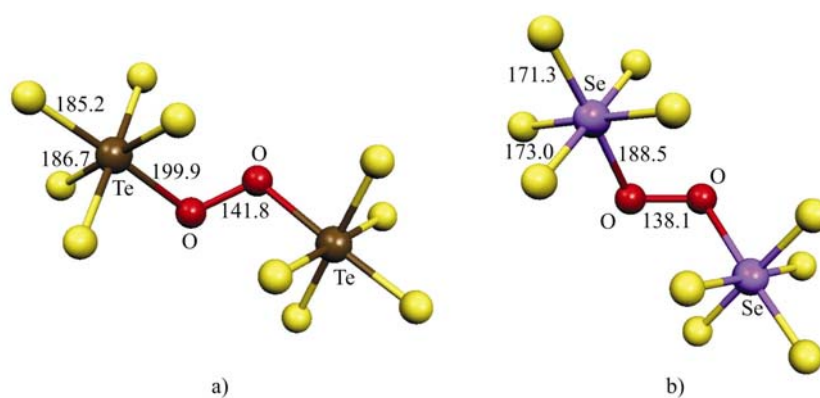


**Figure 4.2-9** Optimised structures for peroxide species  $[OTeF_5]_2$  and  $[OSeF_5]_2$ . a)  $[OTeF_5]_2$ . b)  $[OSeF_5]_2$ .

The other primary products of  $X_2$  elimination from  $HgX_4$  or of  $F_2$  elimination from  $HgF_2X_2$  are the peroxidic  $[OEF_5]_2$  dimers, shown in Figure 4.2-9. They exhibit  $C_2$  symmetry with an E-O-O-E dihedral angle of  $118.5^\circ$ , similar to the parent compound hydrogen peroxide. The O-O bond is somewhat shorter for the selenium system. The O-O distances in both systems are shorter than the computed O-O bond length of  $H_2O_2$  at the same level (145.3 pm). Experimental O-O bond lengths are  $145 \pm 4$  pm and  $148 \pm 1$  pm for  $F_5TeOOTEF_5$ <sup>[158]</sup> and  $H_2O_2$ <sup>[159]</sup>, respectively. It has been argued that the O-O bonds in the  $F_5EO-OEF_5$  derivatives are made particularly strong by the electron-withdrawing nature of the  $EF_5$ -substituents.<sup>[108]</sup> However, as we will show below, this is not the case.

#### 4.2.4 Thermochemical Stability of Hg<sup>IV</sup> versus Hg<sup>II</sup> Complexes

The most important decomposition channels towards which the Hg<sup>IV</sup> complexes may be unstable are a) elimination of F<sub>2</sub>, and b) elimination of X<sub>2</sub> (where possible). Elimination of FX was not explicitly considered, as the energies of this reaction are expected to be intermediate between those of the other two routes. We will thus investigate energies of the reactions HgF<sub>2</sub>X<sub>2</sub> → HgX<sub>2</sub> + F<sub>2</sub> and HgF<sub>2</sub>X<sub>2</sub> → HgF<sub>2</sub> + X<sub>2</sub>. The latter pathway is only a viable one for X = OEF<sub>5</sub> (E = Se, Te), as the X<sub>2</sub> elimination products will be unfavourable in the other cases. Elimination of F<sub>2</sub> may in some cases be followed in principle by subsequent reactions, e.g. Hg[EF<sub>6</sub>]<sub>2</sub> → HgF<sub>2</sub> + 2EF<sub>5</sub> (E = As, Sb). As these reactions are relevant with respect to the overall competitiveness of a given ligand set, we will also consider them. For the HgX<sub>4</sub> complexes, the reaction HgX<sub>4</sub> → HgX<sub>2</sub> + X<sub>2</sub> is expected to be competitive only for OEF<sub>5</sub>-ligands. In all other cases, F<sub>2</sub> elimination with ligand fragmentation is expected to be the dominant decomposition channel, e.g., as Hg[EF<sub>6</sub>]<sub>4</sub> → Hg[EF<sub>6</sub>]<sub>2</sub> + [EF<sub>5</sub>]<sub>2</sub> + F<sub>2</sub> (E = As, Sb).

[X]<sup>-</sup> = [AlF<sub>4</sub>]<sup>-</sup>, [Al<sub>2</sub>F<sub>7</sub>]<sup>-</sup>. As shown in Table 4.2-2, Hg[AlF<sub>4</sub>]<sub>4</sub> is rather unfavourable thermochemically. In addition to the exothermic F<sub>2</sub> elimination accompanied by ligand fragmentation, there is an even more exothermic channel that involves the attachment of intermediately formed AlF<sub>3</sub> entities to the initial elimination product Hg[AlF<sub>4</sub>]<sub>2</sub> to form the more stable Hg[Al<sub>2</sub>F<sub>7</sub>]<sub>2</sub>.

**Table 4.2-2** Computed reaction energies (in kJ mol<sup>-1</sup>) for complexes with AlF<sub>4</sub><sup>-</sup> and Al<sub>2</sub>F<sub>7</sub><sup>-</sup>-ligands.

Reaction	Structure	ΔE
Hg[AlF <sub>4</sub> ] <sub>4</sub> → Hg[AlF <sub>4</sub> ] <sub>2</sub> + [AlF <sub>3</sub> ] <sub>2</sub> + F <sub>2</sub>		-180.5
Hg[AlF <sub>4</sub> ] <sub>4</sub> → Hg[Al <sub>2</sub> F <sub>7</sub> ] <sub>2</sub> + F <sub>2</sub>		-307.0
HgF <sub>2</sub> [AlF <sub>4</sub> ] <sub>2</sub> → Hg[AlF <sub>4</sub> ] <sub>2</sub> + F <sub>2</sub>	<i>trans</i>	-106.3
HgF <sub>2</sub> [AlF <sub>4</sub> ] <sub>2</sub> → Hg[AlF <sub>4</sub> ] <sub>2</sub> + F <sub>2</sub>	<i>cis</i>	-100.9
HgF <sub>2</sub> [AlF <sub>4</sub> ] <sub>2</sub> → HgF[Al <sub>2</sub> F <sub>7</sub> ] + F <sub>2</sub>	<i>trans</i>	-93.4
HgF <sub>2</sub> [AlF <sub>4</sub> ] <sub>2</sub> → HgF[Al <sub>2</sub> F <sub>7</sub> ] + F <sub>2</sub>	<i>cis</i>	-88.0
HgF <sub>3</sub> [Al <sub>2</sub> F <sub>7</sub> ] → HgF[Al <sub>2</sub> F <sub>7</sub> ] + F <sub>2</sub>		-25.6
HgF <sub>3</sub> [Al <sub>2</sub> F <sub>7</sub> ] → Hg[AlF <sub>4</sub> ] <sub>2</sub> + F <sub>2</sub>		-38.5
HgF <sub>2</sub> [Al <sub>2</sub> F <sub>7</sub> ] <sub>2</sub> → Hg[Al <sub>2</sub> F <sub>7</sub> ] <sub>2</sub> + F <sub>2</sub>		-126.0
Hg[AlF <sub>4</sub> ] <sub>2</sub> → HgF <sub>2</sub> + [AlF <sub>3</sub> ] <sub>2</sub>		+129.2
Hg[Al <sub>2</sub> F <sub>7</sub> ] <sub>2</sub> → HgF <sub>2</sub> + 2 [AlF <sub>3</sub> ] <sub>2</sub>		+255.7
HgF[Al <sub>2</sub> F <sub>7</sub> ] → HgF <sub>2</sub> + [AlF <sub>3</sub> ] <sub>2</sub>		+116.3
[AlF <sub>3</sub> ] <sub>2</sub> → 2 AlF <sub>3</sub>		+188.7



We have not identified such extremely exothermic decomposition pathways for the  $\text{HgF}_2[\text{AlF}_4]_2$  isomers. Interestingly, the rearrangement product  $\text{HgF}_3[\text{Al}_2\text{F}_7]$  is about 60-70  $\text{kJ mol}^{-1}$  more stable than the latter complexes – see above and Figure 4.2-1. However, it appears an unlikely species to be formed in a superacid condensed-phase environment.  $\text{HgF}_2[\text{Al}_2\text{F}_7]_2$  decomposes also exothermically.

$[\text{X}]^- = [\text{EF}_6]^-$  (**M=As, Sb**). Table 4.2-3 summarises reaction energies for the  $\text{Hg}[\text{EF}_6]_4$  and  $\text{HgF}_2[\text{EF}_6]_2$  complexes. While all species are again thermochemically unstable towards elimination of  $\text{F}_2$ , the reaction energies are in the range from -60 to -120  $\text{kJ mol}^{-1}$ . The more favourable cases are thus less endothermic than the  $\text{AlF}_4$ - or  $\text{Al}_2\text{F}_7$ -complexes. The *cis*- $\text{HgF}_2[\text{EF}_6]_2$  complexes are marginally more stable than their *trans* isomers – cf. above. Interestingly, the  $\text{AsF}_6$ -complexes tend to be less endothermic than their  $\text{SbF}_6$ -analogues, in spite of the ready removal of  $\text{AsF}_5$  from  $\text{AsF}_6$ -ligands bound to  $\text{Hg}^{\text{IV}}$ . This has to do with the fact that the strongly endothermic fragmentation of the  $\text{Hg}[\text{EF}_6]_2$  elimination product into  $\text{HgF}_2$  and  $\text{EF}_5$  is energetically much more costly with  $\text{E} = \text{Sb}$  than with  $\text{E} = \text{As}$ . Indeed, the less favourable thermochemistry relative to gas-phase  $\text{HgF}_4$  may also be viewed as a consequence of the stronger binding of  $\text{EF}_5$  in the  $\text{Hg}^{\text{II}}$  species compared to the  $\text{Hg}^{\text{IV}}$  complexes. As this differential effect (Table 4.2-3) is more pronounced with  $\text{SbF}_6$ -ligands, the  $\text{Hg}^{\text{IV}}$  complexes with  $\text{AsF}_6$ -ligands exhibit a more favourable thermochemistry. This becomes even more pronounced when we consider that  $\text{SbF}_5$  has a much larger tendency to aggregate than  $\text{AsF}_5$  – cf. dimerization energies for  $\text{EF}_5$  in Table 4.2-3. Indeed,  $\text{SbF}_5$  is an oil at room temperature (mp. 8.3°C, bp. 141°C), with polymeric zig-zag chains of *cis*-interlinked octahedra.<sup>[115, 116]</sup> It exhibits tetramers in the solid-state. In the gas-phase at 252°C, dimers dominate.<sup>[115, 116]</sup> Already when we take into account the dimerization energy of  $\text{SbF}_5$  in computing the elimination energies (values in parentheses in Table 4.2-3), the  $\text{Hg}^{\text{IV}}$  complexes with  $\text{SbF}_6$ -ligands become still more unfavourable. Many of them are probably not competitive in the condensed phase.

In contrast,  $\text{AsF}_5$  shows little tendency to aggregate. At B3LYP level,  $\text{As}_2\text{F}_{10}$  is unbound. This may arise from a poor description of dispersion interactions by the DFT method used. MP2 calculations provide larger binding energies for both  $\text{As}_2\text{F}_{10}$  and  $\text{Sb}_2\text{F}_{10}$  (cf. Table 4.2-3) but confirm that the aggregation energy of  $\text{AsF}_5$  is indeed very small. At room temperature,  $\text{AsF}_5$  is a monomeric gas (mp. -79.8°C, bp. -52.8°C).<sup>[115, 116]</sup> This lack of aggregation is favourable for the stability of the  $\text{Hg}^{\text{IV}}$  complexes with  $\text{AsF}_6$ -ligands. While  $\text{AsF}_5$  is split off relatively easily from the  $\text{Hg}^{\text{IV}}$  complexes, and less so for

Hg[AsF<sub>6</sub>]<sub>2</sub>, the associated differential energy effect is less pronounced than for SbF<sub>6</sub>-ligands (Table 4.2-3). Moreover, there is little extra energetic penalty provided by aggregation of the elimination products. This makes complexes like HgF<sub>2</sub>[AsF<sub>6</sub>]<sub>2</sub> or Hg[AsF<sub>6</sub>]<sub>4</sub> good candidates for a mercury(IV) chemistry.

**Table 4.2-3** Computed reaction energies (in kJ mol<sup>-1</sup>) for complexes with EF<sub>6</sub>-ligands (E = As, Sb)

Reaction	Structure	ΔE
Hg[AsF <sub>6</sub> ] <sub>4</sub> → Hg[AsF <sub>6</sub> ] <sub>2</sub> + 2 AsF <sub>5</sub> + F <sub>2</sub>		-61.4 <sup>[a]</sup>
Hg[SbF <sub>6</sub> ] <sub>4</sub> → Hg[SbF <sub>6</sub> ] <sub>2</sub> + 2 SbF <sub>5</sub> + F <sub>2</sub>		-85.9 (-160.9) <sup>[b]</sup>
HgF <sub>2</sub> [AsF <sub>6</sub> ] <sub>2</sub> → Hg[AsF <sub>6</sub> ] <sub>2</sub> + F <sub>2</sub>	<i>cis</i>	-76.1
	<i>trans</i>	-76.8
HgF <sub>2</sub> [SbF <sub>6</sub> ] <sub>2</sub> → Hg[SbF <sub>6</sub> ] <sub>2</sub> + F <sub>2</sub>	<i>cis</i>	-110.5
	<i>trans</i>	-120.0
Hg[AsF <sub>6</sub> ] <sub>4</sub> → HgF <sub>4</sub> + 4 AsF <sub>5</sub>		+44.0 <sup>[a]</sup>
Hg[SbF <sub>6</sub> ] <sub>4</sub> → HgF <sub>4</sub> + 4 SbF <sub>5</sub>		+115.5 (-34.5) <sup>[b]</sup>
HgF <sub>2</sub> [AsF <sub>6</sub> ] <sub>2</sub> → HgF <sub>4</sub> + 2AsF <sub>5</sub>	<i>cis</i>	+29.3
	<i>trans</i>	+25.2
HgF <sub>2</sub> [SbF <sub>6</sub> ] <sub>2</sub> → HgF <sub>4</sub> + 2SbF <sub>5</sub>	<i>cis</i>	+91.5 (+16.5) <sup>[b]</sup>
	<i>trans</i>	+82.0 (+6.0) <sup>[b]</sup>
Hg[AsF <sub>6</sub> ] <sub>2</sub> → HgF <sub>2</sub> + 2 AsF <sub>5</sub>		+150.6
Hg[SbF <sub>6</sub> ] <sub>2</sub> → HgF <sub>2</sub> + 2 SbF <sub>5</sub>		+247.2 (+172.2) <sup>[b]</sup>
As <sub>2</sub> F <sub>10</sub> → 2 AsF <sub>5</sub>		-19.6 <sup>[c]</sup>
Sb <sub>2</sub> F <sub>10</sub> → 2 SbF <sub>5</sub>		+75.0 <sup>[c]</sup>

<sup>[a]</sup>Cf. HgF<sub>2</sub>[AsF<sub>6</sub>]<sub>2</sub>·2AsF<sub>5</sub>-type structure for Hg[AsF<sub>6</sub>]<sub>4</sub> in Figure 4.2-3a. <sup>[b]</sup>Values in parentheses obtained after taking into account dimerization of SbF<sub>5</sub>. <sup>[c]</sup>MP2 values are +13.2 kJ mol<sup>-1</sup> and +109.9 kJ mol<sup>-1</sup> for As<sub>2</sub>F<sub>10</sub> and Sb<sub>2</sub>F<sub>10</sub>, respectively.

[X]<sup>-</sup> = [E<sub>2</sub>F<sub>11</sub>]<sup>-</sup> (E = As, Sb). The trends discussed for the EF<sub>6</sub>-ligands become even more pronounced for the dinuclear E<sub>2</sub>F<sub>11</sub>-ligands (Table 4.2-4). We did not find a stable minimum for Hg[Sb<sub>2</sub>F<sub>11</sub>]<sub>4</sub>, and Hg[As<sub>2</sub>F<sub>11</sub>]<sub>4</sub> is essentially HgF<sub>4</sub> with only loosely connected AsF<sub>5</sub> units – cf. Figure 4.2-5a. The ready extrusion of AsF<sub>5</sub> from As<sub>2</sub>F<sub>11</sub>-ligands bound to Hg<sup>IV</sup> is apparent (Table 4.2-4). Table 4.2-4 contains also data for the free E<sub>2</sub>F<sub>11</sub>-anions. Together, these data indicate that the energy cost of removing an AsF<sub>5</sub>-ligand from an As<sub>2</sub>F<sub>11</sub>-unit costs about +20-25 kJ mol<sup>-1</sup> when the ligand is bound to Hg<sup>IV</sup>,



about +55-60 kJ mol<sup>-1</sup> in Hg<sup>II</sup>[As<sub>2</sub>F<sub>11</sub>]<sub>2</sub>, and ca. +78 kJ mol<sup>-1</sup> in the free anion. The corresponding values for Sb<sub>2</sub>F<sub>11</sub>-ligands are ca. +107 kJ mol<sup>-1</sup>, ca. +167 kJ mol<sup>-1</sup>, and ca. +130 kJ mol<sup>-1</sup>, respectively (Table 4.2-4). This indicates on one side that the antimony systems are held together more tightly, consistent with the higher Lewis-acidity of SbF<sub>5</sub> compared to AsF<sub>5</sub><sup>[113]</sup> – cf. also dimerization energies of EF<sub>5</sub> in Table 4.2-3. Indeed, the As<sub>2</sub>F<sub>11</sub>-unit is less well known and characterised than its Sb analogue.<sup>[160, 161]</sup> On the other side, differential binding effects within the E<sub>2</sub>F<sub>11</sub>-ligands will favour particularly the Hg<sup>II</sup> complexes and thus disfavour the Hg<sup>IV</sup> complexes (Table 4.2-4). This has to do with the more ionic bonding in the Hg<sup>II</sup> compared to the Hg<sup>IV</sup> complexes, which gives rise to less destabilisation of the *trans* E-F bonds in the coordinated ligands – cf. 4.3.

**Table 4.2-4** Computed reaction energies (in kJ mol<sup>-1</sup>) for complexes with E<sub>2</sub>F<sub>11</sub>-ligands (E = As, Sb)

Reaction	Structure	ΔE
Hg[As <sub>2</sub> F <sub>11</sub> ] <sub>4</sub> → Hg[As <sub>2</sub> F <sub>11</sub> ] <sub>2</sub> + 4 AsF <sub>5</sub> + F <sub>2</sub>		-83.6 <sup>[a]</sup>
HgF[Sb <sub>2</sub> F <sub>11</sub> ] <sub>3</sub> → Hg[Sb <sub>2</sub> F <sub>11</sub> ] <sub>2</sub> + F <sub>2</sub> + 2 SbF <sub>5</sub>		-128.5 (-203.5) <sup>[b]</sup>
HgF <sub>2</sub> [As <sub>2</sub> F <sub>11</sub> ] <sub>2</sub> → Hg[As <sub>2</sub> F <sub>11</sub> ] <sub>2</sub> + F <sub>2</sub>	<i>cis</i>	-109.7 <sup>[c]</sup>
	<i>trans</i>	-111.4 <sup>[c]</sup>
HgF <sub>2</sub> [Sb <sub>2</sub> F <sub>11</sub> ] <sub>2</sub> → Hg[Sb <sub>2</sub> F <sub>11</sub> ] <sub>2</sub> + F <sub>2</sub>	<i>cis</i>	-171.1
	<i>trans</i>	-180.3
Hg[As <sub>2</sub> F <sub>11</sub> ] <sub>4</sub> → HgF <sub>2</sub> [As <sub>2</sub> F <sub>11</sub> ] <sub>2</sub> + 4 AsF <sub>5</sub>	<i>cis</i>	+26.1 <sup>[a,c]</sup>
	<i>trans</i>	+27.8 <sup>[a,c]</sup>
Hg[As <sub>2</sub> F <sub>11</sub> ] <sub>4</sub> → HgF <sub>4</sub> + 8 AsF <sub>5</sub>		+78.5 <sup>[a]</sup>
HgF <sub>2</sub> [As <sub>2</sub> F <sub>11</sub> ] <sub>2</sub> → HgF <sub>2</sub> [AsF <sub>6</sub> ] <sub>2</sub> + 2AsF <sub>5</sub>	<i>cis</i>	+23.1 <sup>[c]</sup>
	<i>trans</i>	+25.5 <sup>[c]</sup>
HgF <sub>2</sub> [Sb <sub>2</sub> F <sub>11</sub> ] <sub>2</sub> → HgF <sub>2</sub> [SbF <sub>6</sub> ] <sub>2</sub> + 2SbF <sub>5</sub>	<i>cis</i>	+107.0 (+32.0) <sup>[b]</sup>
	<i>trans</i>	+107.3 (+32.3) <sup>[b]</sup>
Hg[As <sub>2</sub> F <sub>11</sub> ] <sub>2</sub> → Hg[AsF <sub>6</sub> ] <sub>2</sub> + 2AsF <sub>5</sub>		+56.8
Hg[Sb <sub>2</sub> F <sub>11</sub> ] <sub>2</sub> → Hg[SbF <sub>6</sub> ] <sub>2</sub> + 2SbF <sub>5</sub>		+167.6 (+92.8) <sup>[b]</sup>
As <sub>2</sub> F <sub>11</sub> <sup>-</sup> → AsF <sub>6</sub> <sup>-</sup> + AsF <sub>5</sub>		+78.5
Sb <sub>2</sub> F <sub>11</sub> <sup>-</sup> → SbF <sub>6</sub> <sup>-</sup> + SbF <sub>5</sub>		+130.5

<sup>[a]</sup>Cf. Figure 4.2-5a for the “HgF<sub>4</sub>·8AsF<sub>5</sub>-type” structure of Hg[As<sub>2</sub>F<sub>11</sub>]<sub>4</sub>.

<sup>[b]</sup>Values in parentheses obtained after taking into account dimerization of SbF<sub>5</sub> (cf. Table 4.2-3). <sup>[c]</sup>Cf. Figure 4.2-5c,d for the “Hg[AsF<sub>6</sub>]<sub>2</sub>·2AsF<sub>5</sub>-type” structure of HgF<sub>2</sub>[As<sub>2</sub>F<sub>11</sub>]<sub>2</sub>.

As  $\text{EF}_5$  units are thus bound much more loosely in  $\text{Hg}[\text{E}_2\text{F}_{11}]_4$  or  $\text{HgF}_2[\text{E}_2\text{F}_{11}]_2$  than in  $\text{Hg}[\text{E}_2\text{F}_{11}]_2$  (cf. Figure 4.2-5,6), aggregation of the ligands to multinuclear entities shifts the  $\text{F}_2$  elimination reactions to the  $\text{Hg}^{\text{II}}$  side and is thus actually unfavourable for the stability of the  $\text{Hg}^{\text{IV}}$  complexes. However, the additional exothermicity is only about  $-20 \text{ kJ mol}^{-1}$  and about  $-30 \text{ kJ mol}^{-1}$  for  $\text{Hg}[\text{As}_2\text{F}_{11}]_4$  and for  $\text{HgF}_2[\text{As}_2\text{F}_{11}]_2$ , respectively (Table 4.2-3,4). In contrast,  $\text{HgF}_2[\text{Sb}_2\text{F}_{11}]_2$  features about  $60 \text{ kJ mol}^{-1}$  more exothermic fluorine elimination than  $\text{HgF}_2[\text{SbF}_6]_2$  (Table 4.2-3,4), consistent with the above discussion of more pronounced differential aggregation effects for the antimony species. Once we consider also aggregation of formed  $\text{SbF}_5$  (see above), the  $\text{Hg}^{\text{IV}}$  complexes with  $\text{Sb}_2\text{F}_{11}$ -ligands exhibit rather unfavourable thermochemistry. In contrast, the  $\text{As}_2\text{F}_{11}$ -complexes are only marginally less favourable than their respective  $\text{AsF}_6$ -analogues, and not much further energy penalty from aggregation of  $\text{AsF}_5$  has to be paid.

$[\text{X}]^- = [\text{OEF}_5]^-$  ( $\text{E} = \text{Se}, \text{Te}$ ). Of the systems studied in this work, the complexes  $\text{HgF}_2[\text{OEF}_5]_2$  ( $\text{E} = \text{Se}, \text{Te}$ ) are the only ones that are thermochemically stable towards elimination of  $\text{F}_2$ . The reaction energies (Table 4.2-5) are ca.  $+15\text{-}20 \text{ kJ mol}^{-1}$ , not far below the  $+44 \text{ kJ mol}^{-1}$  computed previously at the same theoretical level for the gas-phase reaction  $\text{HgF}_4 \rightarrow \text{HgF}_2 + \text{F}_2$ <sup>[12]</sup> – cf. Table 4.2-1. This is consistent with the similar *trans* influence of  $\text{OEF}_5$ - and fluorine-ligands.<sup>[108]</sup>

Unfortunately, the  $\text{OEF}_5$ -complexes have another pathway of elimination, namely  $\text{HgF}_2[\text{OEF}_5]_2 \rightarrow \text{HgF}_2 + [\text{OEF}_5]_2$  or  $\text{Hg}[\text{OEF}_5]_4 \rightarrow \text{Hg}[\text{OEF}_5]_2 + [\text{OEF}_5]_2$ , respectively – see above. Reaction energies for the former reaction range from ca.  $-100$  to ca.  $-110 \text{ kJ mol}^{-1}$  (without aggregation of  $\text{HgF}_2$ ), those for the latter reaction are between ca.  $-120$  and ca.  $-130 \text{ kJ mol}^{-1}$ . One might expect,<sup>[108]</sup> that this is due to the relatively strong O-O bonds in the peroxides  $\text{F}_5\text{EOOEF}_5$  compared to the weaker F-F bond in  $\text{F}_2$ .<sup>[162-164]</sup> However, the peroxide O-O bonds are only about  $15\text{-}20 \text{ kJ mol}^{-1}$  more stable than the F-F bond (Table 4.2-5). This is clearly not enough to explain the much more facile elimination of  $\text{X}_2$  compared to  $\text{F}_2$ . Notably, the O-O bonds in the substituted peroxides  $[\text{OEF}_5]_2$  are actually  $30\text{-}40 \text{ kJ mol}^{-1}$  weaker than in parent  $\text{H}_2\text{O}_2$  (Table 5), in spite of the smaller bond length<sup>1</sup> (the bond is slightly stronger with  $\text{E} = \text{Te}$  than with  $\text{E} = \text{Se}$ ). Thus, significantly weaker Hg-O than Hg-F bonds in the  $\text{Hg}^{\text{IV}}$  complexes must be the main reason for the more facile elimination of  $[\text{OEF}_5]_2$  compared to fluorine. This

<sup>1</sup> This lack of correlation between bond lengths and binding energies is not uncommon in the case of substitution by electronegative groups. It can be traced back to an interplay between electrostatic contraction effects and hybridization defects – see references [165] and [166] and references therein.

is confirmed by fragmentation energies in Table 4.2-5: breaking of the two Hg-OTeF<sub>5</sub> bonds costs only ca. 60 kJ mol<sup>-1</sup> (40 kJ mol<sup>-1</sup> for Hg-OSeF<sub>5</sub>), compared to ca. 190 kJ mol<sup>-1</sup> for two Hg-F bonds in HgF<sub>4</sub> – cf. Table 4.2-1. Similar values apply to Hg-F and Hg-OEF<sub>5</sub> bonds in mixed complexes (Table 4.2-5). The overall fragmentation energies HgX<sub>4</sub> → Hg + 4 X are more than 200 kJ mol<sup>-1</sup> lower for X = OEF<sub>5</sub> compared to X = F (Table 4.2-1,5; but they are still larger than for X = Cl, at least in the case of teflate).

**Table 4.2-5** Computed reaction energies (in kJ mol<sup>-1</sup>) for complexes with OEF<sub>5</sub>-ligands (E = Se, Te)

Reaction	Structure	ΔE
Hg[OSeF <sub>5</sub> ] <sub>4</sub> → Hg[OSeF <sub>5</sub> ] <sub>2</sub> + [OSeF <sub>5</sub> ] <sub>2</sub>		-131.8
Hg[OTeF <sub>5</sub> ] <sub>4</sub> → Hg[OTeF <sub>5</sub> ] <sub>2</sub> + [OTeF <sub>5</sub> ] <sub>2</sub>		-121.7
HgF <sub>2</sub> [OSeF <sub>5</sub> ] <sub>2</sub> → [OSeF <sub>5</sub> ] <sub>2</sub> + HgF <sub>2</sub>	<i>cis</i>	-111.3
	<i>trans</i>	-110.5
HgF <sub>2</sub> [OTeF <sub>5</sub> ] <sub>2</sub> → [OTeF <sub>5</sub> ] <sub>2</sub> + HgF <sub>2</sub>	<i>cis</i>	-98.4
	<i>trans</i>	-103.4
HgF <sub>2</sub> [OSeF <sub>5</sub> ] <sub>2</sub> → Hg[OSeF <sub>5</sub> ] <sub>2</sub> + F <sub>2</sub>	<i>cis</i>	+21.5
	<i>trans</i>	+22.3
HgF <sub>2</sub> [OTeF <sub>5</sub> ] <sub>2</sub> → Hg[OTeF <sub>5</sub> ] <sub>2</sub> + F <sub>2</sub>	<i>cis</i>	+21.4
	<i>trans</i>	+16.5
[OSeF <sub>5</sub> ] <sub>2</sub> → 2 ·OSeF <sub>5</sub>		+170.8
[OTeF <sub>5</sub> ] <sub>2</sub> → 2 ·OTeF <sub>5</sub>		+182.2
H <sub>2</sub> O <sub>2</sub> → 2 ·OH		+212.4 <sup>[a]</sup>
F <sub>2</sub> → 2 ·F		+154.1 <sup>[b]</sup>
Hg[OSeF <sub>5</sub> ] <sub>4</sub> → Hg[OSeF <sub>5</sub> ] <sub>2</sub> + 2 ·OSeF <sub>5</sub>		+39.0
Hg[OTeF <sub>5</sub> ] <sub>4</sub> → Hg[OTeF <sub>5</sub> ] <sub>2</sub> + 2 ·OTeF <sub>5</sub>		+60.4
Hg[OSeF <sub>5</sub> ] <sub>4</sub> → Hg + 4 ·OSeF <sub>5</sub>		+507.5
Hg[OTeF <sub>5</sub> ] <sub>4</sub> → Hg + 4 ·OTeF <sub>5</sub>		+553.2
HgF <sub>2</sub> [OSeF <sub>5</sub> ] <sub>2</sub> → Hg[OSeF <sub>5</sub> ] <sub>2</sub> + 2 ·F	<i>cis</i>	+175.7
	<i>trans</i>	+176.5
HgF <sub>2</sub> [OTeF <sub>5</sub> ] <sub>2</sub> → Hg[OTeF <sub>5</sub> ] <sub>2</sub> + 2 ·F	<i>cis</i>	+175.7
	<i>trans</i>	+170.7
HgF <sub>2</sub> [OSeF <sub>5</sub> ] <sub>2</sub> → HgF <sub>2</sub> + 2 ·OSeF <sub>5</sub>	<i>cis</i>	+59.5
	<i>trans</i>	+60.3
HgF <sub>2</sub> [OTeF <sub>5</sub> ] <sub>2</sub> → HgF <sub>2</sub> + 2 ·OTeF <sub>5</sub>	<i>cis</i>	+83.7
	<i>trans</i>	+78.8

<sup>[a]</sup>Experimental value 199.8 kJ mol<sup>-1</sup>, cf. <sup>[167]</sup> <sup>[b]</sup>Experimental value 154.2 kJ mol<sup>-1</sup>, cf. <sup>[168]</sup>

An expected advantage of the OEF<sub>5</sub>-ligands is the expected volatility of their Hg<sup>II</sup> complexes. To estimate the tendency towards aggregation, we have computed the dimers of Hg[OTeF<sub>5</sub>]<sub>4</sub> and Hg[OTeF<sub>5</sub>]<sub>2</sub>.

Both feature relatively weak intermolecular interactions and small distortions within the monomeric units. Dimerization energies are ca. -18.4 kJ mol<sup>-1</sup> and ca. -47.0 kJ mol<sup>-1</sup> for the Hg<sup>IV</sup> and Hg<sup>II</sup> system, respectively (without CP corrections). This should be compared to dimerization energies of ca. -33.3 kJ mol<sup>-1</sup> and ca. -60.7 kJ mol<sup>-1</sup> computed for HgF<sub>4</sub> and HgF<sub>2</sub>, respectively, at the same computational level – see refs. [73, 169] for *ab initio* results. This suggests appreciably lower energies of aggregation. In particular, Hg[OTeF<sub>5</sub>]<sub>2</sub> is not expected to aggregate to large units,<sup>[108, 114]</sup> whereas HgF<sub>2</sub> forms an ionic fluorite-type lattice. We note in passing, that dispersion effects are expected to be of minor importance for the aggregation of these particular fluorine-based systems,<sup>[169]</sup> and thus the DFT methods employed should provide reasonable estimates of the dimerization energies.

#### 4.2.5 Bonding Analysis

The role of relativistic effects in stabilizing Hg<sup>IV</sup>F<sub>4</sub> against reductive elimination was found to arise mainly from a relativistic destabilisation of Hg<sup>II</sup>F<sub>2</sub>, due to the relativistic contraction of the mercury 6s-orbital – see Chapter 2.5.1.<sup>[73]</sup> The corresponding loss of ionic bonding contributions on the Hg<sup>II</sup> side, and the resulting relative stabilisation of Hg<sup>IV</sup> depends thus on the presence of very electronegative ligands like fluorine. This explains partly why HgCl<sub>4</sub> or HgH<sub>4</sub> are predicted to be strongly endothermic compounds.<sup>[12, 74, 120]</sup> Electronegativity considerations were thus important for the choice of weakly coordinating anions as ligands in the present work.

Table 6 shows that the EF<sub>6</sub> ligands provide appreciably larger positive metal charge in the Hg<sup>II</sup> complexes, but only slightly more for the Hg<sup>IV</sup> systems. This may have to do partly with the tridentate bonding mode in the Hg[EF<sub>6</sub>]<sub>2</sub> complexes – cf. Figure 4.2-4. But even in the Hg<sup>IV</sup> complexes, the EF<sub>6</sub> ligands may be considered more electronegative than fluorine. From this point of view, they are a reasonable choice in the present context. We think that the less favourable thermochemistry compared to (gas-phase) HgF<sub>4</sub> is mainly due to the coordination number 6 in the Hg<sup>II</sup> complexes. Individual atomic charges within the ligands provide further interesting insights into the bonding. For example, they show a much larger ionicity of Sb-F compared to As-F bonds. This is responsible for the important, more pronounced tendency of the antimony systems to aggregate – see above.

**Table 4.2-6** Computed NPA fragment charges for EF<sub>6</sub>-complexes (E = As, Sb)

Species	Hg	F	EF <sub>6</sub>
HgF <sub>2</sub>	1.460	-0.730	
HgF <sub>4</sub>	2.113	-0.528	
Hg[AsF <sub>6</sub> ] <sub>2</sub>	1.721		-0.860
Hg[SbF <sub>6</sub> ] <sub>2</sub>	1.729		-0.865
<i>trans</i> -HgF <sub>2</sub> [AsF <sub>6</sub> ] <sub>2</sub>	2.162	-0.492	-0.589
<i>cis</i> -HgF <sub>2</sub> [AsF <sub>6</sub> ] <sub>2</sub>	2.161	-0.470	-0.611
<i>trans</i> -HgF <sub>2</sub> [SbF <sub>6</sub> ] <sub>2</sub>	2.190	-0.465	-0.630
<i>cis</i> -HgF <sub>2</sub> [SbF <sub>6</sub> ] <sub>2</sub>	2.180	-0.436	-0.654
Hg[AsF <sub>6</sub> ] <sub>4</sub>	2.164	-0.485 <sup>[a]</sup>	-0.597 <sup>[a]</sup>
Hg[SbF <sub>6</sub> ] <sub>4</sub>	2.204		-0.551

<sup>[a]</sup>Only two intact AsF<sub>6</sub>-ligands, cf. Figure 4.2-3a.

There has been appreciable discussion whether the OEF<sub>5</sub>-ligands (E = Se, Te) exhibit higher or lower electronegativity compared to fluorine. Different experimental measures gave rise to opposite conclusions.<sup>[108]</sup> The charges for the mercury complexes in Table 4.2-7 show a mixed situation: metal charges of the Hg<sup>II</sup>[OEF<sub>5</sub>]<sub>2</sub> complexes are somewhat more positive than in HgF<sub>2</sub>. This would suggest slightly larger electronegativity. The situation is reversed for the Hg<sup>IV</sup> complexes, with slightly lower negative charges for OEF<sub>5</sub> compared to F. This confirms the “soft” nature of the electronegativity concept. In any case, the NPA charges confirm the similarity of the electronegativities of OEF<sub>5</sub> and F.

**Table 4.2-7** Computed NPA fragment charges for OEF<sub>5</sub>-complexes (E = Se, Te)

Species	Hg	F	OEF <sub>5</sub>
HgF <sub>2</sub>	1.460	-0.730	
HgF <sub>4</sub>	2.113	-0.528	
Hg[OSeF <sub>5</sub> ] <sub>2</sub>	1.519		-0.760
Hg[OTeF <sub>5</sub> ] <sub>2</sub>	1.521		-0.760
<i>trans</i> -HgF <sub>2</sub> [OSeF <sub>5</sub> ] <sub>2</sub>	2.051	-0.533	-0.492
<i>cis</i> -HgF <sub>2</sub> [OSeF <sub>5</sub> ] <sub>2</sub>	2.053	-0.528	-0.499
<i>trans</i> -HgF <sub>2</sub> [OTeF <sub>5</sub> ] <sub>2</sub>	2.059	-0.529	-0.500
<i>cis</i> -HgF <sub>2</sub> [OTeF <sub>5</sub> ] <sub>2</sub>	2.061	-0.527	-0.503
Hg[OSeF <sub>5</sub> ] <sub>4</sub>	1.970		-0.493
Hg[OTeF <sub>5</sub> ] <sub>4</sub>	1.979		-0.495

Why are the Hg-OEF<sub>5</sub> bonds much weaker than the Hg-F bonds in the Hg<sup>IV</sup> species – cf. Table 4.2-1? Local charge differences around the donating atoms provide an explanation: due to the bonding of the oxygen atom in the OEF<sub>5</sub> complexes to two relatively electropositive centres (Hg and E), it acquires much larger negative charge (ca. –1.0) than the fluorine atoms (ca. –0.5) in HgF<sub>4</sub> or HgF<sub>2</sub>X<sub>2</sub>. This leads to appreciably larger antibonding interactions with the formally nonbonding d-electrons in the 5d<sup>8</sup> complex. This can be seen, e.g., from inspection of the highest occupied MOs of the HgF<sub>2</sub>[OTeF<sub>5</sub>]<sub>2</sub> systems (not shown), which exhibit much more pronounced Hg-O than Hg-F antibonding interactions. In consequence, the Hg-O bonds are weakened relative to Hg-F bonds due to the relatively high negative local charge on oxygen.

#### 4.2.6 Discussion and Suggestions for Experimental Investigation

None of the Hg<sup>IV</sup> complexes investigated here is thermochemically stable, as they all exhibit one exothermic pathway for reductive elimination. In the case of AlF<sub>4</sub><sup>-</sup>, Al<sub>2</sub>F<sub>7</sub><sup>-</sup>, EF<sub>6</sub><sup>-</sup> or E<sub>2</sub>F<sub>11</sub>-ligands (E = As, Sb), elimination of F<sub>2</sub> is exothermic with reaction energies varying between -60 kJ mol<sup>-1</sup> and -180 kJ mol<sup>-1</sup>. In this sense, the systems are clearly inferior to gas-phase HgF<sub>4</sub> which eliminates F<sub>2</sub> endothermically.<sup>[12, 72, 73, 120]</sup> However, based on previous estimates and the relatively high sublimation energy of HgF<sub>2</sub>,<sup>[73]</sup> we think that several of these complexes may provide a more favourable environment for Hg<sup>IV</sup> than HgF<sub>4</sub> itself in the condensed phase. Indeed, the relatively high sixfold coordination of many of the HgX<sub>2</sub> elimination products (Figure 4.2-2, 4, and 6) indicates that even these weakly coordinating anions are able to stabilise the more ionic Hg<sup>II</sup> better than the more covalent Hg<sup>IV</sup>. The situation is thus indeed intermediate between that of gas-phase and condensed-phase HgF<sub>4</sub>. We note also, that the more stable ones of the systems studied here are predicted to be less endothermic than (gas-phase) HgCl<sub>4</sub> or HgH<sub>4</sub> – cf. Table 4.2-1.<sup>[12, 74, 120]</sup>

Are the systems investigated here promising targets for experimental study? In view of the computed endothermicity of all complexes with respect to either F<sub>2</sub> or X<sub>2</sub> elimination, the answer to this question depends on the presence of sufficiently high activation barriers for the reductive elimination reactions. Unfortunately, the complicated electronic structure of the transition state does not allow us at this point to provide these activation barriers quantitatively. The transition state for H<sub>2</sub> elimination from HgH<sub>4</sub> in the gas-phase is comparably easy to locate.<sup>[12, 74]</sup> It exhibits C<sub>2v</sub> symmetry and is about 50 kJ mol<sup>-1</sup> above HgH<sub>4</sub> (about 250 kJ mol<sup>-1</sup> above HgH<sub>2</sub> + H<sub>2</sub>). Unfortunately, we found that the

barriers for F<sub>2</sub> elimination from HgF<sub>4</sub> and for Cl<sub>2</sub> elimination from HgCl<sub>4</sub> are much more difficult to compute, due to large non-dynamical correlation effects – see Chapter 4.1.<sup>[12]</sup> These seem to be related to repulsions between lone-pair electrons on the halide ligands and the semi-core 5p-shell on the metal. The transition state has in both cases appreciable multi-reference character and is not described correctly by single-reference coupled-cluster approaches or by DFT methods. As the active space for a multi-configuration self-consistent-field (CASSCF) wave function has to include the metal d-orbitals plus several orbitals from the ligands, the required expansions for a multi-reference configuration interaction (MR-CI) calculation are expected to be large. We currently perform such calculations for HgF<sub>4</sub> itself. However, there is no realistic chance to obtain reliable activation barriers for the larger systems studied here with currently available computational resources. DFT and CCSD(T) calculations, although certainly unreliable quantitatively, provided considerably larger barriers for the X<sub>2</sub> elimination from HgX<sub>4</sub> (X = F, Cl) than for X = H.<sup>[12]</sup> Intuitively, this appears reasonable, as the electronic reorganization upon splitting two Hg-X bonds, forming the X-X bond, and rearranging the HgX<sub>2</sub> framework is expected to be much more pronounced for the halide complexes than for their hydride analogue. This should hold largely also for the related, larger HgX<sub>4</sub> and HgF<sub>2</sub>X<sub>2</sub> systems studied here. It is therefore quite likely that most of the Hg<sup>IV</sup> systems investigated in this work will have appreciable barriers for F<sub>2</sub> and X<sub>2</sub> elimination. As the exothermicity of most elimination reactions computed is much more moderate than, e.g., that of HgH<sub>4</sub> → HgH<sub>2</sub> + H<sub>2</sub> (cf. Table 4.2-1-5), chances to observe some of the computed Hg<sup>IV</sup> minima appear quite realistic.

Thermochemically, the AsF<sub>6</sub><sup>-</sup> or As<sub>2</sub>F<sub>11</sub><sup>-</sup>-complexes are more favourable than their SbF<sub>6</sub><sup>-</sup> or Sb<sub>2</sub>F<sub>11</sub><sup>-</sup>-analogues, already when we consider only small molecular complexes as products. The computed thermochemistry of Hg<sup>IV</sup> complexes with SbF<sub>6</sub><sup>-</sup> or Sb<sub>2</sub>F<sub>11</sub><sup>-</sup>-ligands turned out to be somewhat disappointing. This became even clearer when the much more pronounced aggregation of SbF<sub>5</sub> compared to AsF<sub>5</sub> was taken into account. The exothermicity of F<sub>2</sub> elimination from Hg[AsF<sub>6</sub>]<sub>4</sub> or from HgF<sub>2</sub>[AsF<sub>6</sub>]<sub>2</sub> may be considered very moderate indeed. Moreover, we do also not expect much further stabilisation of the elimination products Hg<sup>II</sup>X<sub>2</sub> ([X]<sup>-</sup> = [AsF<sub>6</sub>]<sup>-</sup>, [As<sub>2</sub>F<sub>11</sub>]<sup>-</sup>) by aggregation. This may indeed leave appreciable room for finding suitable reaction conditions. The obvious practical disadvantage of an AsF<sub>5</sub> matrix (mp. -79.8°C, bp. -52.8°C) compared to an SbF<sub>5</sub> matrix (mp. 8.3°C, bp. 141°C) environment is the need to work at low temperatures. On the other hand, in view of the endothermicity of the target complexes,

and in the absence of reliable reaction barriers, low-temperature reaction conditions are in any case recommended. The high volatility of  $\text{AsF}_5$  might prove favourable for product isolation. Possible oxidation agents are elemental fluorine (possibly with irradiation to create fluorine atoms) or, e.g.,  $\text{KrF}_2$ .

Complexes with the  $\text{OEF}_5$ -anions ( $\text{E} = \text{Se}, \text{Te}$ ) are distinguished by their preference to bind primarily in a monodentate fashion via their single oxygen atom, even for the  $\text{Hg}^{\text{II}}$  elimination products – cf. Figure 4.2-8. Weak additional secondary bonding is present but appears both for the  $\text{Hg}^{\text{II}}$  and  $\text{Hg}^{\text{IV}}$  systems. Consequently, the complexes  $\text{HgF}_2[\text{OEF}_5]_2$  are the only systems studied here that exhibit endothermic elimination of  $\text{F}_2$ , with energetics that are almost competitive with those of gas-phase  $\text{HgF}_4$  – cf. Table 4.2-5. Notably, aggregation of the  $\text{Hg}^{\text{II}}$  complexes is expected to provide only relatively little further stabilisation relative to  $\text{Hg}^{\text{IV}}$  in these systems – cf. dimerization energies above. This agrees with the fact that the well-known  $\text{Hg}[\text{OEF}_5]_2$  complexes are essentially molecular. In contrast to  $\text{HgF}_2$  (but more like  $\text{HgCl}_2$ ), they are volatile and have a high vapor pressure even at room temperature. They sublime thus easily, and they dissolve molecularly in nonpolar solvents.<sup>[108, 114]</sup> Notably, the secondary  $\text{M}\cdots\text{F}$  contacts in the optimised structures appear to be comparable for the  $\text{Hg}^{\text{IV}}$  and  $\text{Hg}^{\text{II}}$  species – cf. Figure 4.2-7,8 respectively. We have thus come very close to our goal of an almost gas-phase-like environment in the condensed phase.

Unfortunately, the complexes of  $\text{OEF}_5$ -ligands are not unchallenged champions either, as they eliminate  $[\text{OEF}_5]_2$  exothermically, with energies that are similar to those of  $\text{F}_2$  elimination from some of the other systems studied here. As shown above, this is only in a small part due to the stronger O-O than F-F bond. It reflects mainly the destabilisation of the Hg-O bonds in the  $\text{Hg}^{\text{IV}}$  complexes by larger antibonding interactions. Another reaction pathway known for teflate complexes of transition metals in high oxidation states is elimination of  $\text{TeF}_6$  and  $\text{F}_5\text{TeOTeF}_5$  (e.g. to give  $\text{O}=\text{Re}[\text{OTeF}_5]_5$  from  $\text{Re}[\text{OTeF}_5]_7$ ).<sup>[108]</sup> This is very unlikely to occur in the present case, as steric crowding is not a problem for the  $\text{Hg}^{\text{IV}}$  complexes (anyway, the reaction would retain  $\text{Hg}^{\text{IV}}$ ).

In any case, the  $\text{Hg}[\text{OTeF}_5]_4$  and  $\text{HgF}_2[\text{OTeF}_5]_2$  complexes appear to be interesting targets for synthetic work. How could they be prepared? The  $\text{Hg}^{\text{II}}$  complexes  $\text{Hg}[\text{OEF}_5]_2$  ( $\text{E} = \text{Se}, \text{Te}$ ) are well known.<sup>[108, 164]</sup> They might be a good starting point. A variety of suitable reagents for oxidations are available, including  $\text{Xe}[\text{OTeF}_5]_2$ ,<sup>[108, 164]</sup>  $\text{Xe}[\text{OTeF}_5]_4$ ,<sup>[156]</sup> or the recently reported  $[\text{XeOTeF}_5][\text{Sb}(\text{OTeF}_5)_6]$ .<sup>[170]</sup>  $\text{B}[\text{OTeF}_5]_3$  is also a well-known reagent to transfer the  $\text{OTeF}_5$ -ligand.<sup>[108]</sup> It could be supplemented by a



suitable oxidation reagent. Moreover, the back-reaction of the exothermic  $X_2$  elimination in Table 4.2-5 appears attractive: photolytic cleavage of the peroxidic bond in  $[\text{OTeF}_5]_2$  would create the reactive  $\cdot\text{OTeF}_5$  radical, which should add exothermically to  $\text{Hg}[\text{OTeF}_5]_2$  – cf. Table 4.2-5. Characterisation of the  $\text{Hg}^{\text{IV}}$  complexes could be provided by IR spectroscopy, or by NMR for various nuclei ( $^{19}\text{F}$ ,  $^{17}\text{O}$ ,  $^{199}\text{Hg}$ ,  $^{125}\text{Te}$ ).<sup>[108]</sup>

**Table 4.2-8** Reaction energies (in  $\text{kJ mol}^{-1}$ ) for noble-gas complexes

Reaction	$\Delta E_{\text{calc}}$ <sup>[a]</sup>	$\Delta H_{\text{exp}}$ <sup>[b]</sup>
$\text{Xe}[\text{OTeF}_5]_4 \rightarrow \text{Xe}[\text{OTeF}_5]_2 + [\text{OTeF}_5]_2$ ( $D_{2d}$ ) <sup>[c]</sup>	-139.2	
$\text{Xe}[\text{OTeF}_5]_4 \rightarrow \text{Xe}[\text{OTeF}_5]_2 + [\text{OTeF}_5]_2$ ( $C_{2h}$ ) <sup>[d]</sup>	-149.0	
$\text{Xe}[\text{TeOF}_5]_2 \rightarrow \text{Xe} + [\text{OTeF}_5]_2$	-80.7 (MP2 -66.4)	
$\text{Kr}[\text{TeOF}_5]_2 \rightarrow \text{Kr} + [\text{OTeF}_5]_2$	-194.3 (MP2 -96.5)	
$\text{Xe}[\text{TeOF}_5]_2 \rightarrow \text{Xe} + 2 \cdot\text{OTeF}_5$	+101.5 (MP2 +181.4)	
$\text{Kr}[\text{TeOF}_5]_2 \rightarrow \text{Kr} + 2 \cdot\text{OTeF}_5$	-12.2 (MP2 +151.3)	
$[\text{OTeF}_5]_2 \rightarrow 2 \cdot\text{OTeF}_5$	+182.2 (MP2 +247.8)	
$\text{XeF}_4 \rightarrow \text{XeF}_2 + \text{F}_2$	+72.5 (MP2 +86.5)	+119.5
$\text{XeF}_2 \rightarrow \text{Xe} + \text{F}_2$	+93.6 (MP2 +86.7)	+117.9
$\text{KrF}_2 \rightarrow \text{Kr} + \text{F}_2$	-46.6 (MP2 -65.7)	-60.2
$\text{XeF}_2 \rightarrow \text{Xe} + 2 \cdot\text{F}$	+247.8	+267.5
$\text{KrF}_2 \rightarrow \text{Kr} + 2 \cdot\text{F}$	+107.5	+97.8

<sup>[a]</sup>B3LYP results with MP2 values in parentheses. <sup>[b]</sup>Cf. <sup>[171]</sup> Note that the reported experimental energies are not completely consistent with the binding energy of  $\text{F}_2$  (cf. footnote b to Table 4.2-5). <sup>[c]</sup>More stable alternating structure of  $\text{Xe}[\text{OTeF}_5]_4$ . <sup>[d]</sup>Less stable nonalternating arrangement of  $\text{Xe}[\text{OTeF}_5]_4$  as found in the solid-state structure (ref. <sup>[156]</sup>).

The comparison with noble-gas teflate complexes provides further support for our optimistic view on the possible preparation of  $\text{Hg}^{\text{IV}}$  teflate systems:  $\text{Xe}[\text{OTeF}_5]_2$  exhibits surprisingly large thermal stability and decomposes only above ca. 130°C ( $\text{Xe}[\text{OSeF}_5]_2$  is only slightly less stable).<sup>[108, 164]</sup> Nevertheless, our computations show that  $\text{Xe}[\text{OTeF}_5]_2$  is endothermic with respect to elimination of  $[\text{OTeF}_5]_2$ , with a reaction energy in a similar range as computed for the  $\text{Hg}^{\text{IV}}$  complexes (Table 4.2-8). Similarly,  $\text{Xe}[\text{OTeF}_5]_4$  is well known but computed to eliminate  $[\text{OTeF}_5]_2$  with even slightly larger exothermicity than

$\text{Hg}[\text{OTeF}_5]_4$  – cf. Table 4.2-5 and 8. There is even some NMR evidence for the formation of  $\text{Kr}[\text{OTeF}_5]_2$ , the first compound with a Kr-O bond, in cocondensation reactions between  $\text{KrF}_2$  and  $\text{B}[\text{OTeF}_5]_3$ , although the compound could not be isolated in pure form.<sup>[172]</sup> According to our computations,  $\text{Kr}[\text{OTeF}_5]_2$  is more endothermic than any of our  $\text{Hg}^{\text{IV}}$  teflate candidates. Actually, our calculations give even a slightly negative energy for fragmentation into  $\text{Kr} + 2 \cdot \text{OTeF}_5$  (Table 4.2-8). For this rather unstable system, the DFT results are probably too low (our validation did not include such noble-gas systems). MP2 calculations provide more positive fragmentation energies, which in turn are probably far too high (MP2 and B3LYP agree much better with each other – and with available experimental data - for more stable Ng fluoride systems; cf. Table 4.2-8). In any case, the thermochemical viability of many of the  $\text{Hg}^{\text{IV}}$  complexes studied here appears superior to that of  $\text{Xe}[\text{OTeF}_5]_4$  or  $\text{Kr}[\text{OTeF}_5]_2$ . As in the  $\text{Hg}^{\text{IV}}$  case (see above), elimination of  $[\text{OTeF}_5]_2$  from the noble-gas teflate complexes is much more facile than that of  $\text{F}_2$  from the fluorides (Table 4.2-8), reflecting appreciably weaker Ng- $\text{OTeF}_5$  than Ng-F bonds. Finally, there exists also the well-known  $\text{KrF}_2$  (Table 4.2-8), which exhibits an endothermicity that is not much lower than that discussed for several of our more promising target systems.

### 4.2.7 Conclusions

The quest for  $\text{Hg}^{\text{IV}}$  continues. Promising avenues exist, which have not yet been pursued experimentally. On one hand we think that the matrix-isolation route to  $\text{HgF}_4$  deserves more attention than it received hitherto. On the other hand, the present work provides a quantum-chemical study of species that might be obtainable in the bulk condensed phase and could thus open a true  $\text{Hg}^{\text{IV}}$  chemistry. While all  $\text{Hg}^{\text{IV}}$  complexes discussed here exhibit one pathway of exothermic reductive elimination, we have reason to believe that many systems will have nonnegligible activation barriers along the way and might thus be observable, at least at low temperatures. This holds in particular for complexes like  $\text{Hg}[\text{OTeF}_5]_4$  or  $\text{Hg}[\text{AsF}_6]_4$ . We have furthermore suggested a number of possible synthetic routes towards such systems. However, we are convinced that the ingenuity of our experimentalist colleagues will come up with further options that we have not been able to envision. Chances to finally enter experimentally into  $\text{Hg}^{\text{IV}}$  chemistry are therefore good.

## 4.3 Has AuF<sub>7</sub> Been Made?<sup>[173]</sup>

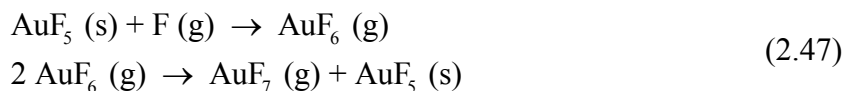
### 4.3.1 Introduction

Pushing the known oxidation states for a main group element or transition metal to the highest possible values is often achieved by utilizing fluorine or oxygen ligands, due to their small size and high electronegativity. The highest oxidation states for the late transition elements are known for their fluorides, e.g., in the case of IrF<sub>6</sub>,<sup>[174]</sup> RhF<sub>6</sub><sup>[175]</sup> or PtF<sub>6</sub><sup>[176, 177]</sup> (claims for high oxidation states in compounds with less electronegative ligands often do not stand up to closer scrutiny of the bonding situation, as e.g. in a recent case of a Pd<sup>VI</sup> complex with supposedly six silyl ligands<sup>[102-105]</sup> – see Chapter 3).

In the case of gold, the highest oxidation state that is experimentally known beyond doubt is Au<sup>V</sup> in the form of various salts of the [AuF<sub>6</sub>]<sup>-</sup> anion,<sup>[178]</sup> and as [AuF<sub>5</sub>]<sub>2</sub>.<sup>[179, 180]</sup> Indeed, the pronounced instability of the monofluoride AuF, which has been obtained only relatively recently, is related to the relativistic destabilisation of the lower +I relative to the higher +III oxidation state in the presence of electronegative ligands.<sup>[181-183]</sup> For similar reasons, ongoing speculations about mercury or element 112 in oxidation state +IV concentrate on the tetrafluorides or on closely related species with very electronegative ligands – see Chapters 4.1 and 4.2.<sup>[12, 72, 73, 75, 76]</sup>

Could gold be oxidised even beyond the +V oxidation state? Almost 20 years ago, the isolation of AuF<sub>7</sub> has been claimed, based on the reaction of solid AuF<sub>5</sub> with atomic fluorine in a vacuum – cf. eq. (2.47) – followed by condensation of the reaction products at liquid-nitrogen temperature, and measurement of their IR and molecular weight data.<sup>[20, 184]</sup> AuF<sub>7</sub> was described as a volatile substance that is stable at room temperature but decomposes at 100°C. However, these claims have never been substantiated nor refuted by other groups, although the observed ready decomposition of [KrF]<sup>+</sup>[AuF<sub>6</sub>]<sup>-</sup> into AuF<sub>5</sub> and F<sub>2</sub> may be viewed as a strong indication of the instability of AuF<sub>7</sub>.<sup>[185]</sup> Even the known 5d hexafluorides range only up to platinum and do not encompass gold.<sup>[186]</sup> It is not clear why the maximum oxidation state should be higher for Au than for Pt. A theoretical study on [AuF<sub>6</sub>]<sup>q-</sup> (q=0,1,2,3) species identified the [AuF<sub>6</sub>]<sup>-</sup> anion as the preferred minimum with respect to molecular charge q.<sup>[187]</sup> AuF<sub>6</sub> has been estimated to have an enormous adiabatic electron

affinity of about 9.5-10.5 eV.<sup>[187-189]</sup> This sheds some doubt on the existence of gold oxidation states beyond +V and on the feasibility of the route described by eq. (2.47). Nevertheless, AuF<sub>7</sub> is sometimes mentioned in the literature as established Au<sup>VII</sup> species.<sup>[190, 191]</sup>



In the next sections approach the question of the existence of oxidation states Au<sup>VI</sup> and Au<sup>VII</sup> by state-of-the-art quantum-chemical calculations.

### 4.3.2 Computational Details

Calculations have been performed at various levels of density functional theory (DFT) and at *ab initio* levels up to CCSD(T). For the HF, MP2 and DFT calculations we used the Gaussian03<sup>[192]</sup> program and the analytical gradient methods implemented therein. The gradient-corrected BP86<sup>[46, 129]</sup> functional, the hybrid functionals B3LYP<sup>[192]</sup> (based on the work of Becke)<sup>[53]</sup> with 20% HF exchange admixture and the “half-and-half” hybrid functional<sup>[192],[52]</sup> with 50% HF exchange (in the following abbreviated BHLYP) were used. This selection of functionals was chosen on purpose, as our experience with similar high-oxidation-state species taught us that the thermochemistry of the redox reactions of such complexes depend crucially on the amount of exact-exchange admixture. Coupled-cluster calculations with single and double substitutions (CCSD), as well as with inclusion of perturbative triple excitations [CCSD(T) level] were carried out with the MOLPRO 2002.6<sup>[193]</sup> program package. All species have been fully optimised at a given computational level, except for some transition states, where coupled-cluster single-point energies were computed at various DFT-optimised structures.

Scalar relativistic effects for gold and platinum were included by a quasirelativistic energy-adjusted, small-core pseudopotential.<sup>[194]</sup> The corresponding (8s6p5d)/[7s3p4d] valence basis set was augmented by two f-type polarization functions. The diffuse function ( $\alpha = 0.2$ ) maximises the static polarizability, and the compact f-function ( $\alpha = 1.0$ ) improves the description of the primary covalent bonding to the metal.<sup>[78]</sup> Calculations for the present systems without these two f-functions led to ca. 2 pm larger bond lengths (data not shown). The fluorine atom was described by an all-electron (9s5p1sp1d)/[4s2p1sp1d]-Dunning-DZ+P<sup>[132]</sup> basis set.

Basis-set superposition errors (BSSE) were evaluated by counterpoise corrections (CP)<sup>[98, 195]</sup> at optimised structures. Zero-point vibrational energy (ZPE) corrections were computed at DFT and *ab initio* levels up to MP2. Spin-orbit (SO) coupling was neglected. Based on our own experience for mercury fluorides<sup>[73]</sup> and on results of other groups for gold complexes,<sup>[196]</sup> SO effects are expected to influence reaction energies involving only closed-shell species negligibly. In the case of the open-shell AuF<sub>6</sub>, we cannot exclude completely some influence of SO effects, but as they derive mainly from the 5d shell, they should not yet be too dramatic either.

### 4.3.3 Structures of Au<sup>V</sup>, Au<sup>VI</sup>, and Au<sup>VII</sup> Fluorides.

Structural data for various species are compared in Table 4.3-1 and 2, and some structures are shown in Figure 4.3-1 - 4. For d<sup>6</sup> Au<sup>V</sup> we have considered monomeric AuF<sub>5</sub>, [AuF<sub>6</sub>]<sup>-</sup>, the dimer [AuF<sub>5</sub>]<sub>2</sub>, and the trimer [AuF<sub>5</sub>]<sub>3</sub>. Before going into the comparison between theory and experiment for individual molecules, it is appropriate to note that comparison of our B3LYP results with relativistic Au PP provide generally about 4-5 pm shorter bond lengths than comparative calculations with a nonrelativistic PP (last column in Table 4.3-1).

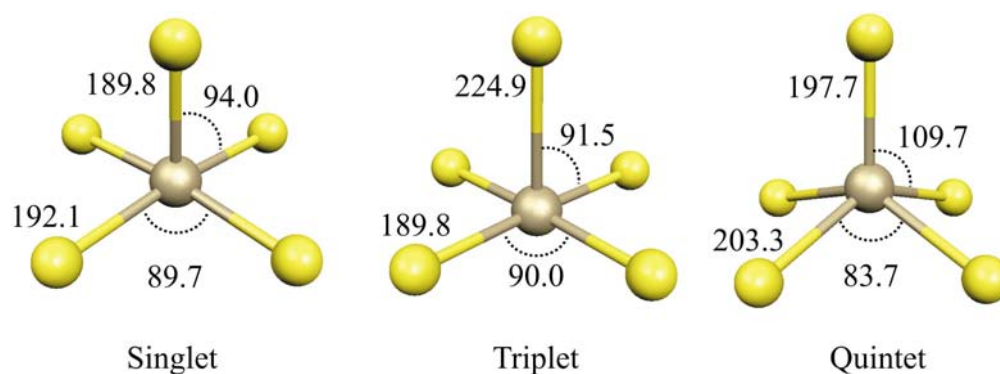


**Figure 4.3-1** B3LYP-optimised structures for ground and excited-states of AuF<sub>5</sub>. a) singlet ground-state, b) lowest triplet excited-state, c) lowest quintet excited-state. All three states exhibit C<sub>4v</sub> minima on their potential energy surfaces (cf. text).

Our calculations for AuF<sub>5</sub> monomer indicate a square pyramidal (C<sub>4v</sub>) minimum (Table 4.3-1, Figure 4.3-1a), which may scramble its fluorine atoms easily via a trigonal bipyramidal transition state at 9.5 kJ mol<sup>-1</sup> (B3LYP level). We note in passing that BP86 calculations gave a slight puckering of the fluorine ligands in the basal plane of the square-pyramidal minimum structure, with only a marginal stabilisation by 3.4 kJ mol<sup>-1</sup> relative to the C<sub>4v</sub> structure. As

expected, the [AuF<sub>6</sub>]<sup>−</sup> anion exhibits an octahedral (*O<sub>h</sub>*) minimum with an Au-F distance of 193.9 pm at B3LYP level – see Table 4.3-1. Experimentally determined distances in the solid state are somewhat shorter, between 185 and 190 pm (with deviations from an ideal octahedron due to interactions with the countercations).<sup>[179, 185, 190, 197-199]</sup>

**Table 4.3-1** Optimised minimum structures of AuF<sub>5</sub>, [AuF<sub>6</sub>]<sup>−</sup>, AuF<sub>6</sub> and AuF<sub>7</sub><sup>[a]</sup>

Species	HF	MP2	CCSD	CCSD(T)	BP86 <sup>[b]</sup>	BHLYP	B3LYP	<i>nrel.</i> B3LYP <sup>[c]</sup>
<b>AuF<sub>5</sub> (<i>C<sub>4v</sub></i>)</b>								
Au-F <sub>ax</sub>	180.5	188.8	186.7	189.0	192.2	183.7	188.2	193.9
Au-F <sub>eq</sub>	185.8	193.0	190.5	192.3	193.5 (193.9)	188.4	192.1	196.2
∠ (F <sub>ax</sub> -Au-F <sub>eq</sub> )	92.3	92.7	92.5	92.7	85.4 (106.7)	92.9	94.0	93.5
<i>T<sub>J</sub></i> -diagnostic			0.0209	0.0213				
<b>[AuF<sub>6</sub>]<sup>−</sup> (<i>O<sub>h</sub></i>)</b>								
Au-F	187.1	194.3	191.6	193.2	195.8	189.9	193.9	198.1
<i>T<sub>J</sub></i> -diagnostic			0.0186	0.0188				
<b>AuF<sub>6</sub> (<i>D<sub>2h</sub></i>)</b>								
Au-F <sub>ax</sub>	182.1	184.1			192.5		189.9	
Au-F <sub>eq</sub>	186.0	194.7			193.3		191.1	
∠ (F <sub>ax</sub> -Au-F <sub>eq</sub> )	90.0	90.0			90.0		90.0	
∠ (F <sub>eq</sub> -Au-F <sub>eq</sub> )	90.6 (89.4)	90.7 (89.3)			89.6 (90.4)		90.5 (89.5)	
<b>AuF<sub>7</sub> (<i>D<sub>5h</sub></i>)</b>								
Au-F <sub>ax</sub>	186.1	195.5	191.3	194.4	195.3	189.2	193.4	197.2
Au-F <sub>eq</sub>	188.9	196.4	194.1	197.3	196.3 – 196.7	191.2	194.7	199.6
<i>T<sub>J</sub></i> -diagnostic			0.0184	0.0189				

<sup>[a]</sup>Distances in pm, angles in degrees. Different *T<sub>J</sub>*-diagnostics reflect the slight differences in the CCSD and CCSD(T) structures. <sup>[b]</sup>BP86 structures exhibit lower symmetry for AuF<sub>5</sub> and AuF<sub>7</sub>, due to puckering in the basal plane (cf. text). <sup>[c]</sup>Calculations with a nonrelativistic PP on gold.

AuF<sub>5</sub> is experimentally produced by thermal decomposition of [KrF]<sup>+</sup>[AuF<sub>6</sub>]<sup>−</sup> or [O<sub>2</sub>]<sup>+</sup>[AuF<sub>6</sub>]<sup>−</sup>.<sup>[200, 201]</sup> Seppelt *et al.*<sup>[179]</sup> showed that it prefers to crystallise as [AuF<sub>5</sub>]<sub>2</sub> dimer (*D<sub>2h</sub>* symmetry) with two bridging fluorine atoms – see Figure 4.3-2a. Even in a gas-phase electron diffraction experiment at nozzle temperature of ca. 220°C, the dimer was the predominant species, and only a small amount of trimer with presumed *D<sub>3h</sub>* structure was present.<sup>[180]</sup> The computed structure parameters for the dimer agree well with the available X-ray and electron-diffraction measurements – see Table 4.3-2 and Figure 4.3-2a. Similar to earlier comparisons of coupled-cluster and DFT-optimisations for mercury(IV) complexes, the shorter bond lengths obtained with the larger HF exchange admixture at the BHLYP level appear to be more reliable. Our B3LYP optimised structure of the trimer shows a slight bending of the Au-F-Au bridges, leading only to *C<sub>3v</sub>* symmetry – see Figure 4.3-2b.

In addition to the ground-state singlet of AuF<sub>5</sub>, we have also optimised the lowest triplet and quintet states. At B3LYP level, their optimised structures are 5 kJ mol<sup>-1</sup> and 173 kJ mol<sup>-1</sup>, respectively, above the singlet ground-state minimum. Figure 4.3-1b shows that excitation to the low-lying triplet breaks essentially the axial Au-F bond. This indicates already a lability of the monomeric fluoride. In the higher-lying quintet state (Figure 4.3-1c), all bonds are expanded. A B3LYP optimisation for triplet [AuF<sub>5</sub>]<sub>2</sub> gave a minimum 113.6 kJ mol<sup>-1</sup> above the singlet minimum (Figure 4.3-2b), consistent with the enhanced stability of the singlet ground-state by dimerization.

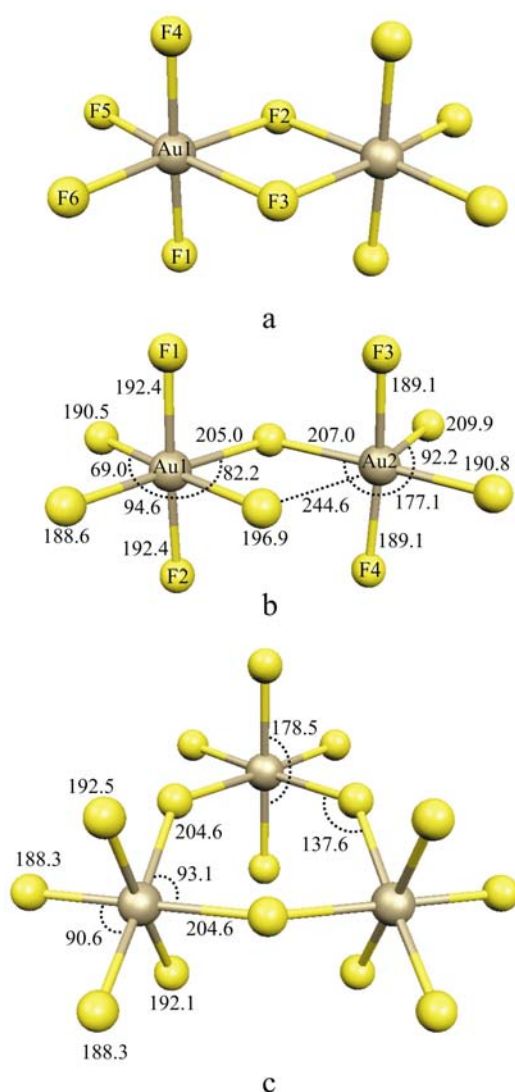


**Figure 4.3-2** B3LYP optimised structures for a) singlet [AuF<sub>5</sub>]<sub>2</sub> (D<sub>2h</sub>), b) triplet [AuF<sub>5</sub>]<sub>2</sub> (F1-Au1-F2 = 177.6, F3-Au2-F4 = 170.9), c) [AuF<sub>5</sub>]<sub>3</sub> (C<sub>3v</sub>).

**Table 4.3-2** Experimental and computed structure parameters for [AuF<sub>5</sub>]<sub>2</sub> in *D*<sub>2h</sub> symmetry<sup>[a]</sup>

[AuF <sub>5</sub> ] <sub>2</sub>	crystal structure <sup>[b]</sup>	electron diffraction <sup>[c]</sup>	MP2 <sup>[b]</sup>	MP2	BP86	B3LYP	BHLYP
Au-F1, Au-F4	189.1(6), 190.1(5)	188.9(9)	196.5	193.8	194.4	192.5	188.7
Au-F2, Au-F3	210.3(5), 203.1(5)	203.0 (7)	207.7	203.9	207.7	206.0	202.4
Au-F5, Au-F6	185.4(6), 187.5(6)	182.2(8)	192.5	190.0	190.4	188.4	184.6
F2-Au-F3	78.4(2)	80.1(5)	79.0	81.4	78.8	78.0	77.4
F1-Au-F4	178.5(3)	181.0(11)	179.3	179.1	178.3	178.7	178.9
F5-Au-F6	87.0(3)	92.3(17)	96.2	88.2	89.2	88.8	88.4

<sup>[a]</sup>Distances in pm, angles in degrees. <sup>[b]</sup>Cf. ref.<sup>[179]</sup> <sup>[c]</sup>Cf. ref.<sup>[180]</sup>

Turning to oxidation state +VI, we have looked at the lowest-lying electronic states of the open-shell AuF<sub>6</sub> molecule (d<sup>5</sup> configuration). Both the low-spin doublet (*D*<sub>2h</sub> symmetry) and the high-spin sextet (*O*<sub>h</sub>) are minima on their respective hypersurfaces – cf. Figure 4.3-3 for structures. No quartet minimum could be located. At B3LYP level, the optimised sextet lies 369.6 kJ mol<sup>-1</sup> above the optimised doublet ground-state. This is in agreement with previous HF calculations.<sup>[187]</sup> The doublet exhibits a slight Jahn-Teller compression of the axial Au-F bonds by 12 pm and a small symmetry breaking in the equatorial plane from *D*<sub>4h</sub> to *D*<sub>2h</sub>.

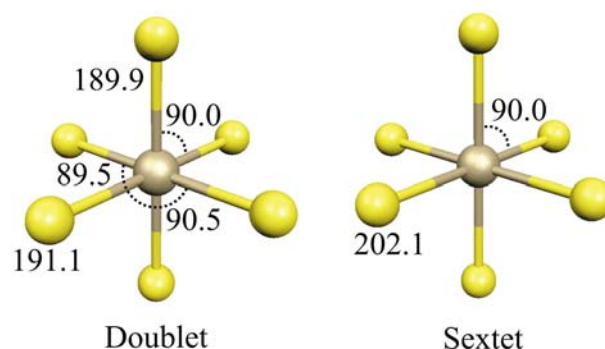


**Figure 4.3-3** B3LYP-optimised structures for ground and lowest excited-state of AuF<sub>6</sub>: a) doublet ground-state (*D*<sub>2h</sub>), b) lowest sextet excited-state (*O*<sub>h</sub>).

Turning finally to Au<sup>VII</sup>, we were able to locate only one minimum on the singlet ground-state potential energy surface of d<sup>4</sup> AuF<sub>7</sub>, the pentagonal bipyramid (*D*<sub>5h</sub>) (Figure 4.3-4a; as for AuF<sub>5</sub> above, BP86 calculations lead to a slight puckering of the Au-F bonds within the basal plane; see supporting information in ref. <sup>[173]</sup> for detailed coordinates). The lowest vibrational frequency for the *D*<sub>5h</sub> minimum is 87 cm<sup>-1</sup> (B3LYP). At all computational levels used, the two axial Au-F bonds are shorter than the five equatorial ones by 1-3 pm, consistent with some crowding in the equatorial plane – see below. No stable triplet or quintet minima could be located. B3LYP single-point calculations for the triplet and quintet state at the



singlet ground-state structure provide excitation energies of 55 kJ mol<sup>-1</sup> and 127 kJ mol<sup>-1</sup>, respectively.

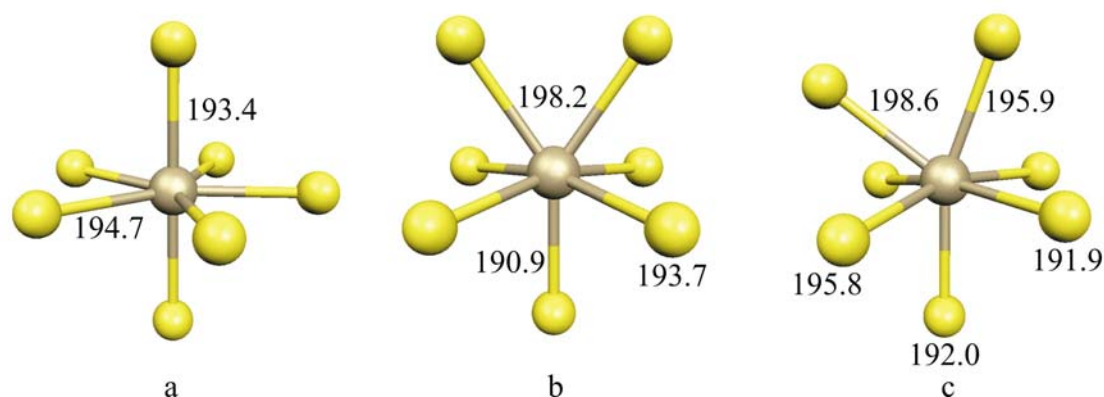


**Figure 4.3-4** B3LYP-optimised structures of stationary points on the AuF<sub>7</sub> potential energy surface: a) pentagonal bipyramidal ( $D_{5h}$ ) minimum, b) monocapped trigonal prismatic ( $C_{2v}$ ) transition state, c) monocapped octahedral ( $C_{3v}$ ) stationary point with two imaginary frequencies.

Apart from the pentagonal bipyramid, the VSEPR model favours two further coordination polyhedra for heptacoordination,<sup>[202]</sup> namely the monocapped trigonal prism ( $C_{2v}$ ) and the monocapped octahedron ( $C_{3v}$ ). The monocapped trigonal prism AuF<sub>7</sub> (Figure 4.3-4b) is calculated to be a transition state (with an imaginary frequency of 70.3 cm<sup>-1</sup>). Optimisations of the monocapped octahedral ( $C_{3v}$ ) structure provided a stationary point with two imaginary frequencies (50.7 cm<sup>-1</sup> and 37.0 cm<sup>-1</sup>; cf. Figure 4.3-4c). At B3LYP level, the optimised structures for these stationary points are 16.5 kJ mol<sup>-1</sup> ( $C_{2v}$ ) and 17.2 kJ mol<sup>-1</sup> ( $C_{3v}$ ) above the pentagonal bipyramidal minimum.

In view of the existence of AuF<sub>5</sub> as dimer (see above), we have searched also for a [AuF<sub>7</sub>]<sub>2</sub> dimer structure. However, neither MP2 nor B3LYP-optimisations provided indications for a stable dimer.

#### 4.3.4 Vibrational Frequencies

The presumable identification of AuF<sub>7</sub> was based in particular on vibrational spectroscopy. A computational evaluation of the spectrum seems thus a good way to prove or disprove the assignment. Calculated harmonic vibrational frequencies at different computational levels are provided in Supporting Information of ref. <sup>[173]</sup>. As these depend nonnegligibly on computational level, we needed to calibrate the reliability of the frequency calculations. To our knowledg, no IR spectrum but one Raman spectrum has been reported for [AuF<sub>5</sub>]<sub>2</sub>.<sup>[179]</sup>

B3LYP and MP2 calculations underestimate these Raman frequencies by ca. 20 cm<sup>-1</sup> – see Supporting Information of ref. [173]. BHLYP underestimates the lower frequencies and overestimates the higher frequencies substantially. In particular, the highest Raman frequency is overestimated by 56 cm<sup>-1</sup> using BHLYP, whereas while B3LYP (11 cm<sup>-1</sup>) and MP2 (6 cm<sup>-1</sup>) are closer to the experiment.

Based on this, we rely in the following on the B3LYP data for AuF<sub>7</sub>. The vibrational frequency of 734 ± 3 cm<sup>-1</sup> was assigned to AuF<sub>7</sub> in refs. [20, 178] is not found computationally. The highest computed Au-F stretching frequencies at B3LYP level are 634, 592, and 589 cm<sup>-1</sup> for the pentagonal bipyramidal (*D*<sub>5h</sub>), monocapped trigonal prismatic (*C*<sub>2v</sub>) and monocapped octahedral (*C*<sub>3v</sub>) stationary points, respectively. The highest frequencies computed for AuF<sub>6</sub> (631 cm<sup>-1</sup>), AuF<sub>5</sub> (633 cm<sup>-1</sup>) and for [AuF<sub>5</sub>]<sub>2</sub> (647 cm<sup>-1</sup>) are also appreciably lower than the 734 cm<sup>-1</sup> value. It thus unclear at the moment what species has given rise to the reported band.

### 4.3.5 Reaction Energies for Concerted and Homolytic Elimination

Calculated energies for the elimination reactions AuF<sub>7</sub> → AuF<sub>5</sub> + F<sub>2</sub> and AuF<sub>5</sub> → AuF<sub>3</sub> + F<sub>2</sub> are summarised in Table 4.3-3. Taking the CCSD(T) energy as reference value, CCSD underestimates and MP2 overestimates the elimination energy. This appreciable level dependence of the results indicates a significant influence of non-dynamical correlation, as has been discussed previously for Hg<sup>IV</sup> (d<sup>8</sup>) species – see Chapter 4.1. [12, 73] The comparison of HF and CCSD(T) results shows the tremendous importance of electron correlation for the description of these elimination reactions. In agreement with our previous systematic calibration of DFT methods for the thermochemistry of Hg<sup>IV</sup> complexes, the B3LYP functional compares well with the CCSD(T) result, whereas the gradient-corrected BP86 provides larger and the BHLYP functional lower values. Also in analogy with the previous studies on Hg<sup>IV</sup>, the agreement between B3LYP and CCSD(T) results is expected to improve even further when considering the larger basis-set dependence of the energies at coupled-cluster compared to DFT levels.

Available computational resources (and the low symmetry of the CP calculations) did not allow a full counterpoise procedure at coupled-cluster levels. CP corrections at the HF and DFT levels tend to lower the reaction energies by ca. 2-6 kJ mol<sup>-1</sup>. CP corrections at MP2 level are ten times larger. We expect the coupled-cluster values to be intermediate but closer to the MP2 value. ZPE corrections amount to ca. 6 kJ mol<sup>-1</sup>. There is thus no doubt that the elimination reaction is exothermic by more than 150 kJ mol<sup>-1</sup>. This renders the existence of

AuF<sub>7</sub> unlikely under the conditions reported, unless the system would exhibit unusually high barriers. This does not seem to be the case – see below.

**Table 4.3-3** Computed reaction energies (kJ mol<sup>-1</sup>) for the elimination AuF<sub>n+2</sub> → AuF<sub>n</sub> + F<sub>2</sub> and for the homolytic reaction AuF<sub>n+1</sub> → AuF<sub>n</sub> + F

AuF <sub>7</sub> → AuF <sub>5</sub> + F <sub>2</sub>	HF	MP2	CCSD <sup>[b]</sup>	CCSD(T) <sup>[b]</sup>	BP86	BHLYP	B3LYP	<i>nrel.</i> B3LYP <sup>[d]</sup>
D <sub>e</sub>	-484.8	-52.6	-234.2	-145.2	-104.4	-268.1	-171.2	-244.2
ZPE	-5.8	-5.4			-5.2	-6.3	-6.4	-4.4
BSSE	-3.5	-30.8			-3.4	-2.3	-5.9	-3.6
Sum <sup>[a]</sup>	-494.0	-88.7			-113.0	-276.7	-183.6	-252.2
<b>AuF<sub>5</sub> → AuF<sub>3</sub> + F<sub>2</sub></b>								
D <sub>e</sub>	-121.4	124.2	24.2	61.9	101.6	-6.0	49.3	-48.4
ZPE	-8.2	-5.5			-5.1	-6.7	-5.2	-5.2
BSSE	-3.1	-44.6			-4.9	-2.4	-3.7	-8.3
Sum <sup>[a]</sup>	-132.7	74.1			91.7	-15.0	40.5	-61.9
<b>AuF<sub>7</sub> → AuF<sub>6</sub> + F</b>								
D <sub>e</sub>	-397.6	-10.6	-136.8 <sup>[c]</sup>	-84.5 <sup>[c]</sup>	-101.4		-139.9	
ZPE	-5.0	-2.5			-3.2		-4.9	
BSSE	-2.7	-12.4			-1.4		-1.9	
Sum <sup>[a]</sup>	-397.6	-25.5			-106.0		-146.7	
<b>AuF<sub>6</sub> → AuF<sub>5</sub> + F</b>								
D <sub>e</sub>	-236.0	103.8	13.1 <sup>[c]</sup>	62.6 <sup>[c]</sup>	213.7		120.7	
ZPE	-8.4	-8.7			-8.0		-7.8	
BSSE	-2.5	-29.4			-2.8		-4.8	
Sum <sup>[a]</sup>	-246.8	65.7			203.0		108.2	

<sup>[a]</sup>Results including CP and ZPE corrections. <sup>[b]</sup>No CP correction was possible due to system size. <sup>[c]</sup>Single-point calculations at B3LYP-optimised structures. <sup>[d]</sup>Nonrelativistic PP for Au used.

We have also studied the successive homolytic splitting of Au-F bonds according to the reactions AuF<sub>7</sub> → AuF<sub>6</sub> + F and AuF<sub>6</sub> → AuF<sub>5</sub> + F (Table 4.3-3). While the bond breaking costs energy for AuF<sub>6</sub>, it is actually *exothermic* for AuF<sub>7</sub>! How could AuF<sub>7</sub> then still be a minimum on the potential energy surface? A B3LYP calculation of AuF<sub>6</sub> + F at the AuF<sub>7</sub> structure (with one equatorial fluorine atom removed to a large distance) gives an energy 161 kJ mol<sup>-1</sup> above the AuF<sub>7</sub> minimum. It is thus only the barrier due to structural rearrangement (presumably in the overcrowded basal plane) that renders AuF<sub>7</sub> a local minimum on the potential energy surface. This provides another indication of the extreme instability of Au<sup>VII</sup>.

### 4.3.6 Transition States for Elimination Reaction

While computational location of the true transition state for homolytic bond dissociation in AuF<sub>7</sub> was not successful so far, we have obtained transition states and barriers (Table 4.3-4) for the concerted F<sub>2</sub> elimination from AuF<sub>7</sub>. Full structure optimisation at coupled-cluster level exceeded the available computational resources in these cases. In addition to full DFT-

optimisations at B3LYP and BHLYP levels, we provide thus single-point MP2, CCSD, and CCSD(T) energies at both B3LYP and BHLYP optimised structures. The transition state exhibits  $C_{2v}$  symmetry, with partial formation of an F-F bond in the equatorial plane of AuF<sub>7</sub> (Figure 4.3-5a). Indeed, the imaginary vibration of the transition state (Figure 4.3-5b) corresponds to the elimination of F<sub>2</sub>, combined with movement of two further equatorial fluorine atoms to give square-pyramidal AuF<sub>5</sub> (cf. Figure 4.3-1a).

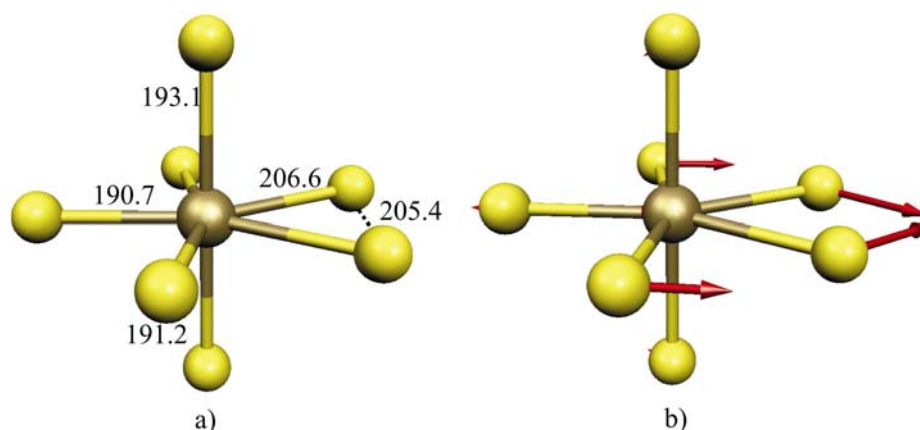


**Figure 4.3-5** a) Transition state structure (B3LYP) for the elimination  $\text{AuF}_7 \rightarrow \text{AuF}_5 + \text{F}_2$ . b) Indication of the imaginary normal vibrational mode by arrows.

**Table 4.3-4** Calculated activation barriers (in  $\text{kJ mol}^{-1}$ ) for the gas-phase elimination of  $\text{AuF}_7 \rightarrow \text{AuF}_5 + \text{F}_2$ <sup>[a]</sup>

Reaction	Input structure	B3LYP	BHLYP	MP2	CCSD <sup>[b]</sup>	CCSD(T) <sup>[b]</sup>
$\text{AuF}_7 \rightarrow \text{AuF}_5 + \text{F}_2$	B3LYP-opt.	24.7	12.9	72.3	27.4	10.0
	BHLYP-opt.	22.3	40.8	102.1	27.1	5.8

<sup>[a]</sup>No ZPE and CP corrections are included here. <sup>[b]</sup>The  $T_1$ -diagnostic of coupled-cluster calculations at the transition state are 0.031 at B3LYP-optimised and 0.033 at BHLYP-optimised structures.

While the computed activation barriers (Table 4.3-4) depend somewhat on the input structure and computational level, they are generally low at both DFT and coupled-cluster levels (even lower for the latter). We consider the larger MP2 values unreliable in view of the appreciable non-dynamical correlation effects (cf.  $T_1$ -diagnostics in footnote to Table 4.3-4). However, the level dependence is much less pronounced than in previous calculations for the transition states of the related eliminations of Hg<sup>IV</sup> complexes,  $\text{HgX}_4 \rightarrow \text{HgX}_2 + \text{X}_2$  ( $\text{X} = \text{F}, \text{Cl}$ ). The  $T_1$ -diagnostic at CCSD level of the corresponding transition states were around 0.04 - 0.06 for elimination from HgF<sub>4</sub> or HgCl<sub>4</sub>.<sup>[12]</sup> The values provided here are thus probably more reliable than what is available for those mercury(IV) systems. Together with the exothermic

reaction energies (Table 4.3-3), this suggests clearly that a stability of AuF<sub>7</sub> up to room temperature, as has been claimed,<sup>[20, 178, 184]</sup> is highly unlikely.

### 4.3.7 Electron Affinities of Hexafluorides

Previous CI calculations predicted an extremely high electron affinity of 9.56 eV for AuF<sub>6</sub>,<sup>[187]</sup> 1.5 eV higher than the value thought to be correct at the time for PtF<sub>6</sub>. An extremely large electron affinity had already been assumed for AuF<sub>6</sub> by Bartlett, using simple extrapolation (personal communication cited in ref. <sup>[188]</sup>). As the electron affinity is another indicator for the (in)stability of the higher oxidation states, we have computed adiabatic electron affinities for AuF<sub>6</sub>, and for comparison for PtF<sub>6</sub>. Our CCSD(T) result of ca. 7.0 eV for platinum hexafluoride agrees well with recent calculations by Schwerdtfeger *et al.*,<sup>[177]</sup> and with the most recent experimental value<sup>[203]</sup> (see Table 4.3-5; older, still larger values for PtF<sub>6</sub> are considered unreliable<sup>[177]</sup>). Given the good agreement, our computed value of ca. 8.5 eV for AuF<sub>6</sub> should be an accurate prediction. While this is about 1 eV lower than Bartlett's estimate, it remains an extremely large electron affinity and characterises the hypothetical AuF<sub>6</sub> as one of the most strongly oxidising species known.

**Table 4.3-5** Calculated adiabatic electron affinities (in eV) for hexafluoride complexes

EA	HF	MP2	CCSD	CCSD(T)	T <sub>1</sub> -dia. <sup>[a]</sup>	BP86	B3LYP	exp.
PtF <sub>6</sub> <sup>[b]</sup> (vertical) <sup>[c]</sup>	6.50	7.57	7.01	6.68			8.66	
PtF <sub>6</sub> <sup>[b]</sup>	8.30	6.43	7.43	6.95			6.78	
PtF <sub>6</sub> (1f-function) <sup>[d]</sup>	8.21	6.50	7.48 <sup>[f]</sup>	6.99 <sup>[f]</sup>	0.030 (0.025)	6.02	6.80	7.00 ± 0.35 <sup>[e]</sup>
AuF <sub>6</sub> (1f-function) <sup>[d]</sup>	9.92	8.38	9.01 <sup>[f]</sup>	8.52 <sup>[f]</sup>	0.020 (0.034)	7.15	8.13	
AuF <sub>6</sub>	9.85	8.33	8.96 <sup>[f]</sup>	8.47 <sup>[f]</sup>	0.021 (0.034)	7.10	8.06	

<sup>[a]</sup>T<sub>1</sub>-diagnostics (in parentheses for the anion [MF<sub>6</sub>]<sup>-</sup>). <sup>[b]</sup>Cf. ref. <sup>[177]</sup>. <sup>[c]</sup>Vertical electron affinities. <sup>[d]</sup>Only one instead of two polarization f-functions was used, with  $\alpha=0.993$ , 1.050 for Pt and Au, respectively.<sup>[204]</sup> This was done for better comparison with ref. <sup>[177]</sup>. <sup>[e]</sup>Cf. ref. <sup>[203]</sup>. <sup>[f]</sup>Single-point calculations at B3LYP-optimised structures.

### 4.3.8 Bonding Comparison of AuF<sub>5</sub> and AuF<sub>7</sub>

Figure 4.3-6 compares the frontier Kohn-Sham MOs for AuF<sub>7</sub>, [AuF<sub>6</sub>]<sup>-</sup> and AuF<sub>5</sub>. Consistent with the high oxidation state of the heptafluoride, the highest occupied MOs are essentially  $\pi$ -type lone pairs on the axial ligands, with only weak metal-ligand antibonding character. In AuF<sub>5</sub>, the three highest occupied MOs derive from the t<sub>2g</sub> set of octahedral [AuF<sub>6</sub>]<sup>-</sup> (cf. Figure 4.3-6c) and exhibit somewhat more pronounced  $\pi$ -antibonding character. The character of the very low-lying virtual orbitals (Figure 4.3-6b) allows us to understand clearly why this Au<sup>V</sup>

species prefers to exist as a dimer (or trimer). The relatively respectable HOMO-LUMO gaps of AuF<sub>7</sub> and [AuF<sub>6</sub>]<sup>-</sup> explain, why they exhibit closed-shell singlet ground-states and relatively high excitation energies.

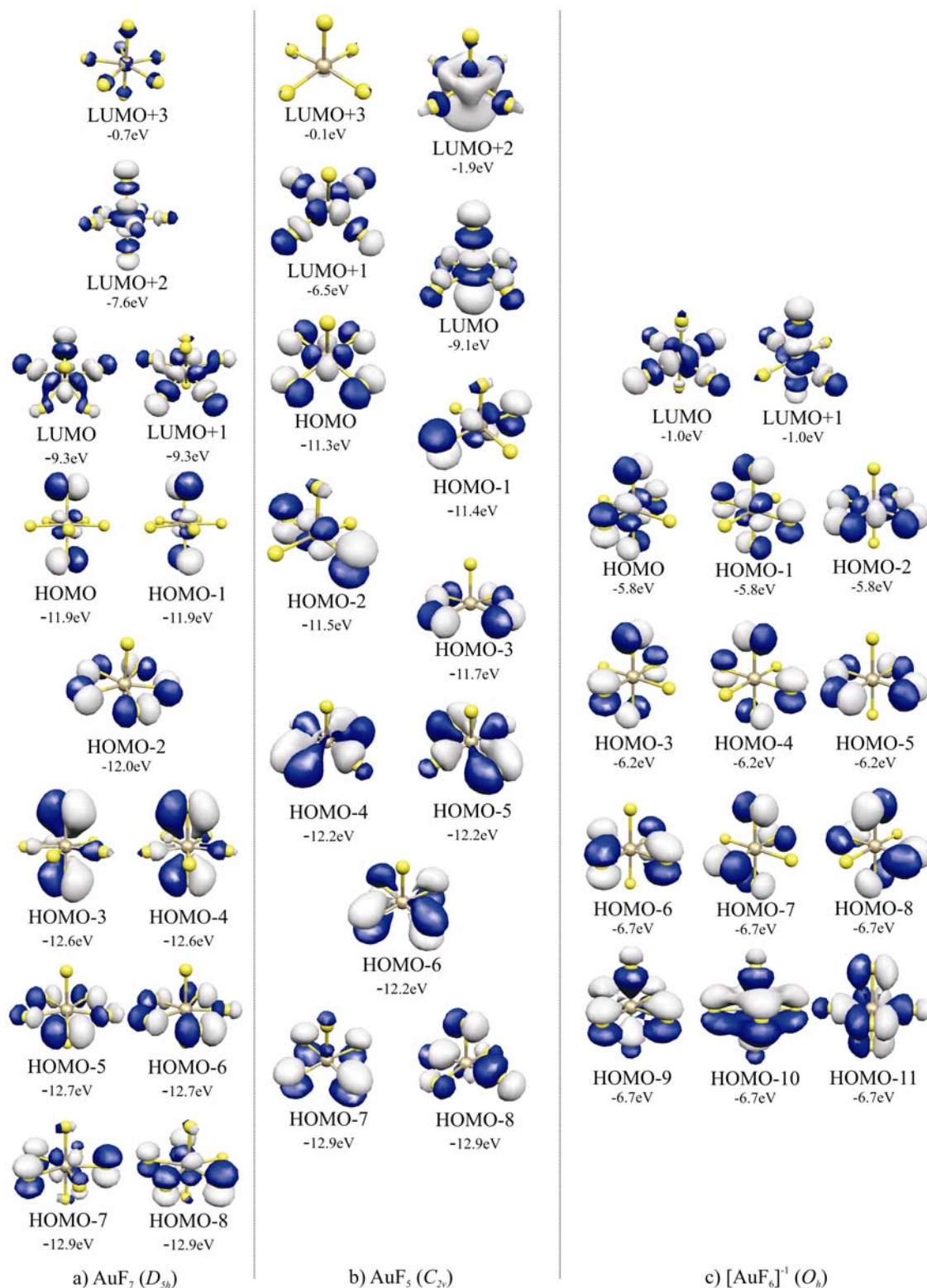


**Figure 4.3-6** Kohn-Sham molecular orbitals of AuF<sub>7</sub> (*D*<sub>5h</sub>), AuF<sub>5</sub> (*D*<sub>3h</sub>) and [AuF<sub>6</sub>]<sup>-</sup> (*O*<sub>h</sub>) at B3LYP level

### 4.3.9 Conclusion

This quantum-chemical study has shown that the experimental observation of AuF<sub>7</sub> reported about 20 years ago is highly improbable. The previously reported, so far unreproduced experimental characterisation of gas-phase AuF<sub>7</sub> by an IR band at  $734\pm 3\text{ cm}^{-1}$  was not confirmed by our calculations. The computed, strongly exothermic elimination of F<sub>2</sub>, with a low activation barrier, is not consistent with the reported stability up to room temperature, and even the existence at liquid-nitrogen temperature is doubtful. Moreover, even the homolytic dissociation of one equatorial Au-F bond is exothermic and has a barrier only due to structural rearrangement. If at all, such a high-energy species will only be accessible in more sophisticated matrix-isolation or mass-spectrometry experiments. In view of the extremely high electron affinity of AuF<sub>6</sub>, this Au<sup>VI</sup> species is also unlikely to exist at most experimentally viable conditions. Oxidation state +V remains thus the highest oxidation state for the group 11 element gold that is known beyond doubt.

## 4.4 Higher Oxidation States of Iridium: the Case of Ir<sup>VII</sup> [112]

### 4.4.1 Introduction

The quest for the highest achievable oxidation states of the transition metal elements is of fundamental interest. Additionally, complexes in very high oxidation states may serve as oxidation agents in other subdisciplines.<sup>[4, 6, 7]</sup> The maximum oxidation states for the early transition metals follow the group number up to group 8 (cf. OsO<sub>4</sub> and RuO<sub>4</sub>, the lack of evidence for an existence of FeO<sub>4</sub> marks the exception). The trends for the later metals tend to be less clear-cut (cf. Figure 1 in ref. [73]). In the 5d series, the trend of the experimentally suggested maximum oxidation states looks irregular – see filled circles and dotted line in Figure 4.4-1.

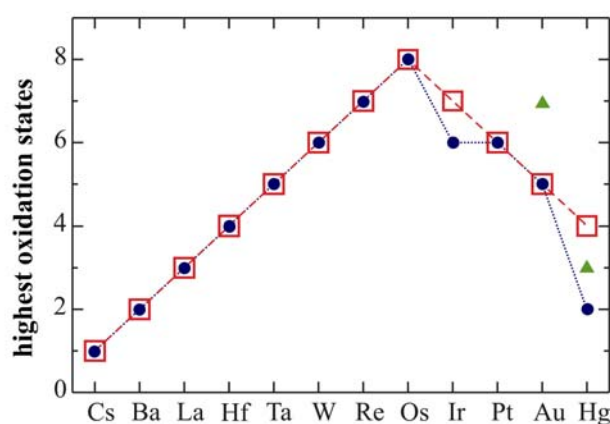


**Figure 4.4-1** Maximum oxidation states of the 5d transition metals: (●) highest experimentally known values, (▲) probably incorrect experimental assignments, (□) suggested most likely values.

The highest experimentally known oxidation states after osmium are represented by the hexafluorides of iridium (IrF<sub>6</sub>)<sup>[174]</sup> and platinum (PtF<sub>6</sub>)<sup>[176]</sup>. The isolation of AuF<sub>7</sub>, claimed almost 20 years ago,<sup>[20]</sup> has recently been shown by high-level quantum-chemical calculations to be highly improbable.<sup>[173]</sup> As the existence of AuF<sub>6</sub> is also unlikely,<sup>[173]</sup> oxidation state +V



remains the highest oxidation state of gold that is known beyond doubt – see Chapter 4.3.<sup>[179]</sup> As we have shown in the Chapters 4.1 and 4.2 quantum-chemical calculations have furthermore strongly supported the thermochemical stability of mercury(+IV) as gaseous HgF<sub>4</sub>,<sup>[12, 72-75, 120]</sup> but no experimental confirmation has been obtained so far.

Combining the results of the most accurate quantum-chemical predictions and of reliable experimental studies, a revised trend of the highest oxidation states of the 5d transition metal row is obtained. Apart from the lack of iridium (+VII), we see a linear descent after osmium – Figure 4.4-1.

To establish the highest achievable iridium oxidation states, we report here structure optimisations by density functional theory (DFT) methods, followed by high-level coupled-cluster calculations of the stabilities of iridium fluoride complexes up to IrF<sub>9</sub>.

#### 4.4.2 Computational Details

All molecular structures have been optimised at the B3LYP<sup>[50, 53, 143, 192]</sup> DFT level, using the Gaussian03<sup>[192]</sup> program. Quasirelativistic energy-adjusted, small-core pseudopotentials of the Stuttgart/Cologne group were used for the transition metals Au,<sup>[194]</sup> Pt,<sup>[137]</sup> and Ir<sup>[137]</sup>. The def-TZVP (7s6p5d)[6s3p3d] valence basis set implemented in the Turbomole 5.6 package<sup>[144]</sup> for Ir, Pt, and Au, augmented by one f-type polarization function<sup>[204]</sup> ( $\alpha = 0.938, 0.993, 1.050$  for Ir, Pt, and Au, respectively), were used together with a fluorine DZ+P<sup>[132]</sup> basis set by Dunning. For the noble-gas atoms Kr and Xe we used energy-consistent, 8-valence-electron pseudopotentials and (6s6p3d1f)/[4s4p3d1f] valence basis sets.<sup>[148]</sup> Stationary points on the potential energy surface were characterised by harmonic vibrational frequency analyses at this level (providing also zero-point energy corrections to the thermochemistry). Subsequent single-point energy calculations at B3LYP DFT as well as coupled-cluster CCSD and CCSD(T) levels had the fluorine basis replaced by a larger aug-cc-pVTZ basis set.<sup>[126]</sup> The coupled-cluster calculations were carried out with the MOLPRO 2002.6<sup>[193]</sup> program package. Contributions of basis-set superposition errors (BSSE) to the energetics were estimated by the counterpoise (CP)<sup>[98]</sup> procedure. Spin-orbit (SO) corrections to the energetics were computed at B3LYP level (with the same basis sets as used in the regular energy calculations above) using a relativistic two-component non-collinear-spin DFT method<sup>[205]</sup> implemented recently into the in-house program ReSpect,<sup>[206]</sup> together with a two-component PP for Ir (made from a scalar relativistic part and an SO potential).

### 4.4.3 Structures and Thermochemistry

Figure 4.4-2 shows the DFT-optimised structures of IrF<sub>9</sub>, IrF<sub>7</sub>, and IrF<sub>5</sub>. While IrF<sub>9</sub> exhibits a minimum with  $D_{3h}$  symmetry on the potential energy surface (singlet state), the gas-phase elimination of F<sub>2</sub> is computed to be highly exothermic – see Table 4.4-1. Calculations on oxo-fluoro complexes of Ir<sup>IX</sup> (e.g. on IrO<sub>3</sub>F<sub>3</sub>) indicate also very exothermic decomposition pathways with low barriers (details of these studies will be provided elsewhere<sup>[123]</sup>). This makes the existence of the highest theoretically possible oxidation state of iridium highly unlikely.

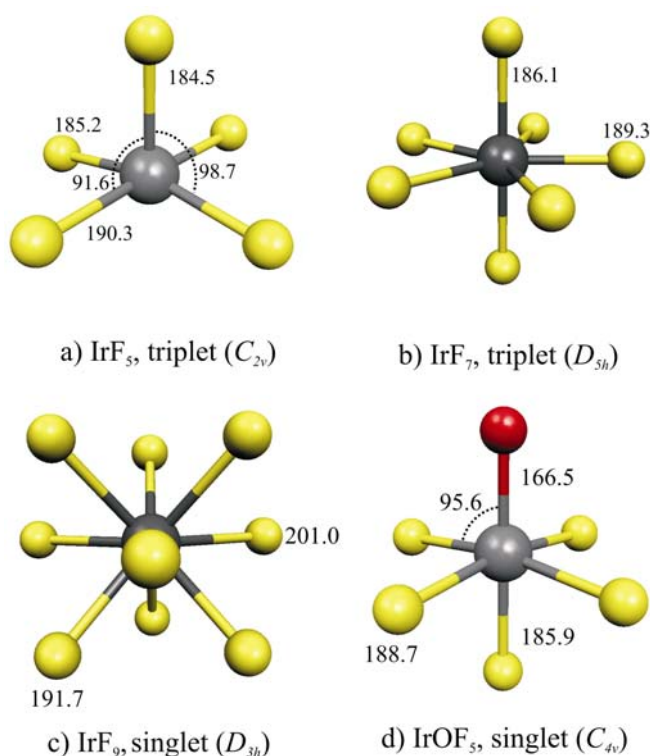


**Figure 4.4-2** B3LYP-optimised minimum structures of IrF<sub>5</sub> ( $C_{2v}$ ), IrF<sub>7</sub> ( $D_{5h}$ ), IrF<sub>9</sub> ( $D_{3h}$ ), and IrOF<sub>5</sub> ( $C_{4v}$ ). Distances in pm, angles in degrees.

What about Ir<sup>VIII</sup>? Synthesis of the most likely Ir<sup>VIII</sup> complex, IrO<sub>4</sub>, has recently been attempted by matrix-isolation but resulted in formation of the peroxide species (O<sub>2</sub>)IrO<sub>2</sub>.<sup>[207]</sup> This reflects the energy gain from formation of an O-O bond. The homoleptic fluoride complex IrF<sub>8</sub> exhibits a square antiprismatic ( $D_{4d}$ ) minimum on the potential-energy surface (not shown). However, concerted F<sub>2</sub> elimination is computed to be highly exothermic (Table 4.4-1). This is likely due to steric crowding in the Ir coordination sphere, which places this complex at very high energies (and probably leads to low barriers). Most mixed fluoro-oxo

complexes of Ir<sup>VIII</sup> are computed to be similarly unstable; only IrOF<sub>6</sub> exhibits somewhat less exothermic decomposition pathways.<sup>[123]</sup>

**Table 4.4-1** Computed reaction energies (kJ mol<sup>-1</sup>) for iridium fluoride complexes<sup>[a]</sup>

Reaction	CCSD	CCSD(T)	B3LYP <sup>[b]</sup>
a. IrF <sub>9</sub> → IrF <sub>7</sub> + F <sub>2</sub>	-401.9	-319.6	-375.5 (-385.9)
b. IrF <sub>8</sub> → IrF <sub>6</sub> + F <sub>2</sub>	-329.6	-249.6	-246.7 (-257.2)
c. IrF <sub>7</sub> → IrF <sub>5</sub> + F <sub>2</sub>	32.8	102.6	130.3 (119.6)
d. IrF <sub>7</sub> → IrF <sub>6</sub> + F	-100.1	-44.3	-32.9 (-40.3)
e. IrF <sub>6</sub> → IrF <sub>5</sub> + F	257.3	299.7	318.5 (308.2)
f. IrF <sub>5</sub> + KrF <sub>2</sub> → IrF <sub>7</sub> + Kr	-117.8	-163.5	-166.0
g. IrOF <sub>5</sub> → IrOF <sub>3</sub> + F <sub>2</sub>			261.6
h. IrOF <sub>5</sub> → IrF <sub>4</sub> + OF			176.9
i. IrOF <sub>5</sub> → IrOF <sub>4</sub> + F			172.8
j. IrOF <sub>5</sub> → IrF <sub>5</sub> + O			256.1
k. [IrF <sub>6</sub> ] <sup>+</sup> → [IrF <sub>4</sub> ] <sup>+</sup> + F <sub>2</sub>			216.7
l. [IrF <sub>6</sub> ] <sup>+</sup> → [IrF <sub>5</sub> ] <sup>+</sup> + F			154.5
m. KrF <sub>2</sub> → Kr + F <sub>2</sub> <sup>[c]</sup>	-85.0	-60.9	-35.7
n. F <sub>2</sub> → 2F <sup>[d]</sup>	124.4	152.7	155.3

<sup>[a]</sup>Reaction energies given at scalar relativistic levels, for singlet IrF<sub>9</sub>, doublet IrF<sub>8</sub>, triplet IrF<sub>7</sub>, quartet IrF<sub>6</sub>, triplet IrF<sub>5</sub>, quartet IrF<sub>4</sub>, triplet IrOF<sub>5</sub>, doublet IrOF<sub>4</sub>, and singlet IrOF<sub>3</sub>. Spin-orbit corrections at B3LYP level to reactions c, d, and e amount to -36.9 kJ mol<sup>-1</sup>, -7.6 kJ mol<sup>-1</sup>, and -29.3 kJ mol<sup>-1</sup>, respectively. <sup>[b]</sup>Values in parentheses are counterpoise and zero-point vibration corrected. <sup>[c]</sup>The experimental value is -60.2 kJ mol<sup>-1</sup>. <sup>[d]</sup>The experimental value is +159.7 kJ mol<sup>-1</sup>.

Things look rather different for Ir<sup>VII</sup> (d<sup>2</sup> configuration): IrF<sub>7</sub> is computed to exhibit a pentagonal bipyramidal triplet ground-state minimum – *D*<sub>5h</sub> symmetry, see Figure 4.4-2. A singlet minimum with *C*<sub>s</sub> symmetry is calculated to be 82 kJ mol<sup>-1</sup> above the triplet ground-state of IrF<sub>7</sub> at scalar relativistic level. For the triplet ground-state, the monocapped trigonal prism is a transition state at 27.1 kJ mol<sup>-1</sup>, and the monocapped octahedron is a second-order saddle point at 29.7 kJ mol<sup>-1</sup> above the *D*<sub>5h</sub> minimum. In contrast to IrF<sub>9</sub>, F<sub>2</sub> elimination from triplet IrF<sub>7</sub> is appreciably endothermic (Table 4.4-1), in fact much more so than the best calculations suggest for the long-sought HgF<sub>4</sub>.<sup>[12, 72-75, 120]</sup> Our coupled-cluster calculations predict an energy of +102.6 kJ mol<sup>-1</sup> (Table 4.4-1). As for related cases,<sup>[12, 73, 173]</sup> triple excitations contribute substantially to this positive value, and B3LYP DFT calculations compare reasonably well with the CCSD(T) results<sup>[12, 173]</sup> (this makes B3LYP energies a good choice for larger systems where coupled-cluster calculations are not feasible). A second potential channel for decomposition of IrF<sub>7</sub> involves the homolytic dissociation of an Ir-F bond to give IrF<sub>6</sub>. While this reaction is calculated to be slightly exothermic (Table 4.4-1;

larger basis sets are expected to render this value less negative<sup>[12, 73]</sup>, the structural rearrangement required for this bond breaking is substantial and creates an appreciable barrier of +100.4 kJ mol<sup>-1</sup> (scalar relativistic DFT results). The transition state is a singly capped octahedron with  $C_{3v}$  symmetry, where the cap represents the IrF bond to be broken.

We note in passing that nonrelativistic pseudopotential calculations provide ca. 100 kJ mol<sup>-1</sup> less positive F<sub>2</sub> elimination energies. Thus, as in all other cases studied hitherto,<sup>[66, 73, 173, 194]</sup> the stability of the highest oxidation states of the 5d elements is largely due to relativistic effects – see Chapter 4.1 – 4.3.

Given the open-shell nature of several of the relevant species involved, we have also evaluated the influence of SO effects on stabilities, using single-point calculations with a recently implemented<sup>[205]</sup> two-component non-collinear spin-density functional approach, see Chapter 4.4.2. Most of the relevant results are in footnote a to Table 4.4-1. While the SO stabilisation increases from IrF<sub>7</sub> to IrF<sub>6</sub> to IrF<sub>5</sub>, its influence on the decomposition reactions of IrF<sub>7</sub> is moderate and does not change the thermochemistry dramatically (the same holds for activation barriers; computed SO corrections to the barrier for homolytic Ir-F bond breakage amount to only -5.7 kJ mol<sup>-1</sup>). Counterpoise corrections for basis-set superposition errors and zero-point vibrational energy corrections are also of no appreciable consequence for the relevant reaction energies (cf. Table 4.4-1). It appears thus likely that IrF<sub>7</sub> is a viable target for gas-phase synthesis (e.g. in molecular-beam experiments) or for access in matrix-isolation studies. Characterisation of IrF<sub>7</sub> by vibrational spectroscopy may be aided by the harmonic vibrational frequency analysis provided in Table S1 in Supporting Information of ref<sup>[112]</sup>. Electronic structure and oxidation state of Ir<sup>VII</sup> species might be accessible also by Ir Mössbauer spectroscopy.

#### 4.4.4 Noble-Gas Complexes

Oxidation of IrF<sub>5</sub> by the endothermic fluorine compound KrF<sub>2</sub> is substantially exothermic (Table 4.4-1). This holds even more so for the strongest presently known oxidative fluorinating agent [KrF]<sup>+</sup>.<sup>[208]</sup> Formation of the [KrF][IrF<sub>6</sub>] ion-pair complex from (gas-phase) [KrF]<sup>+</sup> and [IrF<sub>6</sub>]<sup>-</sup> is highly exothermic (by -491.6 kJ mol<sup>-1</sup> at B3LYP level) and provides a local minimum on the potential energy surface (analogous to the known complex [XeF][IrF<sub>6</sub>]<sup>[209]</sup>). However, the complex is calculated to decompose exothermically (by -118.5 kJ mol<sup>-1</sup>) into IrF<sub>7</sub> and Kr. Figure 4.4-3 shows the reaction energies [NgF][MF<sub>6</sub>] → MF<sub>7</sub> + Ng

for a range of complexes (Ng = Kr, Xe and M = Ir, Pt, Au) at the corresponding computational level.

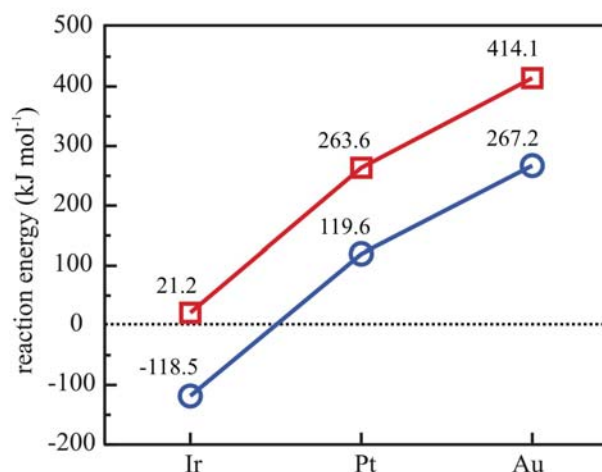


**Figure 4.4-3** Computed energies (B3LYP) for the (gas-phase) reactions  $[\text{NgF}][\text{MF}_6] \rightarrow \text{MF}_7 + \text{Ng}$  (Ng = Kr, Xe; M = Ir, Pt, Au):  $\square$   $[\text{XeF}]^+$  complexes,  $\circ$   $[\text{KrF}]^+$  complexes.

While the formation of the ion-pair complexes from the separated ions is in all cases strongly exothermic (data not shown), only  $[\text{KrF}][\text{IrF}_6]$  decomposes exothermically to give the heptafluoride (note that these energies will be generally somewhat more positive in the condensed phase due to electrostatic stabilisation of the ion-pair complexes). These computational results suggest a possible pathway to obtain Ir<sup>VII</sup>. Interestingly, in contrast to several known  $[\text{KrF}][\text{MF}_6]$  complexes of platinum and gold,<sup>[185, 209, 210]</sup> and in spite of the existence of  $[\text{XeF}][\text{IrF}_6]$ ,<sup>[209]</sup> observation of  $[\text{KrF}][\text{IrF}_6]$  has never been reported.

#### 4.4.5 The Iridium Oxyfluoride IrOF<sub>5</sub>

Initial data for an alternative Ir<sup>VII</sup> target, the  $C_{4v}$ -symmetrical IrOF<sub>5</sub>, have also been obtained (Table 4.4-1, Figure 4.4-2d; data for the triplet state are provided; the singlet is only 2.4 kJ mol<sup>-1</sup> higher at scalar relativistic level, but this difference is enhanced by SO effects). It has the advantage of a lower coordination number. Indeed, in this case elimination of F<sub>2</sub> is even more endothermic than for IrF<sub>7</sub>, and elimination of OF is also still appreciably endothermic (Table 4.4-1). Even the homolytic splitting of an Ir-F bond to give IrOF<sub>4</sub> is

endothermic by 172.8 kJ mol<sup>-1</sup>. The harmonic vibrational frequencies of IrOF<sub>5</sub> are also provided in Supporting Information of ref. [112].

#### 4.4.6 Cationic Iridium Fluoride Species

Another Ir<sup>VII</sup> species that comes to mind is the cation [IrF<sub>6</sub>]<sup>+</sup>. It is computed to prefer a triplet ground-state with a slight Jahn-Teller distortion (*D*<sub>4h</sub> symmetry, d(Ir-F<sub>ax</sub>) = 179.3 pm, d(Ir-F<sub>eq</sub>) = 184.7 pm). The adiabatic ionization potential IrF<sub>6</sub> → [IrF<sub>6</sub>]<sup>+</sup> is calculated to be very large (13.5 eV at B3LYP level). The energies for concerted F<sub>2</sub> elimination and homolytic Ir-F dissociation are calculated to be both appreciably endothermic (Table 4.4-1). As IrF<sub>6</sub> is a volatile complex, it is unclear at the moment why its molecular ion has apparently never been observed in a mass spectrometry experiment.

#### 4.4.7 Conclusions

Our present state-of-the-art quantum-chemical calculations suggest thus that the highest iridium oxidation state that has a realistic chance of experimental observation is Ir<sup>VII</sup>. The experimentally known highest 5d oxidation states for groups 8, 10 and 11 are Os<sup>VIII</sup>, Pt<sup>VI</sup>, and Au<sup>V</sup>, respectively – see ref. [177] for the computationally verified instability of Pt<sup>VIII</sup> and ref. [173] for exclusion of Au<sup>VII</sup> and Au<sup>VI</sup>. Adding the computationally predicted Hg<sup>IV</sup> and Ir<sup>VII</sup> states suggests that the trend for the later 5d metals should become a linear decrease once all computationally suggested possibilities have been exploited experimentally – see solid line and open squares in Figure 4.4-1 and Chapter 5.

## 4.5 Where is the Limit of Highly Fluorinated High Oxidation State Osmium Species?

### 4.5.1 Introduction

The highest oxidation state (+VIII) of the 5d transition-metal osmium (in fact of any element) is best exemplified by the tetroxide,  $\text{OsO}_4$ , which has achieved substantial importance as an oxidation agent, e.g. in organic chemistry.<sup>[7, 211, 212]</sup> In contrast, the octafluoride,  $\text{OsF}_8$ , is presently unknown, in spite of a long speculative history: in 1913, Ruff and Tschirch<sup>[213]</sup> claimed the first synthesis of  $\text{OsF}_8$ . 45 years later, Weinstock and Malm<sup>[214]</sup> showed, that the purported  $\text{OsF}_8$  was in fact  $\text{OsF}_6$ . The isolation of  $\text{OsF}_7$ , reported in 1966,<sup>[215]</sup> also could recently not be reproduced under the indicated conditions<sup>[22]</sup> (reaction of metal powder with  $\text{F}_2$  at 620°C and 400 bar with subsequent rapid cooling). The highest binary osmium fluoride characterised beyond doubt is thus  $\text{OsF}_6$ <sup>[115]</sup> – see Figure 4.5-1.

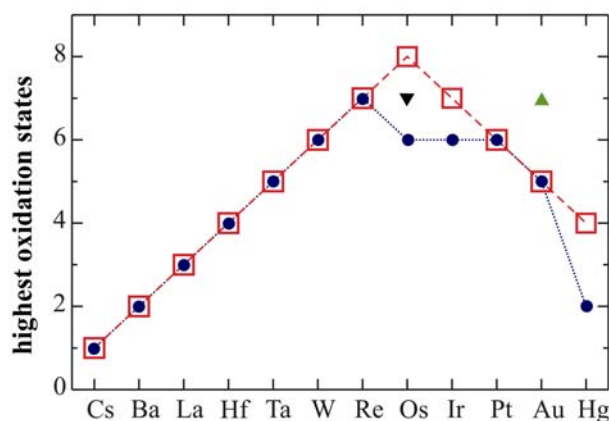


**Figure 4.5-1** Maximum oxidation states of binary 5d transition metal fluorides: (●) highest experimentally known  $\text{MF}_n$  species, (▲) incorrect experimental assignment, (▼) controversial experimental assignment, (□) suggested maximum achievable oxidation states.

Figure 4.5-1 shows also that the decrease of the maximum oxidation states of the fluorides from group 8 through group 13 is irregular if we consider only the experimentally proven cases. Apart from  $\text{OsF}_8$ , the lack of  $\text{IrF}_7$ <sup>[112]</sup> and of  $\text{HgF}_4$ <sup>[12, 72, 73, 75]</sup> prohibits a more regular trend (earlier reports on  $\text{AuF}_7$  have recently been shown to be erroneous<sup>[173]</sup>) – see Chapter 5.

To investigate the chances to prepare species like  $\text{OsF}_8$  and  $\text{OsF}_7$ , we report here quantum-chemical calculations of structures and (gas-phase) stabilities. Additionally, we evaluate also the stabilities of heteroleptic  $\text{Os}^{\text{VIII}}$  oxyfluorides, to find out how they are affected by the number of fluorine atoms present. We will compare our results also to those of an earlier HF and MP2 study of osmium fluorides and oxyfluorides by Veldkamp and Frenking.<sup>[216]</sup> Notably, however, those authors had to rely on various isodesmic reactions to discuss stability, whereas the more refined and advanced computational methods available today allow us to discuss directly the relevant gas-phase elimination and bond-breaking reactions, and to evaluate also activation barriers for some key reactions.

## 4.5.2 Computational Details

Structures were optimised using density-functional theory (hybrid B3LYP<sup>[50, 53, 143, 192]</sup> functional), with the Gaussian03<sup>[192]</sup> program. The transition state optimisations were done using synchronous transit-guided quasi-newton (STQN) methods<sup>[217, 218]</sup> according to the QST2 and QST3 keywords implemented in Gaussian03. Optimisations were followed by single-point energy calculations at DFT, MP2, and high-level coupled-cluster (CCSD and CCSD(T)) levels. Quasirelativistic energy-adjusted, small-core “Stuttgart-type” pseudopotentials were used for the transition metals Os,<sup>[137]</sup> Au,<sup>[137]</sup> Pt,<sup>[137]</sup> and Ir<sup>[137]</sup>. The corresponding (8s7p6d)[6s5p3d] valence basis sets were augmented by one f-type polarization function<sup>[204]</sup> (exponent  $\alpha$ : Os 0.886, Ir 0.938, Pt 0.993, and Au 1.050). Energy-adjusted 8-valence-electron pseudopotentials and (6s6p3d1f)/[4s4p3d1f] valence basis sets were used for the noble-gas atoms Ng = Kr, Xe.<sup>[148]</sup>

In the B3LYP-optimisations, a fluorine DZ+P all-electron basis set by Dunning<sup>[132]</sup> was used. Stationary points on the potential energy surface were characterised by harmonic vibrational frequency analyses at this level (providing also zero-point energy corrections to the thermochemistry). The subsequent single-point energy calculations had the fluorine basis replaced by a larger aug-cc-pVTZ basis set.<sup>[126]</sup> The post-HF calculations were carried out with the MOLPRO 2002.6<sup>[193]</sup> program package. Basis-set superposition errors (BSSE) were estimated by the counterpoise (CP)<sup>[98, 195]</sup> procedure. We note that the methodology used here,



in particular B3LYP-optimisations followed by B3LYP or CCSD(T) single-point energy calculations with larger basis sets, are well established as a reliable tool for redox thermochemistry in the 5d transition metal series, e.g. in previous studies on Hg, Au, Pt, and Ir systems.<sup>[12, 173]</sup> We have furthermore found excellent agreement with structures and relevant thermochemical data in test calculations on  $\text{ReF}_7$  – data not shown. We do not consider spin-orbit corrections in this work. Our previous studies indicated spin-orbit effects to have only a minor influence on the relevant thermochemical data or activation barriers, even when open-shell 5d species were involved.<sup>[112]</sup>

### 4.5.3 Results and Discussion

Figure 4.5-2 shows the B3LYP-optimised structures of  $\text{OsF}_8$ ,  $\text{OsF}_7$ , and  $\text{OsF}_6$ . At this computational level, we find two minima for  $\text{OsF}_8$ . One is a distorted quadratic antiprism with  $D_{2d}$  symmetry and two different Os-F bonds – Table 4.5-1. The other is a regular quadratic antiprism with  $D_{4d}$  symmetry. The energies of the two minima differ only by less than  $5 \text{ kJ mol}^{-1}$ , and the calculations suggest a shallow potential energy surface around the two located minima. An earlier study at HF and MP2 levels indicated a pronounced dependence on computational method. At HF level (with a valence DZP basis for fluorine), a more distorted  $C_{2v}$  structure was obtained, whereas the less distorted antiprism of  $D_{2d}$  symmetry was found at MP2 level.  $\text{OsF}_8$  may indeed be a fluxional species.

Unimolecular gas-phase  $\text{F}_2$  elimination from  $\text{OsF}_8$  to give  $\text{OsF}_6$  is found to be exothermic – see Table 4.5-2, reaction a. However, the computed barrier for concerted elimination at B3LYP level is appreciable,  $203.9 \text{ kJ mol}^{-1}$ . The transition state has  $C_{2v}$  symmetry. A second potential channel for decomposition of  $\text{OsF}_8$  involves the homolytic dissociation of an Os-F bond to give  $\text{OsF}_7$ . This reaction is endothermic (by  $14.4 \text{ kJ mol}^{-1}$  at CCSD(T) level; Table 4.5-2, reaction b) but exhibits an appreciable barrier of  $144.0 \text{ kJ mol}^{-1}$ , due to substantial nuclear reorganization. Bimolecular  $\text{F}_2$  elimination to give  $\text{OsF}_7$  (Table 4.5-3, reaction a) is strongly exothermic and may be a reason why  $\text{OsF}_8$  has not been observed in typical condensed-phase reactions (computation of activation barriers of bimolecular reaction channels is outside the scope of the present work).

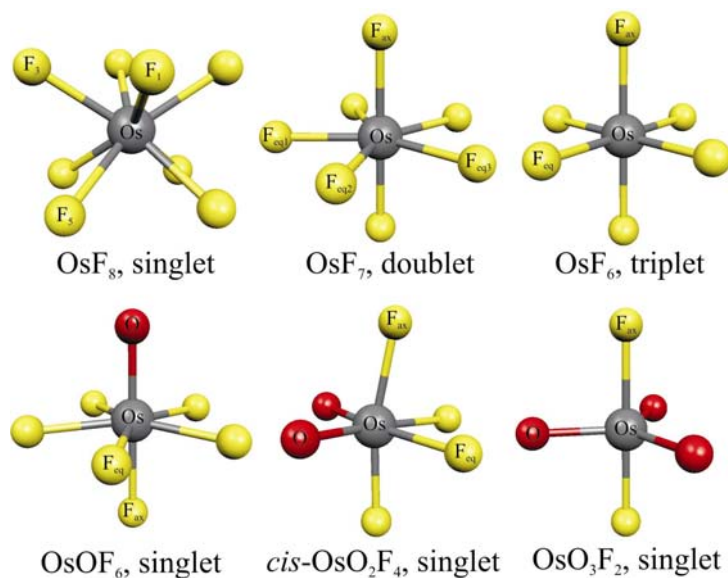


**Figure 4.5-2** B3LYP-optimised minimum structures of OsF<sub>8</sub> ( $D_{4d}$ ), OsF<sub>7</sub> ( $C_{2v}$ ), OsF<sub>6</sub> ( $D_{4h}$ ), OsOF<sub>6</sub> ( $C_{5v}$ ), *cis*-OsO<sub>2</sub>F<sub>4</sub> ( $C_{2v}$ ), and OsO<sub>3</sub>F<sub>2</sub> ( $D_{3h}$ ). Distances and angles are in Table 4.5-1.

**Table 4.5-1** B3LYP-optimised minimum structures<sup>[a]</sup>

Species	Symmetry	Species	Symmetry	Species	Symmetry
<b>OsF<sub>8</sub></b>	$D_{2d}$ ( $D_{4d}$ ) <sup>[b]</sup>	<b>OsF<sub>7</sub></b>	$C_{2v}$	<b>OsF<sub>6</sub></b>	$D_{4h}$
Os-F <sub>1</sub>	186.7	F <sub>ax</sub>	183.9	F <sub>ax</sub>	187.1
Os-F <sub>3</sub>	189.9	F <sub>eq1</sub>	185.6	F <sub>eq</sub>	183.4
Os-F <sub>5</sub>	1.867	F <sub>eq2</sub>	189.0		
F <sub>1</sub> -Os-F <sub>2</sub>	104.0	F <sub>eq3</sub>	186.9		
F <sub>3</sub> -Os-F <sub>4</sub>	123.8	F <sub>eq1</sub> -Os-F <sub>eq2</sub>	71.9		
F <sub>1</sub> -Os-F <sub>5</sub>	86.4 (78.2)	F <sub>eq2</sub> -Os-F <sub>eq3</sub>	72.2		
		F <sub>eq3</sub> -Os-F <sub>eq4</sub>	71.8		
<b>OsOF<sub>6</sub></b>	$C_{5v}$	<b><i>cis</i>-OsO<sub>2</sub>F<sub>4</sub></b>	$C_{2v}$	<b>OsO<sub>3</sub>F<sub>2</sub></b>	$D_{3h}$
Os-O	167.8	Os-F <sub>ax</sub>	186.1	Os-F <sub>ax</sub>	189.3
Os-F <sub>eq</sub>	188.6	Os-O	169.0	Os-O	169.7
Os-F <sub>ax</sub>	186.1	Os-F <sub>eq</sub>	188.8		
O-Os-F <sub>eq</sub>	93.6	F <sub>ax</sub> -Os-O	93.9		
F <sub>eq</sub> -Os-F <sub>eq</sub>	71.8	F <sub>ax</sub> -Os-F <sub>eq</sub>	85.3		
		F <sub>ax</sub> -Os-F <sub>ax</sub>	167.8		

<sup>[a]</sup>Distances in pm and angles in degrees. Cf. Figure 4.5-1 for atom numbering.

<sup>[b]</sup>Values in parentheses are for the  $D_{4d}$  minimum – see text.

**Table 4.5-2** Computed reaction energies (in kJ mol<sup>-1</sup>)<sup>[a]</sup>

Reaction	B3LYP	MP2	CCSD	CCSD(T)
a. OsF <sub>8</sub> → OsF <sub>6</sub> + F <sub>2</sub> <sup>[b]</sup>	-79.1 (-97.3)	63.0	-150.8	-73.1
b. OsF <sub>8</sub> → OsF <sub>7</sub> + F <sup>[b]</sup>	6.6 (-7.8)	94.2	-38.4	14.4
c. OsF <sub>7</sub> → OsF <sub>5</sub> + F <sub>2</sub> <sup>[b]</sup>	218.9 (206.8)	303.7	108.7	186.5
d. OsF <sub>7</sub> → OsF <sub>6</sub> + F <sup>[b]</sup>	69.6 (59.5)	142.4	12.0	65.2
e. OsF <sub>6</sub> → OsF <sub>5</sub> + F <sup>[b]</sup>	304.6 (296.4)	334.9	221.1	274.1
f. OsF <sub>6</sub> + KrF <sub>2</sub> → OsF <sub>8</sub> + 2Kr	43.4	-91.6	65.8	12.2
g. OsF <sub>5</sub> + KrF <sub>2</sub> → OsF <sub>7</sub> + 2Kr	-254.6	-332.2	-193.7	-247.4
h. [OsF <sub>6</sub> ] <sup>-</sup> + [KrF] <sup>+</sup> → OsF <sub>7</sub> + Kr <sup>[c]</sup>	-688.7	-746.3	-552.7	-633.5
i. OsOF <sub>6</sub> → OsOF <sub>4</sub> + F <sub>2</sub>	138.7	298.2	59.5	133.6
j. OsOF <sub>6</sub> → OsF <sub>5</sub> + OF	170.3	507.4	116.2	233.7
k. OsOF <sub>6</sub> → OsF <sub>6</sub> + O	97.5	390.0	73.7	164.7
l. OsOF <sub>6</sub> → OsOF <sub>5</sub> + F	54.2	150.1	4.1	54.8
m. OsO <sub>2</sub> F <sub>4</sub> + 2F <sub>2</sub> → OsF <sub>8</sub> + O <sub>2</sub>	-205.6	-129.2	-104.8	-110.2
n. OsO <sub>2</sub> F <sub>4</sub> + 2KrF <sub>2</sub> → OsF <sub>8</sub> + 2Kr + O <sub>2</sub>	-276.9	-186.3	-274.8	-232.1
o. OsO <sub>4</sub> + 4KrF <sub>2</sub> → OsF <sub>8</sub> + 4Kr + 2O <sub>2</sub>	-836.9	-711.9	-921.3	-805.0
p. OsO <sub>4</sub> + 2KrF <sub>2</sub> → OsO <sub>2</sub> F <sub>4</sub> + 2Kr + O <sub>2</sub>	-560.0	-525.7	-646.5	-572.9
q. OsO <sub>2</sub> F <sub>4</sub> + KrF <sub>2</sub> → OsOF <sub>6</sub> + Kr + O	96.7	95.0	28.6	71.5
r. OsO <sub>2</sub> F <sub>4</sub> + F <sub>2</sub> → OsOF <sub>6</sub> + O	132.4	123.5	113.7	132.4
s. OsO <sub>2</sub> F <sub>4</sub> + 2F <sub>2</sub> → OsOF <sub>6</sub> + OF + F	55.9	79.6	59.5	80.1
t. OsO <sub>3</sub> F <sub>2</sub> + 2F <sub>2</sub> → OsOF <sub>6</sub> + O <sub>2</sub>	-473.3	-387.2	-348.1	-337.9
u. KrF <sub>2</sub> → Kr + F <sub>2</sub> <sup>[d]</sup>	-35.7	-28.5	-85.0	-60.9
v. F <sub>2</sub> → 2F <sup>[e]</sup>	155.3	173.6	124.4	152.7

<sup>[a]</sup>Reaction energies for singlet OsF<sub>8</sub>, doublet OsF<sub>7</sub>, triplet OsF<sub>6</sub>, quartet OsF<sub>5</sub>, singlet OsOF<sub>6</sub>, singlet OsO<sub>2</sub>F<sub>4</sub>, singlet OsO<sub>3</sub>F<sub>2</sub>, and singlet OsO<sub>4</sub>. <sup>[b]</sup>Values in parentheses are counterpoise and zero-point vibration corrected. <sup>[c]</sup>Energies for the separate steps are: (i) formation of the ion-pair complex -545.2 kJ mol<sup>-1</sup>, and (ii) decomposition to OsF<sub>7</sub> and Kr -143.5 kJ mol<sup>-1</sup> (B3LYP result). <sup>[d]</sup>The experimental value is -60.2±3.4 kJ mol<sup>-1</sup>. <sup>[219, 220]</sup> <sup>[e]</sup>The experimental value is +158.3 kJ mol<sup>-1</sup>. <sup>[110, 168]</sup>

We note in passing the good agreement between B3LYP and CCSD(T) thermochemistry, whereas MP2 tends to overestimate and CCSD tends to underestimate the stabilities of the high-oxidation-state species significantly. These trends are consistent with appreciable differential non-dynamical correlation effects and agree with our earlier experience on redox reactions of 5d transition metal fluoride complexes.<sup>[12, 72, 73, 173, 221]</sup> We consider the B3LYP and CCSD(T) results to provide faithful estimates of the reaction energies. The good performance of B3LYP in this field of 5d-metal fluoride redox reactions (compared to pure gradient-corrected functionals or hybrid functionals with larger exact-exchange admixtures<sup>[12, 173]</sup>) is notable also in view of an apparently nonuniform quality of B3LYP in other areas of transition metal thermochemistry.<sup>[222]</sup>

**Table 4.5-3** Computed bimolecular decomposition reactions (in kJ mol<sup>-1</sup>)<sup>[a]</sup>

Reaction	B3LYP	MP2	CCSD	CCSD(T)
a. 2OsF <sub>8</sub> → 2OsF <sub>7</sub> + F <sub>2</sub>	-142.0	3.4	-212.2	-131.9
b. 2OsF <sub>7</sub> → 2OsF <sub>6</sub> + F <sub>2</sub>	-16.1	111.3	-100.4	-22.4
c. 2OsF <sub>6</sub> → 2OsF <sub>5</sub> + F <sub>2</sub>	453.9	496.1	317.7	395.4
d. 2OsOF <sub>6</sub> → 2OsF <sub>6</sub> + O <sub>2</sub>	-319.6	200.4	-295.5	-151.1
e. 2OsOF <sub>6</sub> → 2OsOF <sub>5</sub> + F <sub>2</sub>	-46.9	126.7	-116.2	-43.1
f. 2OsO <sub>2</sub> F <sub>4</sub> + 2F <sub>2</sub> → 2OsOF <sub>6</sub> + O <sub>2</sub>	-249.7	-332.7	-215.6	-215.7
g. 2OsO <sub>2</sub> F <sub>4</sub> + 2KrF <sub>2</sub> → 2OsOF <sub>6</sub> + O <sub>2</sub> + 2Kr	-321.1	-389.7	-385.6	-337.5
h. 2OsF <sub>6</sub> + KrF <sub>2</sub> → 2OsF <sub>7</sub> + Kr	-19.5	-139.8	15.4	-38.6

<sup>[a]</sup>Cf. footnote 1 to Table 4.5-2

Moving to the next lower homoleptic fluoride, we find OsF<sub>7</sub> to exhibit a minimum with C<sub>2v</sub> symmetry – Figure 4.5-2. Unimolecular F<sub>2</sub> Elimination, OsF<sub>7</sub> → OsF<sub>5</sub> + F<sub>2</sub>, is now appreciably endothermic – by 186.5 kJ mol<sup>-1</sup> at CCSD(T) level, Table 4.5-2. Homolytic bond cleavage costs 65.2 kJ mol<sup>-1</sup> at the same level, with a relatively high barrier of 237.0 kJ mol<sup>-1</sup>, due to extensive nuclear reorganization (B3LYP result). These results suggest appreciable stability for OsF<sub>7</sub> under typical gas-phase conditions. Notably, however, the bimolecular F<sub>2</sub> elimination (Table 4.5-3, reaction b) is exothermic. The characterisation of OsF<sub>7</sub> in ref. <sup>[215]</sup> was mainly based on an IR spectrum that differed from that of OsF<sub>6</sub>. Our computed vibrational spectra (Table 4.5-5) suggest substantial differences between the two species but do not agree too well with the reported solid-state data on OsF<sub>7</sub>. A recent attempt by Seppelt *et al.*<sup>[22]</sup> to reproduce the reaction of ref. <sup>[215]</sup> gave pure OsF<sub>6</sub> as sole product, as indicated by low-temperature Raman spectroscopy. Our computations do not allow us to interpret the experimental results of ref. <sup>[215]</sup> at this point. In any case, OsF<sub>7</sub> appears to be a clearly more stable species and more easily accessible target (at least in gas-phase or matrix-isolation experiments) compared to OsF<sub>8</sub>. It is unclear, however, whether the high-temperature condensed-phase conditions employed in the experiments would allow isolation of such a highly reactive species.

KrF<sub>2</sub> is a well-known, very strong oxidative fluorination agent and might provide a pathway towards the higher fluorides. Table 4.5-2 lists thus also reactions involving krypton, as well as some isoelectronic xenon compounds. The oxidation reaction OsF<sub>6</sub> + KrF<sub>2</sub> → OsF<sub>8</sub> + Kr is calculated to be slightly endothermic – Table 4.5-2, reaction f. This indicates that preparation of OsF<sub>8</sub> will indeed be a great challenge. In contrast, oxidation of OsF<sub>5</sub> (Table 4.5-2, reaction g) or of OsF<sub>6</sub> (Table 4.5-3, reaction h) by KrF<sub>2</sub> is substantially exothermic. This holds even more so for the strongest presently known oxidative fluorinating agent [KrF]<sup>+</sup>:<sup>[208]</sup> formation of the [KrF][OsF<sub>6</sub>] ion-pair complex from (gas-phase) [KrF]<sup>+</sup> and quartet [OsF<sub>6</sub>]<sup>-</sup> is highly exothermic (-545.2 kJ mol<sup>-1</sup> at B3LYP level) and provides a local

minimum on the potential energy surface. However,  $[\text{KrF}][\text{OsF}_6]$  is calculated to decompose exothermically (by  $-143.5 \text{ kJ mol}^{-1}$ ) into  $\text{OsF}_7$  and Kr. Reaction of the related complex  $[\text{XeF}][\text{OsF}_6]$  is calculated to be endothermic (experimentally, this ion-pair complex decomposes at  $20^\circ\text{C}$  according to  $3[\text{XeF}][\text{OsF}_6] \rightarrow [\text{Xe}_2\text{F}_3][\text{OsF}_6] + 2\text{OsF}_6 + \text{Xe}^{[209]}$ ).

Figure 4.5-3 shows the reaction energies  $[\text{NgF}][\text{MF}_6] \rightarrow \text{MF}_7 + \text{Ng}$  for a range of complexes ( $\text{Ng} = \text{Kr}, \text{Xe}$  and  $\text{M} = \text{Os}, \text{Ir}, \text{Pt}, \text{Au}$ ) at the corresponding computational level (note that these energies will be generally somewhat more positive in the condensed phase due to electrostatic stabilisation of the ion-pair complexes). Reaction of  $[\text{KrF}][\text{IrF}_6]$  to give  $\text{IrF}_7$  is also exothermic and has recently been suggested as a possible pathway towards  $\text{Ir}^{\text{VII}}$ .<sup>[112]</sup> Figure 4.5-3 suggests analogous access to  $\text{OsF}_7$ . Interestingly, in contrast to several known  $[\text{KrF}][\text{MF}_6]$  complexes of platinum and gold, and in spite of the existence of  $[\text{XeF}][\text{IrF}_6]$ ,<sup>[209]</sup> the corresponding osmium  $[\text{NgF}][\text{OsF}_6]$  and  $[\text{KrF}][\text{IrF}_6]$  complexes have never been observed.

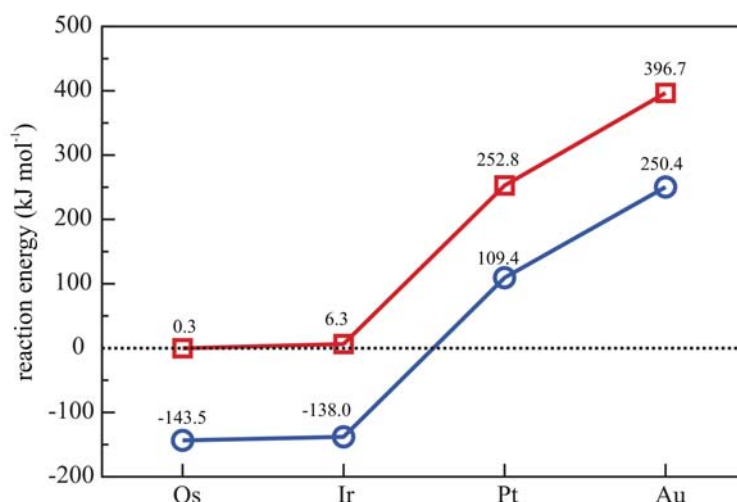


**Figure 4.5-3** Computed energies (B3LYP) in  $\text{kJ mol}^{-1}$  for the (gas-phase) reactions  $[\text{NgF}]^+[\text{MF}_6]^- \rightarrow \text{MF}_7 + \text{Ng}$  ( $\text{Ng} = \text{Kr}, \text{Xe}$ ;  $\text{M} = \text{Os}, \text{Ir}, \text{Pt}, \text{Au}$ ): ( $\square$ )  $[\text{XeF}]^+$  complexes, ( $\circ$ )  $[\text{KrF}]^+$  complexes.

Veldkamp and Frenking<sup>[216]</sup> had discussed isodesmic fluorination reactions of  $\text{Os}^{\text{VIII}}$  oxofluorides as possible pathway towards  $\text{OsF}_8$ . Unfortunately, experimental investigations suggest that these types of fluorinations, either with  $\text{F}_2$  or with  $\text{KrF}_2$ , stop at the known  $\text{OsO}_2\text{F}_4$  stage,<sup>[223-225]</sup> and further fluorination is unsuccessful. Thus, even  $\text{OsOF}_6$  is not known (and a structure could not be located at HF or MP2 level in ref. <sup>[216]</sup>). Most likely, the reason is

the increasing steric hindrance in the Os coordination sphere, leading to an increasing oxidising power along the series  $\text{OsO}_4 < \text{OsO}_3\text{F}_2 < \text{OsO}_2\text{F}_4$ .<sup>[226]</sup> Interestingly, our computations (B3LYP or CCSD(T), Table 4.5-2) indicate exothermic fluorination, both with  $\text{F}_2$  and with  $\text{KrF}_2$ , up to and including  $\text{OsF}_8$  as product. Maybe the kinetics of these reactions are unfavourable (this will be subject of future studies). Experimental evidence suggests in any case that homoleptic lower osmium fluorides provide a better starting point for the synthesis of the higher fluorides than the  $\text{Os}^{\text{VIII}}$  oxyfluorides.

**Table 4.5-4** Computed adiabatic first ionization potentials (in eV) of neutral osmium fluoride complexes and decomposition reaction energies of cationic species (in  $\text{kJ mol}^{-1}$ )<sup>[a]</sup>

Reaction	B3LYP	MP2	CCSD	CCSD(T)
a. $\text{OsF}_7 \rightarrow [\text{OsF}_7]^+$	12.6	11.4	13.3	12.5
b. $\text{OsOF}_5 \rightarrow [\text{OsOF}_5]^+$	12.3	11.1	12.8	12.2
c. $[\text{OsF}_7]^+ \rightarrow [\text{OsF}_6]^+ + \text{F}$	32.3	128.1	-24.5	33.5
d. $[\text{OsF}_7]^+ \rightarrow [\text{OsF}_5]^+ + \text{F}_2$	88.3	257.9	-36.3	76.7
e. $[\text{OsOF}_5]^+ \rightarrow [\text{OsOF}_4]^+ + \text{F}$	116.6	245.2	34.7	114.5
f. $[\text{OsOF}_5]^+ \rightarrow [\text{OsOF}_3]^+ + \text{F}_2$	277.7	469.4	185.1	279.6

<sup>[a]</sup>Reaction energies for doublet  $\text{OsF}_7$ , singlet  $[\text{OsF}_7]^+$ , doublet  $[\text{OsF}_6]^+$ , triplet  $[\text{OsF}_5]^+$ , doublet  $\text{OsOF}_5$ , singlet  $[\text{OsOF}_5]^+$ , doublet  $[\text{OsOF}_4]^+$ , and triplet  $[\text{OsOF}_3]^+$ .

All attempts to synthesise the highest oxyfluoride  $\text{OsOF}_6$  were unsuccessful (a claimed preparation was later shown to have led to  $\text{OsO}_2\text{F}_4$ <sup>[223, 227]</sup>), and even the computational search for this complex failed.<sup>[216]</sup> In contrast to that older computational study, we have been able to locate a minimum for  $\text{OsOF}_6$  at B3LYP level (a similar structure is obtained at HF or MP2 levels), namely a pentagonal bipyramidal structure ( $C_{5v}$  symmetry, Figure 4.5-2; a monocapped octahedral  $C_{3v}$  structure is a transition state at  $61.6 \text{ kJ mol}^{-1}$ , and the monocapped trigonal prism of  $C_{2v}$  symmetry is a second-order saddle point at  $110.2 \text{ kJ mol}^{-1}$  above the  $C_{5v}$  minimum). All unimolecular gas-phase decomposition channels of  $\text{OsOF}_6$  are endothermic (Table 4.5-2), including homolytic Os-F bond-breaking to give  $\text{OsOF}_5$  (doublet), or Os-O bond cleavage to give  $\text{OsF}_6$  (triplet). Inclusion of bimolecular channels leads to exothermic decomposition pathways – Table 4.5-3, reactions d,e. As for  $\text{OsF}_8$  or  $\text{OsF}_7$ , this suggests gas-phase or matrix-isolation techniques as preferred tools for the preparation of  $\text{OsOF}_6$ .

The cations  $[\text{OsF}_7]^+$  and  $[\text{OsOF}_5]^+$  are of particular interest as potential precursors for the missing targets  $\text{OsF}_8$  and  $\text{OsOF}_6$ . Singlet  $[\text{OsF}_7]^+$  exhibits a slightly compressed pentagonal bipyramidal structure (Os-F<sub>ax</sub> 180.0 pm, Os-F<sub>eq</sub> 184.7 pm). The adiabatic ionization potential  $\text{OsF}_7 \rightarrow [\text{OsF}_7]^+$  is calculated to be appreciable 12.5 eV (CCSD(T) result). Os-F bond

homolysis and concerted F<sub>2</sub> elimination are computed to be endothermic – Table 4.5-4. [OsOF<sub>5</sub>]<sup>+</sup> exhibits C<sub>4v</sub> symmetry. Due to the *trans* influence of the oxo ligand, the axial Os-F bond is somewhat lengthened (Os-O 167.5 pm, Os-F<sub>ax</sub> 183.9 pm, and Os-F<sub>eq</sub> 181.2 pm). Unimolecular decomposition channels for this cation are all computed to be endothermic.

**Table 4.5-5** Experimental and computed vibrational frequencies (with IR- and Raman intensities) for OsF<sub>7</sub> and OsF<sub>6</sub><sup>[a]</sup>

	exp. IR freq. (solid-state)	exp. IR freq. (gas-phase)	exp. Raman freq.	comp. freq.	comp. IR inten.	comp. Raman activities
<b>OsF<sub>7</sub></b>	282			67	-	9
	336			193	9	-
	366			268	-	4
	483			293	21	21
	550			303	-	4
	715			346	20	-
				481	-	9
				500	-	4
				648	-	13
				661	150	-
				680	150	-
				706	-	46
				722	186	-
<b>OsF<sub>6</sub></b>	303	268	252	160	3	-
	328	720	632	249	22	-
	384	894	733	290	12	-
	514	969		320	-	4
	555	1453		650	-	13
	628			662	-	12
	700			689	207	-
	900			718	205	-
	870			724	-	44
	968			1520	-	389
	1020					
	1190					
	1315					
	1400					
	1435					
1473						

<sup>[a]</sup>Frequencies in cm<sup>-1</sup>, computed IR-intensities in KM Mole<sup>-1</sup>, computed Raman scattering activities in (Å<sup>4</sup> AMU<sup>-1</sup>). Experimental solid-state results for OsF<sub>7</sub> from ref. <sup>[215]</sup> and for OsF<sub>6</sub> from ref. <sup>[228]</sup>. Gas-phase data for OsF<sub>6</sub> from ref. <sup>[229]</sup>.

#### 4.5.4 Conclusions

The evaluation of structures and stabilities of higher fluorides and oxyfluorides of osmium indicates that  $\text{OsF}_7$  is a viable target for preparation. But in view of potential exothermic bimolecular decomposition pathways, this might be better achieved in a gas-phase or matrix-isolation experiment than in an earlier<sup>[215]</sup> direct condensed-phase fluorination experiment that has recently been put into question.<sup>[22]</sup>  $\text{OsF}_8$  is much less stable thermochemically but appears to exhibit appreciable activation barriers for its unimolecular decomposition pathways. Its experimental observation under matrix-isolation conditions appears thus also possible. The last missing  $\text{Os}^{\text{VIII}}$  oxyfluoride,  $\text{OsOF}_6$ , is even somewhat more stable against unimolecular decomposition. Overall, the highest fluorides and oxyfluorides do thus remain interesting challenges for matrix-isolation spectroscopists, or possibly for mass spectrometrical identification in the gas-phase, whereas classical condensed-phase syntheses appear difficult.



## 5 Chapter

# Conclusions and Outlook

In this thesis we have suggested, by state-of-the-art quantum-chemical calculations, that several hitherto unknown high oxidation state 5d transition metal complexes have a realistic chance of experimental preparation. To enable the search for high oxidation state species by quantum-chemical methods, we have validated several density functional methods against CCSD(T) results for structures, reaction energies and activation barriers for Hg<sup>IV</sup> species like HgF<sub>4</sub>, HgCl<sub>4</sub>, and HgH<sub>4</sub>. Hybrid functionals with ca. 20% Hartree-Fock exchange (B3LYP, B1LYP or MPW1PW91) provide the best energetics compared with the CCSD(T) results – see Chapter 4.1.<sup>[12]</sup> Our study further confirms that HgF<sub>4</sub><sup>[12, 72, 73, 75, 120]</sup> is clearly a thermochemically stable species in the gas-phase whereas HgCl<sub>4</sub><sup>[12, 75, 120]</sup> is suggested to be thermochemically unstable with respect to Cl<sub>2</sub> elimination. HgH<sub>4</sub><sup>[12, 74, 75]</sup> is calculated to decompose exothermically into HgH<sub>2</sub> and H<sub>2</sub>, but it is also shown that the H<sub>2</sub> elimination has a moderate activation barrier – see Chapter 4.1.

Based on the calibration results we have used the B3LYP functional to explore alternative species that might provide access to condensed-phase Hg<sup>IV</sup> chemistry – see Chapter 4.2.<sup>[75]</sup> Several Hg<sup>IV</sup>X<sub>4</sub> and Hg<sup>IV</sup>F<sub>2</sub>X<sub>2</sub> species using so-called weakly coordinating anions, WCAs ([X]<sup>-</sup> = [AlF<sub>4</sub>]<sup>-</sup>, [Al<sub>2</sub>F<sub>7</sub>]<sup>-</sup>, [AsF<sub>6</sub>]<sup>-</sup>, [SbF<sub>6</sub>]<sup>-</sup>, [As<sub>2</sub>F<sub>11</sub>]<sup>-</sup>, [Sb<sub>2</sub>F<sub>11</sub>]<sup>-</sup>, [OSeF<sub>5</sub>]<sup>-</sup>, [OTeF<sub>5</sub>]<sup>-</sup>), have been calculated and were compared with each other or with analogous noble-gas compounds and the aforementioned gas-phase HgX<sub>4</sub> species. Several complexes studied show an exothermic F<sub>2</sub> elimination channel, with energies ranging from only about -60 kJ mol<sup>-1</sup> up to appreciable -180 kJ mol<sup>-1</sup>. The stability of these species is lower compared with the HgX<sub>4</sub> gas-phase species (HgF<sub>4</sub>, HgH<sub>4</sub> and HgCl<sub>4</sub>), and this is mainly due to the higher coordination number six of the Hg<sup>II</sup> species which stabilises the elimination products. It is shown that the [AsF<sub>6</sub>]<sup>-</sup> ligand is a more promising ligand system than the analogous [SbF<sub>6</sub>]<sup>-</sup> because of different aggregation effects in the Hg<sup>II</sup> and Hg<sup>IV</sup> complexes. In the case of [OSeF<sub>5</sub>]<sup>-</sup> and [OTeF<sub>5</sub>]<sup>-</sup> complex, fluorine elimination is calculated to be endothermic. This is partly due to the weaker interactions in the Hg<sup>II</sup> complexes. But a second elimination channel has to be considered for

this kind of ligand systems. The coupling product of two ligands will form the peroxidic  $[\text{OTeF}_5]_2$  species. These corresponding exothermic elimination energies lie between  $-100$  and  $-130 \text{ kJ mol}^{-1}$ . However, comparison between  $\text{Hg}^{\text{IV}}[\text{OTeF}_5]_4$  and the experimentally known  $\text{Xe}[\text{OTeF}_5]_4$  indicates that the noble-gas species has a slightly higher exothermicity of elimination than  $\text{Hg}^{\text{IV}}[\text{OTeF}_5]_4$  – see Chapter 4.2. We furthermore believe that many of the systems discussed will have nonnegligible activation barriers. The most promising complexes stabilizing the +IV oxidation state of mercury are  $\text{Hg}[\text{OTeF}_5]_4$  and  $\text{Hg}[\text{AsF}_6]_4$ .

Shifting one group left from mercury to the lighter element gold, a Russian research group had previously claimed the synthesis of  $\text{AuF}_7$  with gold in oxidation state +VII.<sup>[20, 184]</sup> We have performed calculations at DFT (BP86, B3LYP, BHLYP), MP2, CCSD and CCSD(T) levels on various fluorine containing compounds of gold in oxidation states +V through +VII – see Chapter 4.3.<sup>[173]</sup> Our calculations indicate clearly that the  $\text{F}_2$  elimination from  $\text{AuF}_7$  is strongly exothermic with a low activation barrier. This is inconsistent with the claimed stability of  $\text{AuF}_7$  at room temperature, and its existence at liquid-nitrogen temperature looks doubtful. Even homolytic Au-F bond breaking is exothermic and has only a low activation barrier. In view of its extremely high electron affinity (ca. 8.5 eV),  $\text{AuF}_6$  is also unlikely to exist. The oxidation state +V in, e.g.,  $[\text{AuF}_5]_2$  thus remains the highest oxidation state for gold<sup>[78, 178-180]</sup> that is known beyond doubt – see Chapter 4.3.

The highest known oxidation state of iridium is +VI in  $\text{IrF}_6$ .<sup>[115, 174]</sup> Our calculations suggest that the highest possible oxidation state of iridium having a realistic chance of experimental observation is +VII – see Chapter 4.4.<sup>[112]</sup> In the case of  $\text{IrF}_7$  we found an endothermic  $\text{F}_2$  elimination where the homolytic Ir-F bond breaking is actually slightly exothermic. However, the structural rearrangement required for this decomposition is substantial and creates an appreciable barrier of  $+100.4 \text{ kJ mol}^{-1}$ . An alternative  $\text{Ir}^{\text{VII}}$  compound is  $\text{IrOF}_5$  which has the advantage of a lower coordination number – see Chapter 3. All possible decomposition pathways for this species are computed to be endothermic; thus, this species has also a realistic chance for experimental observation. Another possible  $\text{Ir}^{\text{VII}}$  species is  $[\text{IrF}_6]^+$ , where concerted  $\text{F}_2$  elimination and homolytic bond breaking are calculated to be endothermic. This species would be an ideal precursor for a possible synthesis of  $\text{IrF}_7$  – see Chapter 4.4.<sup>[112]</sup>

For the next lightest element, osmium, all possible positive oxidation states are experimentally known.<sup>[115]</sup> In contrast to the other high oxidation states discussed in this thesis, the highest oxidation states of osmium are stabilised more by oxo ligands than by fluoride. The oxidation state +VIII is best known in form of  $\text{OsO}_4$ , and even the oxidation

state +VII is known without any doubt only for oxyfluorides. The isolation of OsF<sub>7</sub>, reported in 1966, could not be reproduced<sup>[22]</sup> under the conditions described<sup>[215]</sup>. The highest binary osmium fluoride characterised beyond doubt is thus OsF<sub>6</sub>.<sup>[115]</sup> We have studied various osmium fluorides and oxyfluorides up to oxidation state +VIII – see Chapter 4.5.<sup>[221]</sup> Our calculations indicate that the homoleptic fluorides all the way up to OsF<sub>8</sub> may exist. Homolytic Os-F bond breaking is calculated to be endothermic whereas concerted F<sub>2</sub> elimination from OsF<sub>8</sub> is exothermic. However, this elimination channel is prevented by an activation barrier of ~ 200 kJ mol<sup>-1</sup> at B3LYP level. For the next lower homoleptic fluoride, OsF<sub>7</sub>, both unimolecular F<sub>2</sub> elimination and homolytic bond cleavage are computed to be endothermic. This indicates appreciable stability of OsF<sub>7</sub> in the gas-phase. We have also studied the last missing oxyfluoride, OsOF<sub>6</sub>, which is computed to have only unimolecular gas-phase decomposition pathways. Only the inclusion of bimolecular channels leads to exothermic decomposition pathways – see Chapter 4.5.<sup>[221]</sup> This strongly suggests that the synthesis of such compounds in a gas-phase or matrix-isolation experiment is may be possible.

For the highest oxidation states of the remaining 5d transition metals (rhenium to lanthanum) we may refer to the experimental literature. Rhenium has its highest known oxidation state in ReF<sub>7</sub>, which is up to now the highest valence neutral transition metal fluoride species known.<sup>[230-234]</sup> For the next lighter element, the highest oxidation state is seen in the octahedral tungsten hexafluoride WF<sub>6</sub>.<sup>[235]</sup> It was recently discovered that this species exhibits an intramolecular ligand exchange (trigonal twist) with a relatively low barrier of 62 kJ mol<sup>-1</sup>.<sup>[186, 236]</sup> In the case of tantalum all pentahalides are known, but with different structures. The pentafluoride shows a tetrameric unit [TaF<sub>5</sub>]<sub>4</sub> in the crystal whereas in the gas-phase electron diffraction, mass- and infrared-spectroscopy suggest a trimer, [TaF<sub>5</sub>]<sub>3</sub>, or dimer, [TaF<sub>5</sub>]<sub>2</sub>.<sup>[237]</sup> The highest known oxidation state of hafnium is +IV, stabilised with all four halides (HfF<sub>4</sub> – HfI<sub>4</sub>) which display regular tetrahedral structures.<sup>[237]</sup> To complete the series we have to consider also the lightest 5d metal lanthanum. All trihalides of lanthanum are experimentally known.<sup>[237-239]</sup>

If we combine the highest oxidation states reliably known by experiment for the 5d transition metals with the high-level quantum-chemical predictions in this thesis, we observe a revised trend in the periodic table – see below. Before considering quantum-chemical predictions the trend of the highest oxidation states of 5d transition metals looks irregular from group 8 through group 13 – see Figure 5-1.

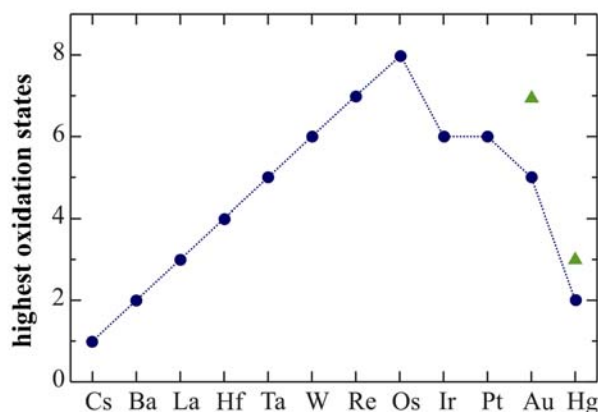


**Figure 5-1** Maximum oxidation states of the 5d transition metals: (●) highest experimentally known values, (▲) probably incorrect experimental assignments.

The maximum oxidation states for the early transition metals follow the group number up to Group 8 (e.g.  $\text{OsO}_4$ ). But the trend for the later transition metals is less clear-cut (see filled circles and dotted line in Figure 5-1). As we have seen above the highest experimentally known oxidation state of iridium is +VI in  $\text{IrF}_6$ . For platinum the highest possible oxidation state is +VI is in the  $\text{PtF}_6$  species (see ref. <sup>[177]</sup> and Table 5-1 for computational verification of the instability of  $\text{Pt}^{\text{VIII}}$  and  $\text{Pt}^{\text{VII}}$ , respectively). The highest oxidation state for gold known without any doubt is  $\text{Au}^{\text{V}}$ , and our quantum-chemical calculations have shown that  $\text{Au}^{\text{VII}}$  and  $\text{Au}^{\text{VI}}$  are highly improbable. In the case of mercury, the early reports of electrochemically generated, spectroscopically characterised short-lived  $[\text{Hg}^{\text{III}}(\text{cyclam})][\text{BF}_4]_3$  species have not been reproduced and therefore the experimentally well-known oxidation state +II ( $\text{HgF}_2$ ) should be taken as highest.

Once we include our predictions we obtain a revised picture of the highest oxidation states of the 5d transition metals, displaying a clear trend. Now, we observe a linear descent from osmium +VIII to mercury +IV – see red squares and dashed line in Figure 5-2.

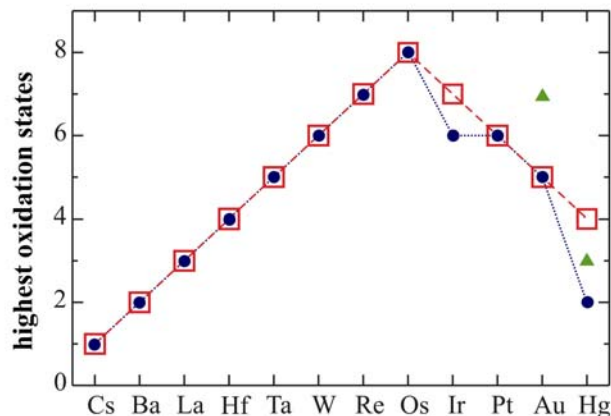


**Figure 5-2** Maximum oxidation states of the 5d transition metals: (●) highest experimentally known values, (▲) probably incorrect experimental assignments, (□) suggested maximum achievable oxidation states.

Except for osmium, the highest oxidation states are generally stabilised as fluorides. As discussed in Chapter 4.5,  $\text{OsF}_7$  and  $\text{OsF}_8$  also have a chance of experimental realisation, which would therefore complete the trend of the fluoride series of the 5d transition metals – see red squares and dashed line in Figure 5-3. A rough overview of the highest experimental and predicted oxidation states of the 5d row stabilised by fluoride ligands is given in Table 5-1.

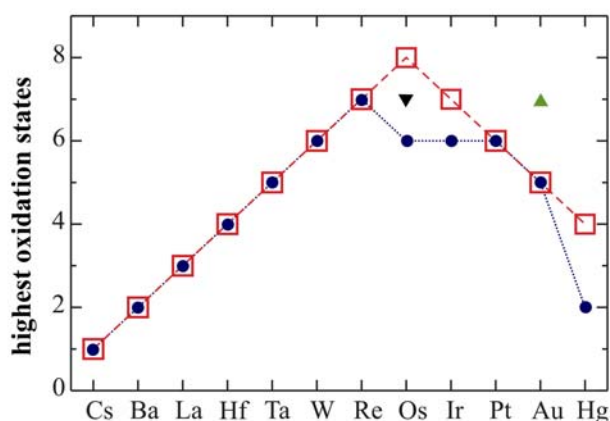


**Figure 5-3** Maximum oxidation states of binary 5d transition metal fluorides: (●) highest experimentally known  $\text{MF}_n$  species, (▲) probably incorrect experimental assignment, (▼) controversial experimental assignment, (□) suggested maximum achievable oxidation states.

**Table 5-1** The highest experimental and predicted 5d transition metal fluorides.

Element	Species	Ox. state	Status	Theor. Ref.	Exp. Ref.
La	LaF <sub>3</sub>	3	[b]	[240]	[237, 241]
Hf	HfF <sub>4</sub>	4	[b]	[242]	[237]
Ta	TaF <sub>5</sub> <sup>[d]</sup>	5	[b]	[243]	[237, 241]
W	WF <sub>6</sub>	6	[b]	[244-246]	[115, 116, 186, 247, 248]
Re	ReF <sub>7</sub>	7	[b]		[230, 231, 234, 249]
Os	OsF <sub>6</sub>	6	[b]	[221, 244]	[115, 116, 186, 226, 248]
	<i>OsF</i> <sub>7</sub>	7	[a]	[216, 221]	[22, 215]
	<i>OsF</i> <sub>8</sub>	8	[c]	[216, 221]	
Ir	IrF <sub>6</sub>	6	[b]	[112, 244]	[115, 116, 186, 248]
	<i>IrF</i> <sub>7</sub>	7	[c]	[112]	
Pt	PtF <sub>6</sub>	6	[b]	[177, 244]	[115, 116, 186]
Au	AuF <sub>3</sub> <sup>[e]</sup>	5	[b]	[173]	[179, 180, 200]
Hg	HgF <sub>2</sub>	2	[b]	[169, 250]	[115, 116]
	<i>HgF</i> <sub>4</sub>	4	[c]	[12, 72-75, 118-120]	

Species written in *italic* are predicted to be stable. <sup>[a]</sup>Controversial experimental assignment. <sup>[b]</sup>Experimentally known. <sup>[c]</sup>Predicted to be stable. <sup>[d]</sup>Pentafluorides have tetrameric units. <sup>[e]</sup>Pentafluorides have dimeric units.

The trend in the highest oxidation states continues even beyond the 5d transition metals. The elements caesium and barium fit the trend at the beginning of period six, as shown in the Figures 5.1 – 5.3. The element thallium also fits in the trend with the highest experimentally known oxidation state +III in TaF<sub>3</sub>.<sup>[237]</sup>

Do the 3d and 4d transition metal rows exhibit similar trends? In the case of the 4d transition metal row we also observe a linear increase of the oxidation states up to ruthenium (+ VIII), e.g. RuO<sub>4</sub>, but afterwards the trend looks irregular. The highest observed oxidation state for rhodium is only +VI in RhF<sub>6</sub><sup>[115, 190]</sup>, missing the oxidation state +VII needed for linear descent. Moving towards silver the maximum oxidation states decrease with increasing atomic number, with the relevant complexes being [O<sub>2</sub>][PdF<sub>6</sub>]<sup>[190, 251]</sup> and [Cs]<sub>2</sub>[AgF<sub>6</sub>]<sup>[252, 253]</sup>. PdF<sub>6</sub> was reported in 1982 by a Russian research group, but this has never been confirmed.<sup>[190, 254]</sup> Note that Schwerdtfeger *et al.* have predicted, on the basis of quantum-chemical calculations, the possible existence of the oxidation state +V in the silver fluoride [AgF<sub>6</sub>]<sup>-</sup>.<sup>[145]</sup> For the next element, cadmium, there is no doubt that the highest reachable oxidation state is +II. The predicted thermochemistry of CdF<sub>4</sub> strongly suggests exothermic F<sub>2</sub> elimination.<sup>[73]</sup> This is mainly due to the lack of relativistic stabilisation compared with its heavier homologue mercury.

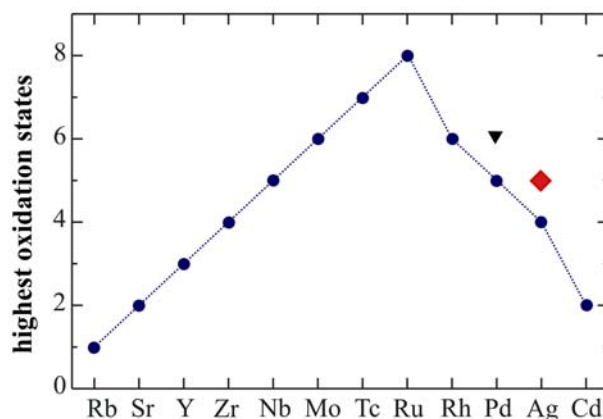


**Figure 5-4** Maximum oxidation states of 4d transition metals: (●) highest experimentally known species, (◆) computationally predicted species, (▼) controversial experimental assignment.

For the 3d transition metals we also observe a linear increase of the highest oxidation states, but only up to oxidation state +VII in  $[\text{MnO}_4]^-$  – see Figure 5-5.  $\text{Fe}^{\text{VIII}}$ , was reported<sup>[255, 256]</sup> in 1987 in the form of the tetraoxide,  $\text{FeO}_4$ , but this is certainly incorrect. Attempts to prepare and characterise  $\text{FeO}_4$  in a matrix experiment were unsuccessful.<sup>[257, 258]</sup> DFT calculations on several  $\text{FeO}_4$  isomers show that the peroxide  $[\text{O}_2]\text{FeO}_2$  in oxidation state +VI is much more stable species. It has been observed in a matrix-isolation experiment.<sup>[257]</sup> Therefore, oxidation state +VI remains the highest oxidation state of iron that is known beyond doubt.<sup>[259]</sup> Cobalt has nine electrons in its valence shell, but only the +V oxidation state is considered accessible.<sup>[260-262]</sup>  $[\text{NiF}_6]^{2-}$  is an example of nickel in oxidation state +IV; no higher state has been discovered so far.<sup>[263, 264]</sup> In the case of copper, two experimental species of oxidation state +IV were reported:  $\text{Cs}_2[\text{CuF}_6]$  and  $\text{Rb}_2[\text{CuF}_6]$ .<sup>[265-268]</sup> The copper oxidation state +III<sup>[269]</sup> is well known in ionic form, e.g., in  $[\text{CuF}_6]^{3-}$ , although neutral  $\text{CuF}_3$  is still unknown.<sup>[115, 267]</sup> As we have seen already, for cadmium oxidation states +IV or +III are most likely unstable due to a lack of relativistic effects, and this is also the case for zinc. The highest reachable oxidation state for zinc is therefore +II in, e.g.,  $\text{ZnF}_2$ .<sup>[73]</sup>

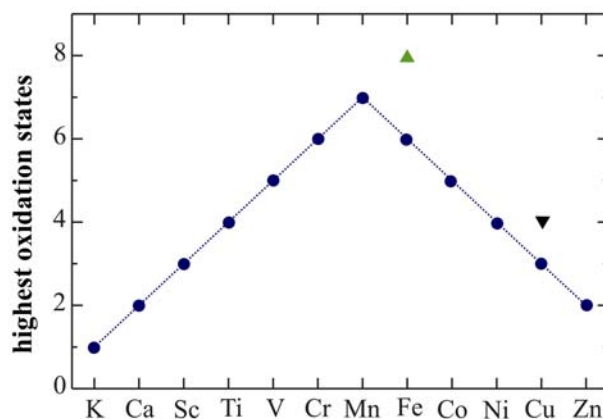


**Figure 5-5** Maximum oxidation states of 3d transition metals: (●) highest experimentally known species, (▲) incorrect experimental assignment, (▼) controversial experimental assignment.

To recapitulate the trends in the highest transition metal oxidation states: we observe a linear trend for the 5d transition metal row, whereas the trend of the 4d transition metals looks irregular for the last four elements Rh, Pd, Ag, and Cd. Inspection of the 3d row results in a more or less clear linear trend with the exception of the controversial copper +IV. All the trends presented in this thesis are based on experimentally confirmed species and high-level quantum-chemical predictions. Experimental verification of the predicted species and therefore of the suggested trends should be possible by using matrix-isolation or gas-phase experiments.<sup>[121]</sup>



*„Es mag interessant sein zu spekulieren, warum sich bestimmte Verbindungen so lange der Entdeckung entzogen und dann plötzlich mühelos herstellbar wurden. Obwohl jeder Fall sicherlich begründet werden kann, war es doch meistens so, dass ein anfänglicher Misserfolg auf intelligente Weise erklärt wurde. Danach wurde die Erklärung akzeptiert, und es mangelte an Bemühungen, diese zu widerlegen. Wenn daraus eine Lehre zu ziehen ist, dann die, dass man besser nicht so kategorisch behauptet, welcher experimentelle Weg viel versprechend ist oder nicht.“*

*E. A. Appelman cited in „Nichtexistierende Verbindungen“  
Konrad Seppelt, Chemie in unserer Zeit, 1978, 2*

## 6 Chapter

### References

- [1] D. I. Mendeleev, *Principles of Chemistry*, **1870**.
- [2] J. L. Meyer, *Justus Liebigs Annalen der Chemie* **1870**, 7, 354.
- [3] J. H. Holloway, E. G. Hope, P. J. Townson, R. L. Powell, *J. Fluorine Chem.* **1996**, 76, 105.
- [4] W. W. Dukat, J. H. Holloway, E. G. Hope, M. R. Rieland, P. J. Townson, R. L. Powell, *J. Chem. Soc., Chem. Commun.* **1993**, 1429.
- [5] J. H. Canterford, T. A. O'Donnell, *Inorg. Chem.* **1967**, 6, 541.
- [6] N. Bartlett, *Angew. Chem. Int. Ed.* **1968**, 7, 433.
- [7] B. C. Bales, P. Brown, A. Dehestani, J. M. Mayer, *J. Am. Chem. Soc.* **2005**, 127, 2832.
- [8] B. L. Pagenkopf, E. M. Carreira, *Chem. Eur. J.* **1999**, 5, 3437.
- [9] K. Khanbabaee, *Nachr. Chem. Tech. Lab.* **2003**, 51, 442.
- [10] P. Pyykkö, N. Runebeg, *THEOCHEM* **1991**, 80, 279.
- [11] K. O. Christe, W. W. Wilson, J. A. Sheehy, J. A. Boatz, *Angew. Chem. Int. Ed.* **1999**, 38, 2004.
- [12] S. Riedel, M. Straka, M. Kaupp, *Phys. Chem. Chem. Phys.* **2004**, 6, 1122.
- [13] M. C. Holthausen, *J. Comput. Chem.* **2005**, 26, 1505.
- [14] W. Koch, M. C. Holthausen, *A Chemist's Guide to Density Functional Theory, 2nd Edition*, Wiley-VCH, Weinheim, **2001**.
- [15] O. V. Gritsenko, E. J. Baerends, *Theor. Chem. Acc.* **1997**, 96, 44.
- [16] P. R. T. Schipper, O. V. Gritsenko, E. J. Baerends, *Theor. Chem. Acc.* **1998**, 99, 329.
- [17] P. Rother, F. Wagner, U. Zahn, *Radiochim. Acta* **1969**, 11, 203.
- [18] Y. M. Kiselev, *Russ. J. Inorg. Chem.* **1999**, 44, 652.
- [19] A. I. Dement'ev, M. L. Kuznetsov, Y. M. Kiselev, *Zh. Neorg. Khim.* **1997**, 42, 1167.
- [20] A. A. Timakov, V. N. Prusakov, Y. V. Drobyshevskii, *Dokl. Akad. Nauk SSSR* **1986**, 291, 125.
- [21] Y. M. Kiselev, Y. D. Tretiyakov, *Russ. Chem. Rev.* **1999**, 68, 365.
- [22] H. Shorafa, K. Seppelt, *Inorg. Chem.* **2006**, in press.
- [23] A. Szabo, N. S. Ostlund, *Modern Quantum Chemistry: Introduction to Advanced Electronic Structure Theory. 1st Ed. Revised*, Dover, New York, **1989**.
- [24] F. Jensen, *Introduction to computational chemistry*, John Wiley & Sons, Weinheim, **1999**.
- [25] W. Kutzelnigg, *Introduction to Theoretical Chemistry, Vol. 1: Quantum Mechanical Principles*, Verlag Chemie, Weinheim, **1975**.
- [26] P.-O. Windmak, B. O. Roos, *European Summerschool in Quantum Chemistry, Vol. 4*, Lund University, Lund, **2005**.
- [27] J. A. Pople, M. Head-Gordon, K. Raghavachari, *J. Chem. Phys.* **1987**, 87, 5968.
- [28] T. J. Lee, G. E. Scuseria, *Understanding Chemical Reactivity* **1995**, 13, 47.
- [29] T. H. Dunning, Jr., K. A. Peterson, *J. Chem. Phys.* **2000**, 113, 7799.
- [30] O. Sinanoglu, *Adv. Chem. Phys.* **1964**, 6, 358.
- [31] D. K. W. Mok, R. Neumann, N. C. Handy, *J. Phys. Chem.* **1996**, 100, 6225.
- [32] M. A. Buijse, E. J. Baerends, *J. Chem. Phys.* **1990**, 93, 4129.

- [33] M. Kaupp, *Journal of Computational Chemistry* **2006**, in press.
- [34] D. Jayatilaka, T. J. Lee, *J. Chem. Phys.* **1993**, *98*, 9734.
- [35] I. M. B. Nielsen, C. L. Janssen, *Chem. Phys. Lett.* **1999**, *310*, 568.
- [36] C. L. Janssen, I. M. B. Nielsen, *Chem. Phys. Lett.* **1998**, *290*, 423.
- [37] M. L. Leininger, I. M. B. Nielsen, T. D. Crawford, C. L. Janssen, *Chem. Phys. Lett.* **2000**, *328*, 431.
- [38] T. J. Lee, *Chem. Phys. Lett.* **2003**, *372*, 362.
- [39] A. C. Hurley, *Electron correlation in small molecules*, Academic Press, London, **1976**.
- [40] T. J. Lee, P. R. Taylor, *Int. J. Quantum Chem.* **1989**, *23*, 199.
- [41] T. J. Lee, J. E. Rice, G. E. Scuseria, H. F. Schaefer, III, *Theor. Chim. Acta* **1989**, *75*, 81.
- [42] P. Hohenberg, W. Kohn, *Phys. Rev. B* **1964**, *136*, 864.
- [43] P. A. M. Dirac, *Proc. Cambridge Phil. Soc.* **1930**, *26*, 376.
- [44] S. H. Vosko, L. Wilk, M. Nusair, *Can. J. Phys.* **1980**, *58*, 1200.
- [45] A. D. Becke, *J. Chem. Phys.* **1986**, *84*, 4524.
- [46] A. D. Becke, *Phys. Rev. A* **1988**, *38*, 3098.
- [47] J. P. Perdew, in *Electronic Structures of Solids* (Eds.: P. Ziesche, H. Eschrig), Akademie Verlag, Berlin, **1991**.
- [48] J. P. Perdew, K. Burke, M. Ernzerhof, *Phys. Rev. Lett.* **1996**, *77*, 3865.
- [49] J. P. Perdew, *Phys. Rev. B* **1986**, *33*, 8822.
- [50] C. Lee, W. Yang, R. G. Parr, *Phys. Rev. B* **1988**, *37*, 785.
- [51] J. P. Perdew, Y. Wang, *Phys. Rev. B* **1992**, *45*, 13244.
- [52] A. D. Becke, *J. Chem. Phys.* **1993**, *98*, 1372.
- [53] A. D. Becke, *J. Chem. Phys.* **1993**, *98*, 5648.
- [54] K. Burke, M. Ernzerhof, J. P. Perdew, *Chem. Phys. Lett.* **1997**, *265*, 115.
- [55] J. C. Slater, *Phys. Rev.* **1930**, *57*.
- [56] S. F. Boys, *Proc. Roy. Soc. (London)* **1950**, *A200*, 542.
- [57] W. J. Hehre, R. F. Stewart, J. A. Pople, *J. Chem. Phys.* **1969**, *51*, 2657.
- [58] R. Ditchfield, W. J. Hehre, J. A. Pople, *J. Chem. Phys.* **1971**, *54*, 724.
- [59] P. A. M. Dirac, *Proc. Roy. Soc. (London)* **1929**, *A123*, 714.
- [60] W. Kutzelnigg, *Theor. Chem. Acc.* **2000**, *103*, 182.
- [61] P. Pyykkö, J. P. Desclaux, *Acc. Chem. Res.* **1979**, *12*, 276.
- [62] K. S. Pitzer, *Acc. Chem. Res.* **1979**, *12*, 271.
- [63] H. H. Schmidtke, *Quantenchemie, Vol. 2*, VCH, Weinheim, **1994**.
- [64] V. Pershina, in *Relativistic Electronic Structure Theory, Part 2 Applications, Vol. 14* (Ed.: P. Schwerdtfeger), Elsevier, Amsterdam, **2004**, pp. 1.
- [65] P. Pyykkö, J. P. Desclaux, *Chem. Phys.* **1978**, *34*, 261.
- [66] P. Pyykkö, *Chem. Rev.* **1988**, *88*, 563.
- [67] V. Pershina, in *Chemistry of Superheavy Elements* (Ed.: M. Schädel), Kluwer, Dordrecht, **2003**, pp. 31.
- [68] W. H. E. Schwarz, E. M. Van Wezenbeek, E. J. Baerends, J. G. Snijders, *J. Phys. B* **1989**, *22*, 1515.
- [69] E. J. Baerends, W. H. E. Schwarz, P. Schwerdtfeger, J. G. Snijders, *J. Phys. B* **1990**, *23*, 3225.
- [70] J. Autschbach, S. Siekierski, M. Seth, P. Schwerdtfeger, W. H. E. Schwarz, *J. Comput. Chem.* **2002**, *23*, 804.
- [71] P. Schwerdtfeger, M. Seth, in *Relativistic effects on the Superheavy Elements, Vol. 4*, Wiley, New York, **1998**, pp. 2480.
- [72] M. Kaupp, H. G. von Schnering, *Angew. Chem. Int. Ed.* **1993**, *32*, 861.
- [73] M. Kaupp, M. Dolg, H. Stoll, H. G. von Schnering, *Inorg. Chem.* **1994**, *33*, 2122.
- [74] P. Pyykkö, M. Straka, M. Patzschke, *Chem. Commun.* **2002**, 1728.

- [75] S. Riedel, M. Straka, M. Kaupp, *Chem. Eur. J.* **2005**, *11*, 2743.
- [76] M. Seth, P. Schwerdtfeger, M. Dolg, *J. Chem. Phys.* **1997**, *106*, 3623.
- [77] J. P. Desclaux, *Atomic Data and Nuclear Data Tables* **1973**, *12*, 311.
- [78] P. Pyykkö, *Angew. Chem. Int. Ed.* **2004**, *43*, 4412.
- [79] L. J. Norrby, *J. Chem. Educ.* **1991**, *68*, 110.
- [80] P. Pyykkö, S. Riedel, M. Patzschke, *Chem. Eur. J.* **2005**, *11*, 3511.
- [81] M. Kaupp, *Spektrum der Wissenschaft* **2005**, 166.
- [82] L. L. Foldy, S. A. Wouthuysen, *Phys. Rev.* **1950**, *78*, 29.
- [83] M. Douglas, N. M. Kroll, *Ann. Phys.* **1974**, *82*, 89.
- [84] B. A. Hess, C. M. Marian, S. D. Peyerimhoff, in *Advanced Series in Physical Chemistry, Vol. 2* (Ed.: D. R. Yarkony), World Scientific, **1995**, pp. 152.
- [85] B. A. Hess, *Ber. Bunsen-Ges. Phys. Chem.* **1997**, *101*, 1.
- [86] E. van Lenthe, E. J. Baerends, J. G. Snijders, *J. Chem. Phys.* **1996**, *105*, 2373.
- [87] E. van Lenthe, J. G. Snijders, E. J. Baerends, *J. Chem. Phys.* **1996**, *105*, 6505.
- [88] C. Van Wüllen, *J. Comput. Chem.* **1999**, *20*, 51.
- [89] B. A. Hess, *Relativistic Effects in Heavy-Element Chemistry and Physics, Vol. 1*, Wiley, Sussex, **2003**.
- [90] M. Reiher, B. A. Hess, in *Modern Methods and Algorithms of Quantum Chemistry* (Ed.: J. Grotendorst), NIC Proceedings, Jülich, **2000**, pp. 451.
- [91] K. G. Dyall, *J. Chem. Phys.* **1994**, *100*, 2118.
- [92] H. Hellmann, *J. Chem. Phys.* **1935**, *3*, 61.
- [93] P. Gombas, *Z Phys.* **1935**, *94*, 473.
- [94] G. Frenking, I. Antes, M. Boehme, S. Dapprich, A. W. Ehlers, V. Jonas, A. Neuhaus, M. Otto, R. Stegmann, et al., in *Reviews in Computational Chemistry, Vol. 8* (Eds.: K. B. Lipkowitz, D. B. Boyd), Wiley-VCH, New York, **1996**, pp. 63.
- [95] T. R. Cundari, M. T. Benson, M. L. Lutz, S. O. Sommerer, in *Reviews in Computational Chemistry, Vol. 8* (Eds.: K. B. Lipkowitz, D. B. Boyd), Wiley-VCH, New York, **1996**, pp. 145.
- [96] J. C. Phillips, L. Kleinman, *Phys. Rev.* **1959**, *116*, 287.
- [97] B. Liu, A. D. McLean, *J. Chem. Phys.* **1989**, *91*, 2348.
- [98] S. F. Boys, F. Bernardi, *Mol. Phys.* **1970**, *19*, 553.
- [99] M. Kaupp, H. G. von Schnering, *Angew. Chem., Int. Ed. Engl.* **1995**, *34*, 986.
- [100] J. E. Ellis, *Inorg. Chem.* **2006**, *45*, 3167.
- [101] C. K. Jørgensen, *Oxidation numbers and Oxidation States*, Springer, New York, **1969**.
- [102] W. Chen, S. Shimada, M. Tanaka, *Science* **2002**, *295*, 308.
- [103] R. H. Crabtree, *Science* **2002**, *295*, 288.
- [104] E. C. Sherer, C. R. Kinsinger, B. L. Kormos, J. D. Thompson, C. J. Cramer, *Angew. Chem. Int. Ed.* **2002**, *41*, 1953.
- [105] G. Aullon, A. Lledos, S. Alvarez, *Angew. Chem. Int. Ed.* **2002**, *41*, 1956.
- [106] M. L. H. Green, *J. Organomet. Chem.* **1995**, *500*, 127.
- [107] D. Lentz, K. Seppelt, *Angew. Chem. Int. Ed.* **1978**, *17*, 355.
- [108] K. Seppelt, *Angew. Chem. Int. Ed.* **1982**, *21*, 877.
- [109] C. Esterhuysen, G. Frenking, *Theor. Chem. Acc.* **2004**, *111*, 381.
- [110] L. E. Forslund, N. Kaltsoyannis, *New J. Chem.* **2003**, *27*, 1108.
- [111] K. Seppelt, *Angew. Chem. Int. Ed.* **1979**, *18*, 186.
- [112] S. Riedel, M. Kaupp, *Angew. Chem. Int. Ed.* **2006**, *45*, 3708.
- [113] I. Krossing, I. Raabe, *Angew. Chem. Int. Ed.* **2004**, *43*, 2066.
- [114] S. H. Strauss, *Chem. Rev.* **1993**, *93*, 927.
- [115] A. F. Holleman, E. Wiberg, *Lehrbuch der Anorganischen Chemie. 71-101th ed, Vol. 101*, Walter de Gruyter, Berlin, **1995**.

- [116] N. N. Greenwood, A. Earnshaw, *Chemistry of the Elements, 2nd Edition*, Elsevier, Oxford, **1997**.
- [117] R. L. Deming, A. L. Allred, A. R. Dahl, A. W. Herlinger, M. O. Kestner, *J. Am. Chem. Soc.* **1976**, *98*, 4132.
- [118] C. K. Jørgensen, *J. Chimie Physique* **1979**, *76*, 630.
- [119] C. K. Jørgensen, *Z. Anorg. Allg. Chem.* **1986**, *540/541*, 91.
- [120] W. Liu, R. Franke, M. Dolg, *Chem. Phys. Lett.* **1999**, *302*, 231.
- [121] I. R. Beattie, *Angew. Chem. Int. Ed.* **1999**, *38*, 3294.
- [122] S. Riedel, Diplomarbeit, Bayerische Julius-Maximilians-Universität Würzburg (Würzburg), **2003**.
- [123] S. Riedel, M. Kaupp, *work in progress*.
- [124] U. Häussermann, M. Dolg, H. Stoll, H. Preuss, P. Schwerdtfeger, R. M. Pitzer, *Mol. Phys.* **1993**, *78*, 1211.
- [125] D. E. Woon, T. H. Dunning, Jr., *J. Chem. Phys.* **1993**, *98*, 1358.
- [126] T. H. Dunning, Jr., *J. Chem. Phys.* **1989**, *90*, 1007.
- [127] H.-J. Werner, P. J. Knowles, R. Lindh, M. Schütz, P. Celani, T. Korona, F. R. Manby, G. Rauhut, R. D. Amos, A. Bernhardsson, A. Berning, D. L. Cooper, M. J. O. Deegan, A. J. Dobbyn, F. Eckert, C. Hampel, G. Hetzer, A. W. Lloyd, S. J. McNicholas, W. Meyer, M. E. Mura, A. Nicklass, P. Palmieri, R. Pitzer, U. Schumann, H. Stoll, A. J. Stone, R. Tarroni, T. Thorsteinsson, 2001.1 ed., **2001**.
- [128] M. J. Frisch, G. W. Trucks, H. B. Schlegel, G. E. Scuseria, M. A. Robb, J. R. Cheeseman, J. A. Montgomery, J. T. Vreven, K. N. Kudin, J. C. Burant, J. M. Millam, S. S. Iyengar, J. Tomasi, V. Barone, B. Mennucci, M. Cossi, G. Scalmani, N. Rega, G. A. Petersson, H. Nakatsuji, M. Hada, M. Ehara, K. Toyota, R. Fukuda, J. Hasegawa, M. Ishida, T. Nakajima, Y. Honda, O. Kitao, H. Nakai, M. Klene, X. Li, J. E. Knox, H. P. Hratchian, J. B. Cross, C. Adamo, J. Jaramillo, R. Gomperts, R. E. Stratmann, O. Yazyev, A. J. Austin, R. Cammi, C. Pomelli, J. W. Ochterski, P. Y. Ayala, K. Morokuma, G. A. Voth, P. Salvador, J. J. Dannenberg, V. G. Zakrzewski, S. Dapprich, A. D. Daniels, M. C. Strain, O. Farkas, D. K. Malick, A. D. Rabuck, K. Raghavachari, J. B. Foresman, J. V. Ortiz, Q. Cui, A. G. Baboul, S. Clifford, J. Cioslowski, B. B. Stefanov, G. Liu, A. Liashenko, P. Piskorz, I. Komaromi, R. L. Martin, D. J. Fox, T. Keith, M. A. Al-Laham, C. Y. Peng, A. Nanayakkara, M. Challacombe, P. M. W. Gill, B. Johnson, W. Chen, M. W. Wong, C. Gonzalez, J. A. Pople, Pittsburg PA, **1998**.
- [129] J. P. Perdew, *Phys. Rev. B* **1986**, *33*, 8822.
- [130] C. Adamo, V. Barone, *Chem. Phys. Lett.* **1997**, *274*, 242.
- [131] A. D. Becke, *J. Chem. Phys.* **1996**, *104*, 1040.
- [132] T. H. Dunning, Jr., *J. Chem. Phys.* **1970**, *53*, 2823.
- [133] T. Clark, J. Chandrasekhar, G. W. Spitznagel, P. v. R. Schleyer, *J. Comput. Chem.* **1983**, *4*, 294.
- [134] T. H. Dunning, P. J. Hay, *Methods of Electronic Structure Theory, Vol. 3*, Plenum Press, **1977**.
- [135] A. Bergner, M. Dolg, W. Kuechle, H. Stoll, H. Preuss, *Mol. Phys.* **1993**, *80*, 1431.
- [136] M. Kaupp, P. v. R. Schleyer, H. Stoll, H. Preuss, *J. Am. Chem. Soc.* **1991**, *113*, 6012.
- [137] D. Andrae, U. Häussermann, M. Dolg, H. Stoll, H. Preuss, *Theor. Chim. Acta* **1990**, *77*, 123.
- [138] P.-O. Windmak, B. O. Roos, *European Summerschool in Quantum Chemistry, Vol. 3*, Lund University, Lund, **1999**.
- [139] A. D. Buckingham, P. W. Fowler, J. M. Hutson, *Chem. Rev.* **1988**, *88*, 963.
- [140] M. W. Chase, Jr., C. A. Davies, J. R. Downey, Jr., D. J. Frurip, R. A. McDonald, A. N. Syverud, *J. Phys. Chem. Ref. Data* **1985**, *14*, 1.

- [141] T. L. Cottrell, *The Strengths of Chemical Bonds*. 2nd ed, Butterworths, London, **1958**.
- [142] K. Millington, PhD, University of Southampton (United Kingdom), **1987**.
- [143] B. Miehlisch, A. Savin, H. Stoll, H. Preuss, *Chem. Phys. Lett.* **1989**, 157, 200.
- [144] R. Ahlrichs, M. Bär, M. Häser, H. Horn, C. Kölmel, *Chem. Phys. Lett.* **1989**, 162, 165.
- [145] M. Seth, F. Cooke, P. Schwerdtfeger, J.-L. Heully, M. Pelissier, *J. Chem. Phys.* **1998**, 109, 3935.
- [146] M. M. Francl, W. J. Pietro, W. J. Hehre, J. S. Binkley, M. S. Gordon, D. J. DeFrees, J. A. Pople, *J. Chem. Phys.* **1982**, 77, 3654.
- [147] S. Huzinaga, J. Anzelm, M. Klobukowski, E. Radzio-Andzelm, Y. Sakai, H. Tatewaki, *Gaussian Basis Sets for Molecular Calculations*, Elsevier, Amsterdam, **1984**.
- [148] A. Nicklass, M. Dolg, H. Stoll, H. Preuss, *J. Chem. Phys.* **1995**, 102, 8942.
- [149] A. E. Reed, F. Weinhold, *J. Chem. Phys.* **1985**, 83, 1736.
- [150] F. Weinhold, 4.M ed., University of Wisconsin, **1999**.
- [151] R. Reviakine, Würzburg, **2004**.
- [152] S. Raugei, M. L. Klein, *J. Chem. Phys.* **2002**, 116, 7087.
- [153] D. Kim, M. L. Klein, *J. Phys. Chem. B* **2000**, 104, 10074.
- [154] P. M. Esteves, A. Ramirez-Solis, C. J. A. Mota, *J. Am. Chem. Soc.* **2002**, 124, 2672.
- [155] P. Huppmann, H. Hartl, K. Seppelt, *Z. Anorg. Allg. Chem.* **1985**, 524, 26.
- [156] L. Turowsky, K. Seppelt, *Z. Anorg. Allg. Chem.* **1992**, 609, 153.
- [157] P. K. Miller, K. D. Abney, A. K. Rappe, O. P. Anderson, S. H. Strauss, *Inorg. Chem.* **1988**, 27, 2255.
- [158] P. Zylka, H. Oberhammer, K. Seppelt, *J. Mol. Struct.* **1991**, 243, 411.
- [159] R. C. Weast, Editor, *CRC Handbook of Chemistry and Physics*, 68 ed., CRC, Boca Raton, **1987**.
- [160] R. Minkwitz, F. Neikes, *Inorg. Chem.* **1999**, 38, 5960.
- [161] K. O. Christe, X. Zhang, R. Bau, J. Hegge, G. A. Olah, G. K. S. Prakash, J. A. Sheehy, *J. Am. Chem. Soc.* **2000**, 122, 481.
- [162] K. Seppelt, *Z. Anorg. Allg. Chem.* **1973**, 399, 87.
- [163] H. A. Carter, J. n. M. Shreeve, *Spectrochim Acta A* **1973**, 29, 1321.
- [164] K. Seppelt, D. Nothe, *Inorg. Chem.* **1973**, 12, 2727.
- [165] M. Kaupp, B. Metz, H. Stoll, *Angew. Chem. Int. Ed.* **2000**, 39, 4607.
- [166] M. Kaupp, S. Riedel, *Inorg. Chim. Acta* **2004**, 357, 1865.
- [167] L. P. Lindeman, J. C. Guffy, *J. Chem. Phys.* **1958**, 29, 247.
- [168] K. P. Huber, G. Herzberg, *Molecular Spectra and Molecular Structure, 4: Constants of Diatomic Molecules*, Van Nostrand, New York, **1979**.
- [169] M. Kaupp, H. G. von Schnering, *Inorg. Chem.* **1994**, 33, 4718.
- [170] H. P. A. Mercier, M. D. Moran, G. J. Schrobilgen, C. Steinberg, R. J. Suontamo, *J. Am. Chem. Soc.* **2004**, 126, 5533.
- [171] N. Bartlett, F. O. Sladky, *Comprehensive Inorganic Chemistry, Vol. 1*, Pergamon, Oxford, **1973**.
- [172] J. C. P. Sanders, G. J. Schrobilgen, *J. Chem. Soc., Chem. Commun.* **1989**, 1576.
- [173] S. Riedel, M. Kaupp, *Inorg. Chem.* **2006**, 45, 1228.
- [174] H. H. Claassen, B. Weinstock, *J. Chem. Phys.* **1960**, 33, 436.
- [175] C. L. Chernick, H. H. Claassen, B. Weinstock, *J. Am. Chem. Soc.* **1961**, 83, 3165.
- [176] B. Weinstock, H. H. Claassen, J. G. Malm, *J. Am. Chem. Soc.* **1957**, 79, 5832.
- [177] R. Wesendrup, P. Schwerdtfeger, *Inorg. Chem.* **2001**, 40, 3351.
- [178] F. Mohr, *Gold Bulletin* **2004**, 37, 164.
- [179] I.-C. Hwang, K. Seppelt, *Angew. Chem. Int. Ed.* **2001**, 40, 3690.
- [180] J. Brunvoll, A. A. Ischenko, A. A. Ivanov, G. V. Romanov, V. B. Sokolov, V. P. Spiridonov, T. G. Strand, *Acta Chem. Scand. A* **1982**, A36, 705.

- [181] P. Schwerdtfeger, *J. Am. Chem. Soc.* **1989**, *111*, 7261.
- [182] P. Schwerdtfeger, P. D. W. Boyd, S. Brienne, A. K. Burrell, *Inorg. Chem.* **1992**, *31*, 3411.
- [183] H. Schwarz, *Angew. Chem. Int. Ed.* **2003**, *42*, 4442.
- [184] V. V. Ostropikov, E. G. Rakov, *Izv. Vyssh. Uchebn. Zaved., Khim. Khim. Tekhnol.* **1989**, *32*, 3.
- [185] J. F. Lehmann, G. J. Schrobilgen, *J. Fluorine Chem.* **2003**, *119*, 109.
- [186] T. Drews, J. Supel, A. Hagenbach, K. Seppelt, *Inorg. Chem.* **2006**, *45*, 3782.
- [187] E. Miyoshi, Y. Sakai, *J. Chem. Phys.* **1988**, *89*, 7363.
- [188] R. N. Compton, P. W. Reinhardt, C. D. Cooper, *J. Chem. Phys.* **1978**, *68*, 2023.
- [189] R. N. Compton, P. W. Reinhardt, *J. Chem. Phys.* **1980**, *72*, 4655.
- [190] S. Cotton, *Chemistry of Precious Metals*, Chapman & Hall, Weinheim, **1997**.
- [191] H. Schmidbaur, *Gold Progress in Chemistry, Biochemistry and Technology*, Wiley-VCH, Weinheim, **1999**.
- [192] M. J. Frisch, G. W. Trucks, H. B. Schlegel, G. E. Scuseria, M. A. Robb, J. R. Cheeseman, J. A. Montgomery, J. T. Vreven, K. N. Kudin, J. C. Burant, J. M. Millam, S. S. Iyengar, J. Tomasi, V. Barone, B. Mennucci, M. Cossi, G. Scalmani, N. Rega, G. A. Petersson, H. Nakatsuji, M. Hada, M. Ehara, K. Toyota, R. Fukuda, J. Hasegawa, M. Ishida, T. Nakajima, Y. Honda, O. Kitao, H. Nakai, M. Klene, X. Li, J. E. Knox, H. P. Hratchian, J. B. Cross, C. Adamo, J. Jaramillo, R. Gomperts, R. E. Stratmann, O. Yazyev, A. J. Austin, R. Cammi, C. Pomelli, J. W. Ochterski, P. Y. Ayala, K. Morokuma, G. A. Voth, P. Salvador, J. J. Dannenberg, V. G. Zakrzewski, S. Dapprich, A. D. Daniels, M. C. Strain, O. Farkas, D. K. Malick, A. D. Rabuck, K. Raghavachari, J. B. Foresman, J. V. Ortiz, Q. Cui, A. G. Baboul, S. Clifford, J. Cioslowski, B. B. Stefanov, G. Liu, A. Liashenko, P. Piskorz, I. Komaromi, R. L. Martin, D. J. Fox, T. Keith, M. A. Al-Laham, C. Y. Peng, A. Nanayakkara, M. Challacombe, P. M. W. Gill, B. Johnson, W. Chen, M. W. Wong, C. Gonzalez, J. A. Pople, Revision B.04 ed., Pittsburgh PA, **2003**.
- [193] H.-J. Werner, P. J. Knowles, R. Lindh, M. Schütz, P. Celani, T. Korona, F. R. Manby, G. Rauhut, R. D. Amos, A. Bernhardsson, A. Berning, D. L. Cooper, M. J. O. Deegan, A. J. Dobbyn, F. Eckert, C. Hampel, G. Hetzer, A. W. Lloyd, S. J. McNicholas, W. Meyer, M. E. Mura, A. Nicklass, P. Palmieri, R. Pitzer, U. Schumann, H. Stoll, A. J. Stone, R. Tarroni, T. Thorsteinsson, MOLPRO 2002.6 ed., Birmingham, UK, **2003**.
- [194] P. Schwerdtfeger, M. Dolg, W. H. E. Schwarz, G. A. Bowmaker, P. D. W. Boyd, *J. Chem. Phys.* **1989**, *91*, 1762.
- [195] S. Simon, M. Duran, J. J. Dannenberg, *J. Chem. Phys.* **1996**, *105*, 11024.
- [196] W. Liu, C. van Wüllen, *J. Chem. Phys.* **1999**, *110*, 3730.
- [197] O. Graudejus, A. P. Wilkinson, L. C. Chacon, N. Bartlett, *Inorg. Chem.* **2000**, *39*, 2794.
- [198] K. Leary, A. Zalkin, N. Bartlett, *J. Chem. Soc., Chem. Commun.* **1973**, 131.
- [199] K. Leary, A. Zalkin, N. Bartlett, *Inorg. Chem.* **1974**, *13*, 775.
- [200] J. H. Holloway, G. J. Schrobilgen, *J. Chem. Soc., Chem. Commun.* **1975**, 623.
- [201] M. J. Vasile, T. J. Richardson, F. A. Stevie, W. E. Falconer, *J. Chem. Soc., Dalton Trans.* **1976**, 351.
- [202] R. Hoffmann, B. F. Beier, E. L. Muetterties, A. R. Rossi, *Inorg. Chem.* **1977**, *16*, 511.
- [203] M. V. Korobov, S. V. Kuznetsov, L. N. Sidorov, V. A. Shipachev, V. N. Mit'kin, *Int. J. Mass Spectrom. Ion Processes* **1989**, *87*, 13.
- [204] A. W. Ehlers, M. Bohme, S. Dapprich, A. Gobbi, A. Hollwarth, V. Jonas, K. F. Kohler, R. Stegmann, A. Veldkamp, G. Frenking, *Chem. Phys. Lett.* **1993**, *208*, 111.
- [205] I. Malkin, O. L. Malkina, V. G. Malkin, M. Kaupp, *J. Chem. Phys.* **2005**, *123*, 244103.

- [206] V. G. Malkin, O. L. Malkina, R. Reviakine, A. V. Arbuznikov, M. Kaupp, B. Schimmelpfennig, I. Malkin, M. Repiský, S. Komorovský, P. Hrobárik, E. Malkin, T. Helgaker, K. Ruud, MAG-ReSpect 2.1 ed., **2005**.
- [207] A. Citra, L. Andrews, *J. Phys. Chem. A* **1999**, *103*, 4182.
- [208] K. O. Christe, D. A. Dixon, *J. Am. Chem. Soc.* **1992**, *114*, 2978.
- [209] F. O. Sladky, P. A. Bulliner, N. Bartlett, *J. Chem. Soc. A* **1969**, *14*, 2179.
- [210] R. J. Gillespie, G. J. Schrobilgen, *Inorg. Chem.* **1976**, *15*, 22.
- [211] H. C. Kolb, M. S. VanNieuwenhze, K. B. Sharpless, *Chem. Rev.* **1994**, *94*, 2483.
- [212] M. A. Andersson, R. Epple, V. V. Fokin, K. B. Sharpless, *Angew. Chem. Int. Ed.* **2002**, *41*, 472.
- [213] O. Ruff, F. W. Tschirch, *Ber.* **1913**, *46*, 929.
- [214] B. Weinstock, J. G. Malm, *J. Am. Chem. Soc.* **1958**, *80*, 4466.
- [215] O. Glemser, H. W. Roesky, K. H. Hellberg, H. U. Werther, *Chem. Ber.* **1966**, *99*, 2652.
- [216] A. Veldkamp, G. Frenking, *Chem. Ber.* **1993**, *126*, 1325.
- [217] C. Peng, H. B. Schlegel, *Isr. J. Chem.* **1994**, *33*, 449.
- [218] C. Peng, P. Ayala, H. B. Schlegel, M. J. Frisch, *J. Comput. Chem.* **1996**, *17*, 49.
- [219] S. R. Gunn, *J. Phys. Chem.* **1967**, *71*, 2934.
- [220] J. F. Lehmann, H. P. A. Mercier, G. J. Schrobilgen, *Coord. Chem. Rev.* **2002**, *233-234*, 1.
- [221] S. Riedel, M. Kaupp, *Inorg. Chem.* **2006**, in press.
- [222] F. Furche, J. P. Perdew, *J. Chem. Phys.* **2006**, *124*, 044103/1.
- [223] K. O. Christe, R. Bougon, *J. Chem. Soc., Chem. Commun.* **1992**, 1056.
- [224] K. O. Christe, D. A. Dixon, H. G. Mack, H. Oberhammer, A. Pagelot, J. C. P. Sanders, G. J. Schrobilgen, *J. Am. Chem. Soc.* **1993**, *115*, 11279.
- [225] R. Bougon, B. Ban, K. Seppelt, *Chem. Ber.* **1993**, *126*, 1331.
- [226] M. Gerken, G. J. Schrobilgen, in *Inorganic Chemistry in Focus II*, **2005**, pp. 243.
- [227] R. Bougon, *J. Fluorine Chem.* **1991**, *53*, 419.
- [228] K. H. Hellberg, A. Mueller, O. Glemser, *Z Naturforsch B* **1966**, *21*, 118.
- [229] B. Weinstock, H. H. Claassen, J. G. Malm, *J. Chem. Phys.* **1960**, *32*, 181.
- [230] J. G. Malm, H. Selig, *J. Inorg. Nucl. Chem.* **1961**, *20*, 189.
- [231] E. J. Jacob, L. S. Bartell, *J. Chem. Phys.* **1970**, *53*, 2231.
- [232] E. W. Kaiser, J. S. Muentner, W. A. Klemperer, W. E. Falconer, *J. Chem. Phys.* **1970**, *53*, 53.
- [233] N. Bartlett, S. Yeh, K. Kourtakis, T. Mallouk, *J. Fluorine Chem.* **1984**, *26*, 97.
- [234] T. Vogt, A. N. Fitch, J. K. Cockcroft, *Science* **1994**, *263*, 1265.
- [235] B. von Ahsen, C. Bach, H. Pernice, H. Willner, F. Aubke, *J. Fluorine Chem.* **2000**, *102*, 243.
- [236] G. S. Quinones, G. Haegele, K. Seppelt, *Chem. Eur. J.* **2004**, *10*, 4755.
- [237] M. Hargittai, *Chem. Rev.* **2000**, *100*, 2233.
- [238] J. Molnar, M. Hargittai, *J. Phys. Chem.* **1995**, *99*, 10780.
- [239] A. Kovacs, R. J. M. Konings, A. S. Booji, *Chem. Phys. Lett.* **1997**, *268*, 9207.
- [240] L. Joubert, G. Picard, J.-J. Legendre, *Inorg. Chem.* **1998**, *37*, 1984.
- [241] M. Hargittai, *Coord. Chem. Rev.* **1988**, *91*, 35.
- [242] S. A. Decker, M. Klobukowski, *J. Chem. Inf. Comput. Sci.* **2001**, *41*, 1.
- [243] C. W. Bauschlicher, Jr., *J. Phys. Chem. A* **2000**, *104*, 5843.
- [244] S. A. Macgregor, K. H. Moock, *Inorg. Chem.* **1998**, *37*, 3284.
- [245] N. Tanpipat, J. Baker, *J. Phys. Chem.* **1996**, *100*, 19818.
- [246] I. W. Parsons, S. J. Till, *J. Chem. Soc., Faraday Trans.* **1993**, *89*, 25.
- [247] H. M. Seip, R. Seip, *Acta Chem Scand* **1966**, *20*, 2698.
- [248] M. Kimura, V. Schomaker, D. W. Smith, *J. Chem. Phys.* **1968**, *48*, 4001.



- [249] J. Supel, R. Marx, K. Seppelt, *Z. Anorg. Allg. Chem.* **2005**, 631, 2979.
- [250] J. Zhao, Y. Zhang, Y. Kan, L. Zhu, *Spectrochim Acta A* **2004**, 60A, 679.
- [251] W. E. Falconer, F. J. DiSalvo, A. J. Edwards, J. E. Griffiths, W. A. Sunder, M. J. Vasile, *Inorg. Nucl. Chem. - Herbert H. Hyman Mem. Vol.* **1976**, 59.
- [252] A. I. Popov, Y. M. Kiselev, V. F. Sukhoverkhov, V. I. Spitsyn, *Dokl. Akad. Nauk SSSR* **1987**, 296, 615.
- [253] A. I. Popov, Y. M. Kiselev, *Zh. Neorg. Khim.* **1988**, 33, 965.
- [254] A. A. Timakov, V. N. Prusakov, Y. V. Drobyshevskii, *Zh. Neorg. Khim.* **1982**, 27, 3007.
- [255] Y. M. Kiselev, N. S. Kopelev, V. I. Spitsyn, L. I. Martynenko, *Dokl. Akad. Nauk SSSR* **1987**, 292, 628.
- [256] Y. M. Kiselev, G. V. Ionova, A. A. Kiseleva, N. S. Kopelev, A. P. Bobylev, A. B. Yatskevich, V. I. Spitsyn, *Dokl. Akad. Nauk SSSR* **1987**, 293, 1407.
- [257] G. V. Chertihin, W. Saffel, J. T. Yustein, L. Andrews, M. Neurock, A. Ricca, C. W. Bauschlicher, Jr., *J. Phys. Chem.* **1996**, 100, 5261.
- [258] Y. Yamada, H. Sumino, Y. Okamura, H. Shimasaki, T. Tominaga, *Appl. Radiat. Isotopes* **2000**, 52, 157.
- [259] J. F. Berry, E. Bill, E. Bothe, S. D. George, B. Mienert, F. Neese, K. Wieghardt, *Science* **2006**.
- [260] M. Ingleson, H. Fan, M. Pink, J. Tomaszewski, K. G. Caulton, *J. Am. Chem. Soc.* **2006**, 128, 1804.
- [261] M. Brookhart, B. E. Grant, C. P. Lenges, M. H. Prosenc, P. S. White, *Angew. Chem. Int. Ed.* **2000**, 39, 1676.
- [262] E. K. Byrne, K. H. Theopold, *J. Am. Chem. Soc.* **1987**, 109, 1282.
- [263] B. Zemva, K. Lutar, A. Jesih, W. J. Casteel, Jr., N. Bartlett, *J. Chem. Soc., Chem. Commun.* **1989**, 346.
- [264] B. Zemva, K. Lutar, L. Chacon, M. Fele-Beuermann, J. Allman, C. Shen, N. Bartlett, *J. Am. Chem. Soc.* **1995**, 117, 10025.
- [265] W. Harnischmacher, R. Hoppe, *Angew. Chem. Int. Ed.* **1973**, 12, 582.
- [266] D. Kissel, R. Hoppe, *Z. Anorg. Allg. Chem.* **1988**, 559, 40.
- [267] T. V. Popova, N. V. Aksenova, *Russ. J. Coord. Chem.* **2003**, 29, 743.
- [268] P. Sorbe, J. Grannec, J. Portier, P. Hagenmuller, *Compt. Rend. (C)* **1976**, 282, 663.
- [269] B. G. Müller, *Angew. Chem. Int. Ed.* **1987**, 26, 1081.

# List of Publications

## List of Publications Included in the Thesis

- I. Sebastian Riedel, Michal Straka, Martin Kaupp, *"Validation of Density Functional Methods for Computing Structures and Energies of Mercury(IV) Complexes"* Phys. Chem. Chem. Phys. **2004**, 6, 1122–1127.
- II. Sebastian Riedel, Michal Straka, Martin Kaupp, *"Can Weakly Coordinating Anions Stabilize Mercury in its Oxidation State +IV?"* Chem. Eur. J. **2005**, 9, 2743–2755.
- III. Sebastian Riedel, Martin Kaupp, *"Has AuF<sub>7</sub> Been Made?"* Inorg. Chem. **2006**, 45, 1228–1234.
- IV. Sebastian Riedel, Martin Kaupp, *"Revising the Highest Oxidation States of the 5d Elements: The Case of Iridium(+VII)"* Angew. Chem. **2006**, 118, 3791–3794 (Angew. Chem. Int. Ed. **2006**, 45, 3708–3711)
- V. Sebastian Riedel, Martin Kaupp, *"Where is the Limit of Highly Fluorinated High-Oxidation State Osmium Species?"* Inorg. Chem. **2006**, in press

## List of other Publications

- I. Martin Kaupp, Sebastian Riedel, *"On the Lack of Correlation between Bond Lengths, Dissociation Energies and Force Constants. The Fluorine-Substituted Ethane Homologues"* Inorg. Chim. Acta **2004**, 6, 1865–1872.
- II. Li Yong, Stephan D. Hoffmann, Thomas F. Fässler, Sebastian Riedel, Martin Kaupp, *"[Pb<sub>5</sub>{Mo(CO)<sub>3</sub>}<sub>2</sub>]<sup>4-</sup> The first Complex Containing a Planar [Pb<sub>5</sub>]<sup>4-</sup> Anion"* Angew. Chem. **2005**, 117, 2129–2133 (Angew. Chem. Int. Ed. **2005**, 44, 2092–2096).
- III. Pekka Pyykkö, Sebastian Riedel, Michael Patzschke, *"Triple-bond Covalent Radii"* Chem. Eur. J. **2005**, 12, 3511–3520.
- IV. Sebastian Riedel, Pekka Pyykkö, Ricardo A. Mata, Hans-Joachim Werner, *"Comparative Calculations for the A-Frame Molecules [S(MPH<sub>3</sub>)<sub>2</sub>] (M=Cu,Ag,Au) at Levels up to CCSD(T)"* Chem. Phys. Lett. **2005**, 405, 148–152.

## List of Poster Presentations and Talks

- I. Sebastian Riedel, Michal Straka, Martin Kaupp "*Validation of Density Functional Methods for Computing Structures and Energies of Mercury(IV) Complexes*" presented on the JungChemikerForum (JCF) Frühjahrssymposium in Heidelberg, 2004.
- II. Sebastian Riedel, Michal Straka, Martin Kaupp "*Can Weakly Coordinating Anions Stabilize Mercury in its Oxidation State +IV*" presented on the "40<sup>th</sup> Symposium for Theoretical Chemistry" in Suhl, 2004.
- III. Michal Straka, Sebastian Riedel, Pekka Pyykkö "*Ab Initio Predictions for Novel Nitrogen Species: Pentazolides, Planar Rings, and N<sub>5</sub><sup>+</sup> Derivatives*" presented on the "Winter School in Theoretical Chemistry 2004" in Helsinki, 2004.
- IV. Sebastian Riedel, Michal Straka, Martin Kaupp "*Hunting for Hg(IV) species*" Relativistic Effects in Heavy Elements (REHE) in Mülheim/Ruhr, 2005.
- V. Sebastian Riedel, Pekka Pyykkö, Michal Patzschke "*Triple-Bonded Covalent Radii of the Periodic Table as a Predictive Tool for New Silicon Triple-Bond Distances*" presented on the "The 14<sup>th</sup> International Symposium on Organosilicon Chemistry ISOS XIV" in Würzburg, 2005.
- VI. Sebastian Riedel, Martin Kaupp "*The Highest Oxidation States of the 5d Transition Metals*" presented on the "Winter School in Theoretical Chemistry 2005" in Helsinki, 2005.
- VII. Sebastian Riedel, Martin Kaupp "*The Highest Oxidation States of the 5d Transition Metals*" presented on the JungChemikerForum (JCF) Frühjahrssymposium in Konstanz, 2006.
- VIII. Sebastian Riedel, Talk: "*The Highest Oxidation States of the 5d Transition Metals*" JungChemikerForum (JCF) Frühjahrssymposium in Konstanz, 2006.

# Lebenslauf

## Sebastian Hasenstab-Riedel

Diplom Chemiker

Geboren: 05.09.1975 in Groß-Gerau

Vater: Wolfgang Riedel (verstorben)

Mutter: Marlies Riedel (geb. Bensel)

### Familienstand

verheiratet, keine Kinder

### Schule

1982-1991

Grund- und Hauptschule Mainaschaff  
(Qualifizierender Hauptschulabschluss)

1991-1993

Berufsfachschule im Berufsfeld Elektrotechnik  
Ludwig-Geissler-Schule Hanau

1996-1997

Fachoberschulabschluss (Chemisch/physikalische Technik)  
Ludwig-Geissler-Schule Hanau

### Berufspraxis vor dem Studium

9/1993-8/1995

Ausbildung zum Chemielaboranten  
Siemens AG Hanau/Wolfgang

9/1995-6/1996

Ausbildung zum Chemielaboranten  
Degussa AG Hanau/Wolfgang

### Studium

Studiengang „Chemie Diplom“

1998-2000

#### Grundstudium

Universität Siegen

9/2000

#### Diplom-Vorprüfung

Erwerb der fachgebundenen Hochschulreife während des Studiums in integrierten Studiengängen.

2000-2002

**Hauptstudium**

Bayerische Julius-Maximilians-Universität Würzburg

**Abschluss des Diplomstudiengangs Chemie**

10/2002

**Diplom-Hauptprüfung (mündlich)**

11/2002-6/2003

**Anfertigung der Diplomarbeit**

in der Arbeitsgruppe von Prof. M. Kaupp

Thema der Diplomarbeit: „Quantenchemische  
Untersuchung zur Existenz von Quecksilber in der  
Oxidationsstufe +IV“

seit 10/2003

**Doktorarbeit**

Bearbeitung der Doktorarbeit in der Arbeitsgruppe von  
Prof. M. Kaupp am Institut für Anorganische Chemie der  
Universität Würzburg

Würzburg den 17.07.2006

Sebastian Hasenstab-Riedel